PATHOGEN CLASSIFICATION USING AI-ENABLED HYPERSPECTRAL MICROSCOPY TO DETECT BIOLOGICAL VARIATIONS

By

MeiLi Papa

A THESIS

Submitted to
Michigan State University
in partial fulfillment of the requirements
for the degree of

Biosystems Engineering – Master of Science

2025

ABSTRACT

Timely detection and identification of pathogens are crucial for safeguarding food safety, public health, and environmental monitoring. However, conventional methods often struggle to account for subtle biological variations in microbial physiology and the nuanced differences among closely related serovars. The objectives of this work were to: i) systematically review AI applications for imaging-based pathogen detection under stress conditions; ii) develop an AI-enabled hyperspectral microscopy framework for rapid detection of stressed cells under low-level antimicrobials; iii) enhance data processing of this framework to classify *Salmonella* serovars. Critical gaps identified from the systematic review highlighted limited research on stressed pathogen detection and inconsistent reporting of laboratory protocols and data pipelines. An optimized laboratory protocol captured distinct hyperspectral profiles of *E. coli* K-12 in both normal (i.e., viable and culturable) and viable but non-culturable (VBNC) states induced by low-level antimicrobials (n = 200). An EfficientNetV2 convolutional neural network (CNN), trained on pseudo-RGB images from these hyperspectral data, achieved a 97.1% accuracy for VBNC classification, outperforming standard color images. Additionally, hyperspectral data detected subtle biological differences of five *Salmonella* serovars, i.e., Kentucky, Johannesburg, Infantis, Enteritidis, and 4,[5],12:i:- (n = 500). Enhanced data preprocessing techniques and multimodal fusion methods were introduced, incorporating both spectral features (via manual feature selection vs. data-driven feature extraction) and spatial features (CNN-based). Data-driven feature extraction outperformed manual selection, and multimodal fusion further improved classification accuracy to 82.40%. These findings demonstrate that integrating hyperspectral microscopy with AI-enabled data analysis enhances classification capabilities, paving the way for practical, streamlined rapid pathogen detection solutions.

ACKNOWLEDGEMENTS

My deepest gratitude to Dr. Jiyoon Yi, my major advisor. Her extensive expertise and unwavering commitment to excellence inspired me to push myself and achieve a level of work I never imagined possible. Her guidance and patience helped me navigate many challenges and become a better researcher.

I would also like to thank Dr. Bosoon Park for sharing his expertise on hyperspectral microscopy. I would not have been able to succeed without his guidance and knowledge. Also, thank you to Dr. Erika Oh for her introduction and guidance on my systematic review.

My committee members, Dr. Teresa Bergholz and Dr. Yuzhen Lu, served as valuable mentors and their expertise, insight, and valuable time greatly contributed to my success.

Thank you to the Food AI & Engineering Lab members for helping expand my knowledge across disciplines. Especially Aarham Wasit and Sid Bhattacharya for their coding expertise, my L.I.A.M, Gillian Kuehnle for her support on my systematic review, and finally Justin Percora for making all of my media (contaminated or not).

Thank you to the Food Safety Engineering Lab staff, Michael James and Dr. Ian Hildebrandt for their support and patience, especially during the beginning of my research journey. Also. Thank you to Phil Hill for fabricating a component of my equipment setup.

Finally, thank you to Boop, who has faithfully tuned into countless lab meetings, writing sessions, and always kept me company through late-night work sessions. And to Boba, for possibly starting a new tradition of getting a new cat for every degree I pursue.

This material is based upon work supported by MSU Startup Funds for Dr. Yi, MSU Research Foundation's Tetrad Award, and USDA ARS Research Support Agreements (No. 58-6040-3-017 and 58-6040-4-041). Any opinion, findings, conclusion, or recommendations expressed in this paper are those of the author(s) and do not necessarily reflect the view of USDA.

TABLE OF CONTENTS

LIST OF TABLES

LIST OF FIGURES

LIST OF ABBREVIATIONS

AI	Artificial Intelligence
ANN	Artificial Neural Network
AOTF	Acoustic-Optic Tunable Filter
AUC	Area Under Curve
CCD	Charge-Coupled Device
CFU	Colony Forming Units
CMOS	Complementary Metal-Oxide-Semiconductor
CNN	Convolutional Neural Network
DA	Discriminant Analysis
EMCCD	Electron-Multiplying Charge-Coupled Device
FN	False Negative
FP	False Positive
GAN	Generative Adversarial Network
HMI	Hyperspectral Microscope Imaging
KNN	*k*-Nearest Neighbors
LDA	Linear Discriminant Analysis
LED	Light-Emitting Diode
LSTM	Long Short-Term Memory
MIL	Multiple Instance Learning
ML	Machine Learning
N/A	Not Applicable
NR	Not Reported
PAA	Peracetic Acid
PCA	Principal Component Analysis

PCR	Polymerase Chain Reaction
PLS-DA	Partial Least Squares Discriminant Analysis
QDA	Quadratic Discriminant Analysis
RF	Random Forest
RFU	Relative Fluorescence Units
RGB	Red Green Blue
RNN	Recurrent Neural Network
ROI	Region of Interest
sCMOS	Scientific CMOS
SIM	Structured Illumination Microscope
SNV	Standard Normal Variate
SVM	Support Vector Machine
TN	True Negative
TRIF	Total Internal Reflection Fluorescence
TP	True Positive
VBNC	Viable but Nonculturable
VNIR	Visible and Near-Infrared

CHAPTER 1: INTRODUCTION

1.1 Background

Evolving technology for pathogen detection is crucial for ensuring food safety, protecting public health, and advancing environmental monitoring. These domains present unique challenges, introducing various stressors that complicate accurate pathogen detection. In food safety, the diversity of food matrices and unfavorable conditions can interfere with detection methods, making it difficult to accurately identify pathogens, especially at low concentrations (Wang and Salazar, 2016; Acuff and Ponder, 2020). In public health, pathogens in medical settings face additional stressors, including the variability of host responses, co-infections, and the presence of non-viable pathogens, which complicate accurate detection (Bliven and Maurelli, 2015; Vicente-Santos et al., 2024). Environmental monitoring similarly deals with complex samples, including water, soil, and air, which are teeming with a wide variety of microorganisms, making it difficult to pinpoint specific pathogens (Dupont et al., 2020). Environmental variability, including fluctuations in temperature, pH, and moisture, further affects pathogen viability, thereby increasing background interference in detection methods.

Optical imaging methods have shown considerable promise in enhancing pathogen detection across these fields. Microscopy-based techniques, particularly hyperspectral microscopy, enable direct, minimally invasive observation of pathogens, capturing detailed spectrochemical data that reveal insights into microbial constituents, intracellular components, and metabolic states (Gowen et al., 2015; Gao and Smith et al., 2016). This is particularly helpful in food safety, where rich hyperspectral information can help differentiate harmful pathogens from natural biological background noise and identify pathogens of different physiological states (Seo et al., 2016; Park et al., 2023; Papa et al., 2025). The near real-time capability of

microscopy-based detection offers advantages in public health, where rapid detection is crucial during outbreaks and for diagnostics by expediting identification, allowing for quicker response times (Akbari et al., 2012; Akgönüllü and Denizli, 2022).

Incorporating artificial intelligence (AI) into these domains has proven useful for improving early detection of pathogens and disease by accelerating and automating the analysis of complex data (Pinto-Coelho, 2023). Specifically, recent studies in the food safety domain have demonstrated the effectiveness of machine learning and deep convolutional neural networks (CNNs) applied to microscopy-based imaging for rapid and accurate detection of foodborne pathogens (Kang et al., 2021; Ma et al., 2023). Moreover, when microscopy is integrated with advanced biosensing techniques that leverage specific biological interactions, CNNs trained on imagery data from lab-cultured bacteria effectively capture these biological patterns and maintain robust detection accuracy even within challenging real-world samples (Yi et al., 2023).

1.2 Research Gaps

Conventional culture-based methods, which depend on non-selective and selective enrichment procedures, often fail to detect pathogens in a timely manner, leading to delayed responses (Law et al., 2015; Hameed et al., 2018). To overcome this limitation, effective pathogen detection requires the identification of unique and stable biomarkers derived from microbial physiological or biochemical signals that can reliably distinguish between infectious and non-infectious material, even amidst biological background noise. However, additional complexity arises in distinguishing viable pathogens from non-viable or stressed cells and accurately identifying causative agents during foodborne outbreaks investigations, which is critical for implementing timely and effective interventions. Complexity further increases when differentiating closely related serovars. Standard serotyping methods, primarily slide

agglutination tests using O and H antigen-specific antisera, remain common but are labor-and resource-intensive, time-consuming, and requires skilled personnel (Herrera-León et al., 2007; Boxrud, 2010; Shi et al., 2015). While advanced molecular methods such as polymerase chain reaction (PCR) offer potential solutions, they still face limitations including extensive sample preparation, high-quality labor, difficulty in differentiating viable from non-viable cells, and interference from non-target DNA (Guo et al., 2021; Pinto et al., 2015). These limitations highlight the need for resource-effective alternative that complements existing technologies by offering rapid screening methods with streamlined sample preparation and automated data analysis. Such innovations can enhance the speed, accuracy, and overall performance of pathogen detection, ultimately leading to more efficient solutions for food safety, public health, and environmental monitoring.

1.3 Goal and Objectives

The goal of this work is to develop an AI-enabled hyperspectral microscopy framework capable of rapidly classifying pathogens and detecting biological variations. The specific objectives are to: i) systematically review AI applications for imaging-based pathogen detection under stress conditions; ii) develop an AI-enabled hyperspectral microscopy framework for rapid detection of stressed cells under low-level antimicrobials; and iii) enhance data processing of this framework to classify *Salmonella* serovars. The findings of this work will serve as a foundation for developing a streamlined rapid pathogen detection and identification system, contributing to enhanced food safety and public health.

BIBLIOGRAPHY

Acuff, J., & Ponder, M. (2020). Interactions of Foodborne Pathogens with the Food Matrix. In A. Demirci, H. Feng, & K. Krishnamurthy (Eds.), *Food Safety Engineering* (pp. 129–156). Springer International Publishing. https://doi.org/10.1007/978-3-030-42660-6_5

Akgönüllü, S., & Denizli, A. (2022). Recent advances in optical biosensing approaches for biomarkers detection. *Biosensors and Bioelectronics: X*, *12*, 100269. https://doi.org/10.1016/j.biosx.2022.100269

Bliven, K. A., & Maurelli, A. T. (2016). Evolution of Bacterial Pathogens Within the Human Host. *Microbiology Spectrum*, *4*(1). https://doi.org/10.1128/microbiolspec.VMBF-0017-2015

Dupont, M. F., Elbourne, A., Cozzolino, D., Chapman, J., Truong, V. K., Crawford, R. J., & Latham, K. (2020). Chemometrics for environmental monitoring: A review. *Analytical Methods*, *12*(38), 4597–4620. https://doi.org/10.1039/D0AY01389G

Gao, L., & Smith, R. T. (2015). Optical hyperspectral imaging in microscopy and spectroscopy – a review of data acquisition. *Journal of Biophotonics*, *8*(6), 441–456. https://doi.org/10.1002/jbio.201400051

Gowen, A. A., Feng, Y., Gaston, E., & Valdramidis, V. (2015). Recent applications of hyperspectral imaging in microbiology. *Talanta*, *137*, 43–54. https://doi.org/10.1016/j.talanta.2015.01.012

Kang, R., Park, B., Ouyang, Q., & Ren, N. (2021). Rapid identification of foodborne bacteria with hyperspectral microscopic imaging and artificial intelligence classification algorithms. *Food Control*, *130*, 108379. https://doi.org/10.1016/j.foodcont.2021.108379

Ma, L., Yi, J., Wisuthiphaet, N., Earles, M., & Nitin, N. (2022). Accelerating the Detection of Bacteria in Food Using Artificial Intelligence and Optical Imaging. *Applied and Environmental Microbiology*, *89*(1), e01828-22. https://doi.org/10.1128/aem.01828-22

Papa, M., Wasit, A., Pecora, J., Bergholz, T. M., & Yi, J. (2025). Detection of Viable but Nonculturable *E. coli* Induced by Low-Level Antimicrobials Using AI-Enabled Hyperspectral Microscopy. *Journal of Food Protection*, *88*(1), 100430. https://doi.org/10.1016/j.jfp.2024.100430

Park, B., Shin, T., Wang, B., McDonogh, B., & Fong, A. (2023). Classification between live and dead foodborne bacteria with hyperspectral microscope imagery and machine learning. *Journal of Microbiological Methods*, *209*, 106739. https://doi.org/10.1016/j.mimet.2023.106739

Pinto, D., Santos, M. A., & Chambel, L. (2015). Thirty years of viable but nonculturable state research: Unsolved molecular mechanisms. *Critical Reviews in Microbiology*, *41*(1), 61–76. https://doi.org/10.3109/1040841X.2013.794127

Seo, Y., Park, B., Hinton, A., Yoon, S.-C., & Lawrence, K. C. (2016). Identification of Staphylococcus species with hyperspectral microscope imaging and classification algorithms. *Journal of Food Measurement and Characterization*, *10*(2), 253–263. https://doi.org/10.1007/s11694-015-9301-0

Vicente-Santos, A., Willink, B., Nowak, K., Civitello, D. J., & Gillespie, T. R. (2023). Host-pathogen interactions under pressure: A review and meta-analysis of stress-mediated effects on disease dynamics. *Ecology Letters*, *26*(11), 2003–2020. https://doi.org/10.1111/ele.14319

Wang, Y., & Salazar, J. K. (2016). Culture-Independent Rapid Detection Methods for Bacterial Pathogens and Toxins in Food Matrices. *Comprehensive Reviews in Food Science and Food Safety*, *15*(1), 183–205. https://doi.org/10.1111/1541-4337.12175

Yi, J., Wisuthiphaet, N., Raja, P., Nitin, N., & Earles, J. M. (2023). AI-enabled biosensing for rapid pathogen detection: From liquid food to agricultural water. *Water Research*, *242*, 120258. https://doi.org/10.1016/j.watres.2023.120258

CHAPTER 2: AI-ENABLED IMAGING FOR PATHOGEN DETECTION UNDER STRESS CONDITIONS: A SYSTEMATIC REVIEW

2.1 Abstract

Advances in pathogen detection incorporating artificial intelligence (AI) can provide insights into bacterial physiology under challenging environmental conditions that traditional methods may miss. This systematic review aims to evaluate the application, efficacy, and technological advancements of AI-enabled imaging for pathogen detection, including its impact on speed, accuracy, and predictive modeling under stress conditions. Studies were systematically identified from five electronic databases using key search terms (i.e., artificial intelligence, pathogen, detection, imaging) and their alternatives. Inclusion criteria, guided by the PICOS framework, focused on microscopy-based pathogen detection enhanced by AI. Data extraction followed PRISMA guidelines, covering aspects such as biological sample preparation, AI-enabled data analyses, and performance metrics. The review evaluated how these methods addressed challenges like biological noise and pathogen viability. Of 2,736 citations retrieved, 120 were reviewed in full and 28 studies met the inclusion criteria. These represented over 40 different pathogens, primarily major foodborne pathogens such as *Salmonella* and *E. coli.* However, only 3 studies addressed bacterial stress conditions. Additionally, many studies lacked conventional detection methods (i.e., culture-based or molecular) as comparators to fully evaluate AI-enabled detection. Reporting inconsistencies in laboratory protocols and data pipeline further complicated reproducibility and meta-analysis. This review provides a comprehensive overview of current methods in AI-enabled pathogen detection from both biological and computational perspectives. Findings emphasize the need for standardized benchmarks and consistent reporting to enhance the credibility, reproducibility, and ultimately

broader adoption of AI-enabled imaging in pathogen detection.

2.2 Introduction

Developing advanced pathogen detection technologies is crucial for ensuring food safety, protecting public health, and enhancing environmental monitoring. However, each of these domains is characterized by inherent biosystems stressors that induce microbiological variations, making accurate pathogen detection challenging without additional biological sample preparation and isolation. In food safety, the diversity of food matrices and processing conditions can interfere with detection methods, especially when pathogens are present at low concentrations (Wang and Salazar, 2016; Acuff and Ponder, 2020). In public health, pathogens in clinical settings face further challenges due to variable host responses, co-infections, and the presence of non-viable pathogens, which complicate detection (Bliven and Maurelli, 2015; Vicente-Santos et al., 2024). Environmental monitoring similarly involves complex samples, including water, soil, and air, teeming with a wide variety of microorganisms, making it difficult to pinpoint specific pathogens (Dupont et al., 2020). Additionally, fluctuations in environmental conditions, such as temperature, pH, and moisture, further affects pathogen viability, complicating detection efforts even more.

Traditional methods often struggle with accuracy, sensitivity, and specificity, which may result in delayed pathogen detection and control (Law et al., 2015; Hameed et al., 2018). The core aim of pathogen detection in food safety, public health, and environmental monitoring is to identify unique and consistent biomarkers from physiological signals that reliably distinguish between infectious and non-infectious material, even amidst biological noise. Additionally, distinguishing between pathogens in different physiological states (e.g., viable cells, viable but stressed cells, and non-viable cells) adds another layer of complexity (Paniel and Noguer 2019).

Standard culture-based methods exacerbate these challenges, requiring extensive biological sample preparation, high-quality labor, and can struggle with detecting non-viable cell DNA (Guo et al., 2021; Pinto et al., 2015). These limitations highlight the need for advanced techniques that minimize biological sample preparation requirements while enhancing data analysis to differentiate among various physiological states. Such techniques can improve the speed and performance of pathogen detection, offering more efficient solutions to address the stressors introduced by food safety, public health, and environmental monitoring.

Optical imaging using microscopy has shown considerable promise in enhancing rapid pathogen detection across these fields. The use of brightfield and darkfield with Gram staining, and fluorescence microscopy with biomarkers has been proven useful for capturing detailed images of pathogens (Kim et al., 2023; Borowa et al., 2021; He et al., 2018). Furthermore, multimodal imaging approaches, such as hyperspectral microscopy, enable direct observation of pathogens without the need for extensive biological sample preparation, while giving insights to spectrochemical information on sample constituents, intracellular components, and metabolic activity (Zhu et al., 2013; Gowen et al., 2015; Gao and Smith et al., 2016). This is particularly helpful in food safety where having rich hyperspectral information can help differentiate harmful pathogens from natural biological background noise and identifying pathogens of different physiological states (Seo et al., 2013; Park et al., 2023). The real-time capability of microscopy-based detection offers advantages in public health, where rapid detection is crucial during outbreaks and for diagnostics by expediting identification, allowing for quicker response times (Akbari et al., 2012; Akgönüllü and Denizli, 2022).

Incorporating artificial intelligence (AI) into these domains has proven useful for improving early detection of pathogens and disease (Pinto-Coelho, 2023). In the food safety

domain, various machine learning (ML) and deep learning classification models have been found to accelerate data analysis and detection of foodborne pathogens (Kang et al., 2021; Ma et al., 2023; Yi et al., 2023). The integration of medical imaging techniques with AI has also demonstrated the ability of extracting valuable insights and patterns that could not be readily discernable to the human eye (Pinto-Coelho, 2023). However, since AI techniques in these domains are relatively new, it is important to standardize methodologies and results reporting, establish clear benchmarks, and ensure fair comparisons with traditional methods.

Therefore, this systematic review aims to provide a comprehensive overview of the techniques and characteristics used in AI applications for imaging-based pathogen detection. By systematically evaluating these methodologies alongside comparisons with traditional pathogen detection approaches reported in the included literature, the review addresses a critical gap in the literature. The insights gained are expected to guide future research, promote the development of standardized protocols, and facilitate the creation of scalable and reliable systems for rapid pathogen detection. Ultimately, this work will enhance our response to emerging challenges in food safety, public health, and environmental monitoring.

2.3 Methods

This systematic review protocol was registered with the International Prospective Register of Systematic Reviews (PROSPERO) under the ID CRD42024547499. It was conducted following the guidelines outlined in the Preferred Reporting Items for Systematic Review and Meta-Analysis Protocols (PRISMA-P).

2.3.1 Research questions

This systematic review rigorously evaluated the application, efficacy, and technological advancements of AI in imaging-based pathogen detection by addressing the following research

questions (RQs):

RQ1. Which AI algorithms have been employed in imaging for pathogen classification?

RQ2. How do AI methods enhance the speed and accuracy of pathogen detection and classification compared to traditional methods?

RQ3. What are the latest advancements in integrating AI with multimodal imaging techniques for pathogen research?

RQ4. How does AI facilitate early detection of pathogens under stress conditions?

2.3.2 Eligibility criteria

Table 2.1 shows the summary of the inclusion and exclusion criteria of the study characteristics based on the PICOS framework (i.e., populations/participants, interventions and comparators, outcome(s) of interest, and study design/type) (Schardt et al., 2007). We included peer-reviewed papers or conference proceedings that focused on bacterial detection by applying AI techniques. Additionally, studies available in full-text and written in English from 2012 to 2024 were selected, with 2012 chosen as the starting point to mark the onset of deep learning's rapid evolution driven by GPU acceleration. (Shao et al., 2022). Studies were excluded if they focused on non-bacterial substrates; used electron microscopy or non-imaging methods without emphasis on morphology; relied on downloaded datasets; or examined only traditional detection methods without AI integration. Additionally, dissertations, theses, reviews, books or book chapters, conference abstracts without full text, editorials, news articles, posters, proposals, retracted publications, studies published outside the 2012–2024 timeframe, or non-English publications were also excluded.

Table 2.1 Inclusion and exclusion criteria guided by the PICOS framework (Schardt et al., 2007).

		Inclusion criteria	Exclusion criteria
P	Population	Studies focusing on bacteria or their physiological signals under stress conditions	Studies focusing on non-bacterial substrates
I	Intervention	Studies applying AI/ML techniques for bacterial detection using optical microscopy focusing on morphology based on original datasets	Studies using electron microscopy or non-imaging methods, not focusing on morphology, or using downloaded datasets
C	Comparison	Comparison of AI-enabled imaging with traditional methods	Studies focusing only on traditional detection methods without AI/ML integration
O	Outcome	Accuracy, speed, and/or predictive capabilities of AI/ML in bacterial detection	N/A
S	Study design	Original research articles from peer-reviewed journals or conference proceedings	Dissertations/theses, reviews, books/book chapters, conference abstracts without full text, editorials, news articles, posters, datasets, patents, proposals, or retracted publications
	Timeframe	2012–2024	Outside of 2012–2024
	Language	English	Non-English

AI: Artificial intelligence. ML: Machine learning. N/A: Not applicable.

2.3.3 Information sources and search strategy

A combination of key search terms was used across five electronic databases (PubMed, IEEE, Scopus, Web of Science, and ACM) to identify studies on AI applications in imaging-based pathogen detection. The searches were completed in May 2024. To build the search strategy, we first identified key terms and their potential synonyms to ensure comprehensive retrieval of relevant literature. The primary keywords and their alternative terms are as below:

- **Artificial intelligence**–machine learning, deep learning
- **Pathogen**–microbe, microorganism, microbial, microbiological, bacteria, bacterial
- **Detection**–diagnostics, classification, prediction, physiological signals, stress phenotype, resilience phenotype
- **Imaging**–image analysis, microscopy, microscope, hyperspectral, multispectral, multimodal

2.3.4 Study selection

All references were imported into the Zotero reference management software. These references were then imported into the Covidence systematic review software (Veritas Health Innovation), and duplicates were removed. Before the full screening of the studies, three reviewers (MeiLi Papa, Gillian Kuehnle, Jiyoon Yi) met to discuss the procedure for title and abstract screening using 10 randomly selected articles to ensure consistency between the reviewers.

2.3.5 Data collection process and data items

Data collection forms were developed based on the PRISMA-P guidelines (Shamseer et al., 2015). The data extraction form includes domains of 1) study characteristics (e.g., authors, year of publication, title, countries of study, study design), 2) pathogen characteristics (e.g.,

bacterial strains, bacterial sample types & origin, bacterial physiological states), 3) AI-enabled detection method characteristics (e.g., biological sample preparation, biological replicates, imaging sample type, imaging modality, imaging parameters–intensity/exposure time/gain, data size for model training/test, data preprocessing methods, AI analysis methods, model architectures, test dataset source), 4) comparator characteristics (e.g., conventional detection methods, additional sample preparation, target detection level–colony/single-cell/subcellular, detection limit), and 5) pathogen detection performances (e.g., evaluation metrics, detection limit, quantification capacity, overall testing time). Two reviewers (MeiLi Papa and Gillian Kuehnle) independently validated the extracted data.

2.3.6 Quality assessment and risk of bias

Selected studies were assessed by two independent reviewers (MeiLi Papa and Gillian Kuehnle) using a modified version of the Quality Assessment of Diagnostic Accuracy Studies 2 (QUADAS-2). This tool was originally designed for systematic reviews evaluating the diagnostic accuracy through four domains, i.e., patient recruitment, index test, reference standards, and flow and timing. We adapted these domains specifically for our review into: 1) pathogen selection, 2) index test (i.e., proposed AI-enabled detection methods), 3) reference standard (i.e., conventional detection methods), and 4) flow and timing. The evaluation was based on a total of 12 signaling questions (3 per domain) assessing risk of bias and applicability, as detailed in **Table 2.2.** Questions unrelated to our research context, such as those addressing responder rates or human participants selection, were excluded. Each study was classified into one of three categories, i.e., "high risk of bias" (<4 "yes" responses), "unclear" (4–8 "yes"), or "low risk of bias" (>8 "yes"). Any disagreements between the primary two reviewers (MeiLi Papa and Gillian Kuehnle) were to be resolved through discussion with a third reviewer (Jiyoon Yi).

Table 2.2 Risk of bias assessment domains and signaling questions used in this systematic review based on a modified QUADAS-2 tool (Whiting et al., 2011).

Domain	Signaling question (SQ)	
Pathogen selection	**SQ1.**	Were the bacterial strains diverse?
	SQ2.	Were the bacterial strains commonly available and easily replicable?
	SQ3.	Were the bacteria from a controlled source?
Index test	**SQ4.**	Were the index test (i.e., AI-enabled detection) results interpreted without the knowledge of the reference stanard?
	SQ5.	Was data preprocessing implemented dynamically wihin the code, rather than being hardcoded?
	SQ6.	Was the data split and final data size clearly explained?
Reference standard	**SQ7.**	Is the reference standard (i.e., conventional detection) likely to correctly classify bacterial samples?
	SQ8.	Were the reference standard results interpreted without the knowledge of the results of the index test?
	SQ9.	Did the reference standard use similar sample preparation methods and target the same cellular level as the index test?
Flow and timing	**SQ10.**	Were the bacterial samples in a consistent status before the index test and the reference standard test?
	SQ11.	Were all bacterial samples for test sets subjected to the reference standard?
	SQ12.	Was the overall testing time for the indext test faster or similar to that of the reference standard?

2.3.7 Synthesis of results

Due to variability in study methods and sample selection, the results were synthesized qualitatively rather than via meta-analysis. No assessment of publication bias was conducted due to this heterogeneity in data and methodologies.

2.4 Results

2.4.1 Study selection

Figure 2.1 shows the study selection process. The database search yielded 3,527 total references from which 791 duplicates were removed. In the first phase of screening, two reviewers (MeiLi Papa and Gillian Kuehnle) independently assessed all study titles and abstracts against the inclusion and exclusion criteria in **Table 2.1**. The agreement in the abstract and title screening between the two reviewers was 98.9%. A total of 2,736 abstracts were screened where 2,616 were deemed ineligible, leaving 120 papers to be read in full text. Then the two reviewers read the resulting studies in full length. The agreement for full text screening was 89.9%. Discrepancies at each stage of the screening process were resolved through discussion with a third reviewer (Jiyoon Yi). In total, 28 papers met the eligibility criteria and were included in this review.

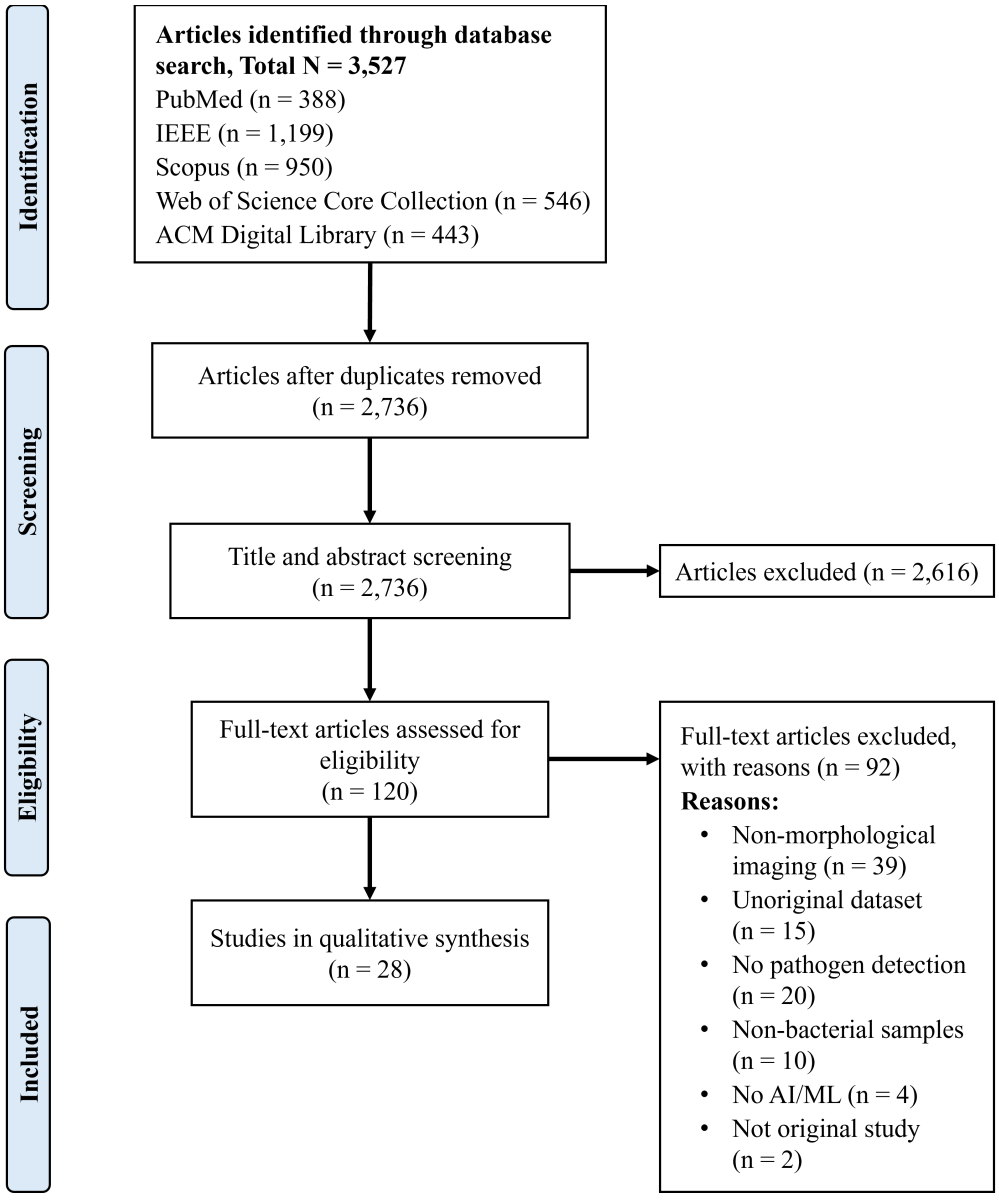

Figure 2.1 Flow diagram illustrating the article screening and selection process for this systematic review.

2.4.2 Main findings

2.4.2.1 Study and pathogen characteristics

The 28 included studies had been published between 2013 and 2024. **Table 2.3** provides detailed characteristics of each study. Of these, 10 were conducted in the United States and the remaining 18 were conducted in China, Italy, Poland, Thailand, Korea, Malaysia, Indonesia, Iran, United Kingdom, Portugal, Finland, Germany, and Japan. Most studies, 26 in total, focused on viable and culturable bacteria grown under optimal laboratory conditions. Only three studies examined bacteria under stress conditions, including predictive modeling of antibiotic susceptibility in *E. coli* (Ali et al., 2020), differentiation of live bacteria from dead ones (Park et al., 2023), and identification of active and inactivated states of *E. coli* following different levels of heat treatment (Wu et al., 2024). Additionally, 17 studies sourced bacterial cultures only from readily available laboratory strains, while the other 11 utilized real-world samples from clinical and environmental settings. Among these, 8 were clinical samples, and 3 included environmental samples (Ali et al., 2020; Borowa et al., 2021; Hoorali et al., 2020; Ibrahim et al., 2021; Kang et al., 2021; Rattray et al., 2023; Kim et al., 2023; Ma et al., 2023; Tao et al., 2023; Yi et al., 2023; Zhu et al., 2023).

The included studies encompass a total of 40 distinct species of bacteria and fungi across a variety of experimental designs. These include 14 species of gram-positive bacteria. A total of 22 gram-negative species were studied, including key foodborne pathogens like *Escherichia coli* (with various strains), *Salmonella* spp.*,* and *Pseudomonas aeruginosa.* Additionally, four other pathogens*, Candida albicans, Mycobacterium tuberculosis, Lactobacillus delbrueckii, and Burkholderia pseudomallei*, were also studied, rounding out the diversity of species investigated. These species are associated with applications in food safety, clinical diagnostics, and

environmental health.

Table 2.3 Summary of study and pathogen characteristics.

No.	1st author (year), country	Bacterial strains	Bacterial sample types & origin	Physiological states
1	Akbar (2021), Malaysia, Indonesia	*Burkholderia pseudomallei, Hemophilus influenzae, Klebsiella pneumoniae, Pseudomonas aeruginosa, Staphylococcus aureus, Streptococcus pneumoniae*	Laboratory strains (Parasitology Lab at University Malaysia Pahang)	Viable and culturable
2	Ali (2020), Germany	*E. coli* AG100 (derived from *E. coli* K12), *E. coli* strains (407, 416, 422, 455, 500, 544, 545, 554, 579, 673, 683)	Laboratory strain; clinical isolates (sepsis patients from Jena University Hospital)	Viable and culturable; antibiotic-treated
3	Borowa (2021), Poland	*Klebsiella pneumoniae*	Clinical isolates (respiratory tract, urine, wound swabs, blood, fecal samples, catheter JJ, and urethral swab)	Viable and culturable
4	Borowa (2023), Poland	*E. coli, Lactobacillus plantarum, Neisseria gonorrhoeae, Staphylococcus aureus*	Laboratory strains (ATCC)	Viable and culturable
5	Fong (2020), US	*Campylobacter jejuni, E. coli, Listeria innocua, Listeria monocytogenes, Salmonella* Typhimurium, *Staphylococcus aureus*	Food processing isolates	Viable and culturable
6	Gu (2020), China	*E. coli, Salmonella* spp., *Staphylococcus aureus*	Laboratory strains (Biological Lab of Animal Science School at Huazhong Agricultural University)	Viable and culturable
7	He (2018), China	*E. coli* MG1655, *Mycobacterium smegmatis* MC155, *Pseudomonas aeruginosa* PAO1	Laboratory strains	Viable and culturable
8	Hoorali (2020), Iran	*Bacillus anthracis*	Clinical samples (cutaneous anthrax disease patient tissues)	Non-viable
9	Ibrahim (2021), Turkey	*Mycobacterium tuberculosis*	Clinical samples (sputum smears from tuberculosis patients, Istanbul Tuberculosis Control Association)	Non-viable
10	Kang (2020a), US, China	*E. coli* serovars (O26, O45, O103, O111, O121, O145)	Laboratory strains (USDA FSIS culture collection)	Viable and culturable

Table 2.3 (cont'd)

No.	1st author (year), country	Bacterial strains	Bacterial sample types & origin	Physiological states
11	Kang (2020b), US, China	*Campylobacter fetus, E. coli, Listeria innocua, Salmonella* Typhimurium, *Staphylococcus aureus*	Laboratory strain (ATCC); Food isolates (chicken carcasses, USDA ARS PMSPRU)	Viable and culturable
12	Kang (2020c), US, China	*Campylobacter jejuni, E. coli, Listeria innocua, Salmonella* Typhimurium, *Staphylococcus aureus*	Laboratory strain (ATCC); food isolates (chicken rinsate, USDA ARS PMSPRU)	Viable and culturable
13	Kang (2021), US, China	*Campylobacter jejuni, E. coli, Listeria innocua, Salmonella* Typhimurium, *Staphylococcus aureus*	Laboratory strain (ATCC); food isolate (chicken carcass rinses, USDA ARS PMSPRU)	Viable and culturable
14	Kim (2023), South Korea	*Cutibacterium acnes, Staphylococcus aureus*, *Staphylococcus epidermidis*	Laboratory strains (ATCC); NR	Viable and culturable
15	Ma (2023), US	*E. coli* strains (LJH 1612, TVS 355, TVS 354, K-12, ATCC 35218, ATCC 11775)	Laboratory strains (ATCC); food, environmental, animal, and clinical isolates (fresh produce, irrigation water, soil); *E. coli*-spiked food sample (romaine lettuce)	Viable and culturable
16	Maeda (2018), Japan	*Pseudomonas aeruginosa, Staphylococcus aureus, Staphylococcus epidermidis, Staphylococcus haemolyticus, Staphylococcus saprophyticus, Staphylococcus simulans*	Laboratory strains (ATCC, NBRC)	Viable and culturable
17	Park (2023), US	*E. coli, Listeria innocua, Salmonella* Enteritidis, *Salmonella* Heidelberg, *Salmonella* Typhimurium, *Staphylococcus aureus*	Laboratory isolates (USDA ARS PMSPRU)	Viable and culturable; dead
18	Rattray (2023), US	*Pseudomonas aeruginosa*	Clinical and environmental isolates	Viable and culturable

Table 2.3 (cont'd)

No.	1st author (year), country	Bacterial strains	Bacterial sample types & origin	Physiological states
19	Seo (2013), US	*Acinetobacter baumannii, Aeromonas salmonicida, Citrobacter koseri, Enterobacter cloacae, E. coli, Klebsiella oxytoca, Pseudomonas putida, Salmonella* Enteritidis, *Salmonella* Typhimurium, *Staphylococcus aureus*	Laboratory strains (USDA ARS PMSPRU); *Salmonella*-spiked food samples (chicken carcass rinses)	Viable and culturable
20	Signoroni (2018), Italy	*E. coli*, *Enterococcus faecalis*, *Klebsiella pneumoniae*, *Proteus mirabilis*, *Proteus vulgaris*, *Pseudomonas aeruginosa*, *Staphylococcus aureus*, *Streptococcus agalactiae*	Laboratory strains (ATCC)	Viable and culturable
21	Spahn (2022), Germany, Portugal, UK, Finland	*Bacillus subtilis, E. coli, Staphylococcus aureus*	Laboratory strains	Viable and culturable
22	Tao (2023), China	*Acinetobacter baumannii, Burkholderia cepacian, Citrobacter afermentans, E. coli, Enterococcus faecalis, Enterococcus faecium, Klebsiella aerogenes, Klebsiella pneumoniae, Moraxella catarrhalis, Morganella morganii, Proteus mirabilis, Proteus vulgaris, Pseudomonas aeruginosa, Serratia marcescens, Staphylococcus aureus, Staphylococcus haemolyticus, Staphylococcus saprophyticus, Staphylococcus warneri, Stenotrophomonas maltophilia, Streptococcus anginosus, Streptococcus constellatus, Streptococcus salivarius* (62 strains)	Laboratory strains (ATCC); clinical isolates (urine, wound secretions, sputum, tissue fluid, articular cavity fluid, ascites, cerebrospinal fluid, purulence, lavage fluid, punctured fluid, drainage fluid, catheter, blood from the Second Affiliated Hospital of Air Force Military Medical University)	Viable and culturable
23	Treebupachatsakul (2019), Thailand	*Lactobacillus delbrueckii, Staphylococcus aureus*	Laboratory strains	Viable and culturable

Table 2.3 (cont'd)

No.	1st author (year), country	Bacterial strains	Bacterial sample types & origin	Physiological states
24	Treebupachatsakul (2020), Thailand	*Lactobacillus delbrueckii, Micrococcus* spp., *Staphylococcus aureus*	Laboratory strains	Viable and culturable
25	Turra (2017), Italy	*E. coli*, *Enterococcus faecalis*, *Klebsiella pneumoniae*, *Proteus mirabilis*, *Proteus vulgaris*, *Pseudomonas aeruginosa*, *Staphylococcus aureus*, *Streptococcus agalactiae*	Laboratory strains (ATCC)	Viable and culturable
26	Wu (2024), China	*E. coli* (EPEC O26: K60, EPEC, CICC 10372)	Laboratory (China General Microbiological Culture Collection Center)	Viable and culturable; heat-treated
27	Yi (2023), US	*Bacillus subtillis, E. coli* BL21, *Listeria innocua, Pseudomonas fluorescens*	Laboratory strains (ATCC); *E. coli*-spiked food and environmental samples (coconut water, spinach wash water, irrigation water)	Viable and culturable
28	Zhu (2023), China	*Bacillus subtilis, E. coli, Pseudomonas aeruginosa, Salmonella* spp., *Staphylococcus aureus*	Clinical isolates (urine, sputum, blood, tissue fluid)	Viable and culturable

ATCC: American Type Culture Collection. NBRC: National Institute of Biotechnological Resource Center, Japan. PMSPRU: Poultry Microbiological Safety and Processing Research Unit. USDA ARS: US Department of Agriculture Agricultural Research Service. USDA FSIS: US Department of Agriculture Food Safety and Inspection Service.

2.4.2.2 AI-enabled detection method characteristics

2.4.2.2.1 Biological sample preparation

Table 2.4 presents a comprehensive overview of the biological sample preparation methods used across the studies, highlighting key aspects such as sample growth time, temperature, treatment conditions prior to data collection. Incubation times varied significantly, reflecting differences in experimental design and pathogen type. While many studies used overnight incubation for sufficient bacterial growth, others extended incubation times to 24–72 h to accommodate slower-growing species or specialized treatments. Precise timings, such as 90 min, 3 h, 4 h, 20 h, 24 h, 48 h, or 72 h, were reported for targeted experimental conditions (Ali et al., 2020; Gu et sl., 2020; Ma et al., 2023; Rattray et al., 2023; Signoroni et al., 2018; Treebupachatsakul et al., 2019, 2020; Yi et al., 2023; Zhu et al., 2023). The studies that list a range (such as 24–48 h) suggest flexibility or adaptation to specific bacteria or experimental objectives (Kang et al., 2020b; Kang et al., 220c; Kang et al., 2021; Park et al., 2023; Seo et al., 2013; Tao et al., 2023; Wu et al., 2024).

Incubation temperatures for 17 studies were set at 37°C to provide the optimal growth temperature for selected bacteria or simulate human physiological conditions. Exceptions included 3 studies where lower temperatures (30°C and 35°C) were used to accommodate specific bacterial strains or environmental conditions (Seo et al., 2013; Treebuchatsakul et al., 2019, 2020). Some studies reported temperature ranges, such as 35–37°C, to allow flexibility in experimental setups (Tao et al., 2023), while the others did not specify temperatures.

Bacterial concentrations used for image collection also showed significant variation. Among the studies, only 7 that utilized pure laboratory cultures provided specific values, ranging from 10–10^8 CFU/mL, ensuring standardized cell densities for reproducibility (Ali et al., 2020;

Gu et al., 2020; Ma et al., 2023; Maeda et al., 2018; Seo et al., 2013; Yi et al., 2023; Zhu et al., 2023). However, the remaining 21 studies did not report these details of concentrations, but did provide other biological sample preparation details, highlighting a lack of standardization in reporting practices.

Imaging sample type—categorized as bacterial suspension, liquid, microcolony, colony, tissue, or sputum—also differed. Tissue or sputum samples, though less frequently used, provided insights into pathogen behavior in complex biological contexts. Bacterial suspension or liquid samples were most common due to their ease of handling, while microcolony or colony samples facilitated direct visualization of bacterial colony morphology. The volume of liquid sample applied to microscope slides ranges from 1 μL to 10 μL, providing insight into the varied preparations for microscopy or other imaging analyses. Smaller volumes (1–3 μL) suggest studies requiring only a minimal sample amount, likely for high-magnification imaging. While larger volumes (10 μL) may accommodate more extensive sample coverage for low-magnification observations. Several entries lack this information, pointing to a lack of consistency in reporting sample preparation.

Table 2.4 Summary of biological characteristics of AI-enabled detection methods.

No.	Reference	Incubation (temperature/time)	Bacterial concentration	Imaging sample type	Other chemical process	Biological replicates
1	Akbar (2021)	NR	NR	NR	Gram stain	NR
2	Ali (2020)	37°C/90 min	5×10^5 CFU/mL	Bacterial suspension (1 or 5 μL)	N/A	1–4
3	Borowa (2021)	NR	NR	NR	Gram stain	2
4	Borowa (2023)	37°C/overnight	NR	Colony suspension	Gram stain	2
5	Fong (2020)	NR	NR	NR	N/A	NR
6	Gu (2020)	37°C/20±2 h	10^2–10^4 CFU/mL	Colony	N/A	NR
7	He (2018)	NR/overnight	NR	Bacterial suspension (3 μL)	Fluorescence staining	NR
8	Hoorali (2020)	N/A	N/A	Tissue	Methanol fixation, Giemsa staining	200
9	Ibrahim (2021)	N/A	N/A	Sputum	Acid-fast staining	100
10	Kang (2020a)	NR	NR	Bacterial suspension (3 μL)	N/A	NR
11	Kang (2020b)	37°C/16–48 h	NR	Bacterial suspension (3 μL)	N/A	10
12	Kang (2020c)	37°C/24–48 h	NR	Bacterial suspension (3 μL)	N/A	NR
13	Kang (2021)	37°C/24–48 h	NR	Bacterial suspension (3 μL)	N/A	NR
14	Kim (2023)	37°C/overnight	NR	Bacterial suspension	Fluorescence staining	NR
15	Ma (2023)	37°C/3 h	10^4–10^7 CFU/mL	Microcolony	N/A	9
16	Maeda (2018)	37°C/overnight	3.2×10^5 cells/mL	Bacterial suspension (1 μL)	N/A	NR
17	Park (2023)	37°C/18–24 h 121°C/15 min (dead)	NR	Bacterial suspension (3 μL)	N/A	3
18	Rattray (2023)	37°C/72 h	NR	Colony	N/A	4
19	Seo (2013)	35°C/18–24 h	10–10^8 CFU/mL	Colony	N/A	5
20	Signoroni (2018)	NR/18 h	NR	Colony	N/A	NR

Table 2.4 (cont'd)

No.	Reference	Incubation (temperature/time)	Bacterial concentration	Imaging sample type	Other chemical process	Biological replicates
21	Spahn (2022)	37°C/overnight	NR	Bacterial suspension	Fluorescence staining	NR
22	Tao (2023)	35–37°C/24–48 h	NR	Bacterial suspension	N/A	NR
23	Treebupachatsakul (2019)	30 or 37°C/24 h	NR	NR	Gram staining	NR
24	Treebupachatsakul (2020)	30°C/24 h, 37°C/48 h	NR	NR	Gram staining	NR
25	Turra (2017)	NR/18 h	NR	Colony	N/A	NR
26	Wu (2024)	37°C/14–16 h	NR	Bacterial suspension (2.5 μL)	N/A	NR
27	Yi (2023)	37°C/4 h	$10–10^3$ CFU/mL	Bacterial suspension (100 μL), liquid	Phage infection, fluorescence staining	5
28	Zhu (2023)	NR/48 h	10^8/mL	Bacterial suspension (10 μL)	N/A	NR

CFU: Colony forming units. N/A: Not applicable. NR: Not reported.

2.4.2.2.2 Imaging modality and parameters

The types of imaging modalities used in these studies varied widely, detailed in **Table 2.5**, indicating an array of experimental goals and bacterial characteristics being investigated. Techniques include conventional microscopy methods with brightfield and darkfield illumination, as well as multimodal techniques like hyperspectral microscopy. Lens-less imaging was also used in some studies to capture wide-field bacterial visualization, demonstrating the versatility and adaptability of imaging techniques to suit specific research needs. Fluorescence microscopy, which leverages targeted staining to visualize bacterial structures with high specificity, was also used, highlighting its relevance in research requiring detailed, molecular-level insights (He et al., 2018). Hyperspectral microscopy, which captures spectral information at each pixel, was applied in several studies to analyze the biochemical composition and structural details of bacterial samples, offering richer spectral and spatial data than conventional microscopy which relies on limited channels with spatial information.

The equipment for these imaging modalities varied across studies, with commonly used microscopes such as the Nikon Eclipse series and Olympus BX series, cameras such as election-multiplying charge-coupled device (EMCCD) and complementary metal-oxide semiconductor (CMOS), each chosen to suit particular imaging conditions. For instance, the use of EMCCD cameras in fluorescence and darkfield microscopy is notable, as their high sensitivity allows for clearer imaging in low-light conditions, a crucial aspect for techniques that rely on capturing fine bacterial details. Custom-built imaging systems, such as a modified Nikon Ti2-U inverted microscope in Kim et al. (2023), were also featured, indicating efforts to tailor equipment for specific bacterial imaging purposes. Other studies used specialized hyperspectral cameras, such as the Specim Spectral Camera V10E, to enhance the spectral range and clarity in analyzing

bacterial morphology and chemical makeup (Signoroni 2018).

Illumination is another critical factor, with studies using varied light sources based on imaging type and bacteria being examined. Halogen lamps were used in 7 studies (Fong et al., 2020; Gu et al., 2020; Ma et al., 2023; Signoroni et al., 2018; Spahn et al., 2022; Tao et al., 2023; Turra et al., 2017). Metal halide was another common light source, particularly for hyperspectral microscopy due to their high-intensity output, with 6 studies reporting using it (Kang et al., 2020a; Kang et al., 2020b; Kang et al., 2020c; Kang et al., 2021; Park et al., 2023; Wu et al., 2024). Lastly, LED light source was reported twice (Maeda et al., 2018; Zhu et al., 2023) and lasers were reported twice (He et al., 2018; Spahn et al., 2022). In fluorescence microscopy studies, specific light sources are often required to match the fluorescence range, though exact details on equipment were not provided in Kim et al. (2023) and Yi et al. (2023).

Magnification levels in the 17 studies that reported it differed based on the study goals. Studies focusing on single cell classification used 100′ oil-immersion objectives for high-detail bacterial observations, especially in darkfield imaging, where capturing micron-scale structural details is essential (Borowa et al., 2023; He et al., 2018; Kang et al., 2020a, 2020b, 2020c, 2021; Park et al., 2023; Spahn et al., 2022; Tao et al., 2023; Treebupachatsakul et al., 2019, 2020; Wu et al., 2024). Contrastingly, Rattray et al. (2023) used a lower magnification of 4′ for colony level imaging to reveal morphological differences.

Imaging parameters, such as exposure time and gain, though not consistently reported, were detailed in 9 studies (Gu et al., 2020; He et al., 2018; Kang et al., 2020a, 2020b, 2020c, 2021; Maeda et al., 2018; Park et al., 2023; Wu et al., 2024). Exposure times of 250 ms and shorter durations, such as 56 ms, were mentioned, which likely reflect efforts to balance image clarity with minimizing motion blur in capturing bacteria under low-light conditions. Gain

settings, recorded in Kang et al. (2020b) and Park et al. (2023) were as low as 1.6% or 16 dB, and as high as 3.5% in Kang et al. (2020c) and Kang et al. (2021).

Table 2.5 Summary of imaging characteristics of AI-enabled detection methods.

No.	Reference	Modality	Equipment	Illumination	Light source	Objective	Gain/ exposure
1	Akbar (2021)	Optical microscopy	Olympus BX40 microscope	Brightfield	NR	NR	NR
2	Ali (2020)	Optical microscopy	Axiobserver.Z1 microscope, scientific CMOS camera	Brightfield	NR	63×	NR
3	Borowa (2021)	Optical microscopy	Olympus XC31 upright microscope, CMOS camera	Brightfield	NR	NR	NR
4	Borowa (2023)	Optical microscopy	Olympus BX63 microscope, CCD camera	Brightfield	NR	100× oil	NR
5	Fong (2020)	Hyperspectral microscopy	Olympus BX43 microscope, HinaLea 4200M camera	Darkfield	Tungsten halogen	NR	NR
6	Gu (2020)	Hyperspectral imaging (non-microscopic)	Specim V10E-CL camera	Reflected	Halogen	N/A	NR/100 ms
7	He (2018)	SIM	Nikon N-SIM microscope, EMCCD camera	Fluorescence (laser-based, SIM)	Laser (488 nm)	100× oil, TIRF	100×/50–100 ms
8	Hoorali (2020)	Optical microscopy	Olympus microscope, camera	Brightfield	NR	NR	NR
9	Ibrahim (2021)	Optical microscopy	NR	Brightfield	NR	NR	NR
10	Kang (2020a)	Hyperspectral microscopy	Nikon Eclipse e80i upright microscope, EMCCD camera, AOTF spectrometer	Darkfield	Metal halide	100× oil	3.5%/250 ms
11	Kang (2020b)	Hyperspectral microscopy	Nikon Eclipse e80i microscope, EMCCD camera, AOTF spectrometer	Darkfield	Metal halide	100× oil	1.6%/250 ms

Table 2.5 (cont'd)

No.	Reference	Modality	Equipment	Illumination	Light source	Objective	Gain/ exposure
12	Kang (2020c)	Hyperspectral microscopy	Nikon Eclipse 80i microscope, EMCCD camera, AOTF spectrometer	Darkfield	Metal halide	100× oil	3.5%/250 ms
13	Kang (2021)	Hyperspectral microscopy	Nikon Eclipse 80i microscope, EMCCD camera, AOTF spectrometer	Darkfield	Metal halide	100× oil	3.5%/250 ms
14	Kim (2023)	Super-resolution fluorescence microscopy	Custom-built Nikon Ti2-U inverted microscope	Fluorescence	NR	NR	NR
15	Ma (2023)	Phase contrast microscopy	Olympus X71 inverted microscope, CCD camera	Phase contrast	Halogen	60× Ph	NR
16	Maeda (2018)	Lensless imaging	CMOS sensor	Transmitted	Blue LED	N/A	NR/56 ms
17	Park (2023)	Hyperspectral microscopy	Nikon Eclipse 80i microscope, EMCCD camera, AOTF spectrometer	Darkfield	Metal halide	100× oil	15 dB/250 ms
18	Rattray (2023)	Optical microscopy	Nikon Eclipse Ti inverted microscope, CCD camera	Brightfield	NR	4×	NR
19	Seo (2013)	Hyperspectral imaging (non-microscopic)	Custom VNIR hyperspectral imaging system	NR	NR	N/A	NR
20	Signoroni (2018)	Hyperspectral imaging (non-microscopic)	Specim V10E camera	Reflected	Halogen	N/A	NR

Table 2.5 (cont'd)

No.	Reference	Modality	Equipment	Illumination	Light source	Objective	Gain/ exposure
21	Spahn (2022)	Optical or fluorescence microscopy, SIM	Nikon Eclipse Ti inverted microscope, Deltavision OMX system, Leica SP8, Nikon Ti-E, EMCCD or scientific CMOS camera	Brightfield, fluorescence (laser-based)	Halogen, lasers (488, 561 nm)	60–100× oil, TIRF	NR
22	Tao (2023)	Hyperspectral microscopy	Olympus BX43 microscope, Basler hyperspectral sensor	Transmitted	Halogen	100× oil	NR
23	Treebupachatsakul (2019)	Optical microscopy	Optika B-292 microscope, CMOS sensor	Brightfield	NR	100× oil	NR
24	Treebupachatsakul (2020)	Optical microscopy	Optika B-292 microscope or Olympus CX31 upright microscope, CMOS sensor	Brightfield	NR	100× oil	NR
25	Turra (2017)	Hyperspectral imaging (non-microscopic)	Specim V10E camera	Reflected	Halogen	N/A	NR
26	Wu (2024)	Hyperspectral microscopy	Nikon Eclipse 100i upright microscope, EMCCD camera, SOC-70 spectrometer	NR	Metal halide	100× oil	NR/99 ms
27	Yi (2023)	Fluorescence microscopy	Olympus IX-71 inverted microscope, CCD camera	Fluorescence	NR	100×	NR
28	Zhu (2023)	Hyperspectral microscopy	Custom hyperspectral microscope imaging system	Transmitted	White LED	40×	NR

AOTF: Acousto-optic tunable filter. CCD: Charge-coupled device. CMOS: Complementary metal-oxide-semiconductor. EMCCD: Electron-multiplying CCD. LED: Light-emitting diode. N/A: Not applicable. NR: Not reported. SIM: Structured illumination microscope. TRIF: Total internal reflection fluorescence. VNIR: Visible and near-infrared.

2.4.2.2.3 Data preprocessing and AI analysis details

Preprocessing techniques varied to address tasks such as data quality control, region of interest (ROI) segmentation, and feature extraction, as summarized in **Table 2.6**. Baseline steps included resizing images to align with deep learning input requirements, along with normalization or standardization to adjust feature scales, reduce bias, and ensure consistent contributions during model training. Other common techniques, such as Savitzky-Golay smoothing for noise reduction and standard normal variate (SNV) for scatter correction, were applied to ensure data consistentcy (Fong et al., 2020; Kang et al., 2020a, 2020b, 2020c, 2021; Park et al., 2023; Seo et al., 2023; Signoroni et al., 2018; Turra et al., 2017; Wu et al., 2024).

To expand biological datasets and focus on individual cells or cellular features, 5 studies divided images into smaller patches (Ali et al., 2020; Borowa et al., 2021, 2023; Hoorali et al., 2020; Spahn et al., 2022), while16 studies utilized ROI segmentation with various techniques (e.g., manual selection, thresholding, watershed, *k*-means clustering, or U-Net) (Fong et al., 2020; Gu et al., 2020; He et al., 2018; Kang et al., 2020a, 2020b, 2020c, 2021; Maeda et al., 2018; Park et al., 2023; Seo et al., 2013; Signoroni et al., 2018; Spahn et al., 2022; Tao et al., 2023; Turra et al., 2017; Wu et al., 2024; Zhu et al., 2013). Additionally, standard image augmentation techniques (e.g., rotation, flipping, scaling, shifting, cropping, shearing, zooming, and adjustments to color, brightness, or contrast) were also applied in 11 studies to increase dataset size and improve model training (Akbar et al., 2021; Borowa et al., 2021, 2023; Hoorali et al., 2020; Ibrahim et al., 2021; Kang et al., 2020b; Ma et al., 2023; Rattray et al., 2023; Spahn et al., 2022; Wu et al., 2024; Yi et al., 2023).

The included studies employed a wide variety of AI model architectures, reflecting the breadth of approaches (**Table 2.6**). Principal component analysis (PCA) was utilized for

dimensionality reduction, often followed by ML classifiers in 12 studies. Traditional ML classifiers such as *k*-nearest neighbors (*k*-NN), support vector machine (SVM), or random forest (RF) were frequently used, either as primary models or as comparative benchmarks in 15 studies. Deep learning approaches, including convolutional neural networks (CNNs) and recurrent neural networks (RNNs), were employed in 23 studies. Common CNN architectures included U-Net for ROI segmentation (e.g., single-cell, colony), as well as historically state-of-the-art models for image classification (e.g., AlexNet, VGG, ResNet, Xception, MobileNet, DenseNet, EfficientNet) for classifying whole images, patches, or ROIs. Additionally, object detection models (e.g., YOLO and R-CNN series) were applied, facilitating bacterial enumeration in addition to detection and identification (Ma et al., 2023; Yi et al., 2023). RNN architectures like long short-term memory (LSTM) networks (Fong et al., 2020; Kang et al., 2020c; Kang et al., 2021; Wu et al., 2024) as well as multiple instance learning (MIL) frameworks (Borowa et al., 2021, 2023) were also applied to analyze pathogen data.

Several studies employed various validation approaches to ensure model robustness and generalizability. The most common method was hold-out validation, where datasets were initially divided into training and test sets using standard split (i.e., 70/30, 80/20, 85/15), and then further partitioned to include an additional hold-out validation set to prevent overfitting during training (Hoorali et al, 2020; Kang et al., 2020a, 2020b, 2020c, 2021; Ma et al., 2023; Park et al., 2023; Rattray et al., 2023; Yi et al., 2023). Other studies used shuffle-and-split cross-validation (i.e., repeated hold-out validation) (Signoroni et al., 2018; Turra et al., 2017). For simpler statistical or traditional ML models, leave-one-replicate-out cross-validation (i.e., full cross-validation) (Ali et al., 2020; Gu et al., 2020; Maeda et al., 2018) or *k*-fold cross-validation (He et al., 2018) was used. Although unusual due to its computational cost, some studies applied

k-fold cross-validation to CNNs models (Borowa et al., 2021; Ibrahim et al., 2021). Notably, one study utilized a fully independent, unseen test set originating from distinct sources to assess model performance against more realistic samples (Yi et al., 2023). However, some studies either did not explicitly mention the use of an unseen test set beyond cross-validation or lacked a separate validation step altogether (Akbar et al., 201; Borowa et al., 2021; He et al., 2018; Maeda et al., 2018; Signoroni et al., 2018; Treebupachatsakul et al., 2019, 2020; Turra et al., 2017; Wu et al., 2024). The variability in validation approaches reflects the adaptability AI-based models to different study designs, data sizes, and pathogen types, highlighting the flexibility of AI-enabled imaging in pathogen classification workflows.

Table 2.6 Summary of data and AI analysis characteristics of AI-enabled detection methods.

No.	Reference	Data type	Data size (train/test)	Preprocessing	AI analysis method	Models
1	Akbar (2021)	Image	31490/13495	Resizing, augmentation	Classification	Proposed: CNN (DensNet-201); Others: CNN (ResNet-18, VGG-19)
2	Ali (2020)	Patch	NR	Resizing, CLAHE, ROI segmentation (U-Net), patching	Segmentation, classification	CNN (U-Net) PCA-ML (OCSVM)
3	Borowa (2021)	Patch	NR	Resizing, patching, filtering, normalization, augmentation	Classification	CNN (ResNet-18) with MIL framework
4	Borowa (2023)	Patch	47149 total	Resizing, patching, filtering, normalization, augmentation	Classification	CNN (ResNet-18) with MIL framework
5	Fong (2020)	ROI	NR/100	ROI segmentation (*k*-means, SAM), grayscale conversion, normalization, thresholding, morphological descriptor extraction, SNV	Classification	Proposed: Multimodal network with RNN (LSTM) & CNN (1D-CNN, ResNet); Others: PCA-ML (SVM, RF, *k*-NN)
6	Gu (2020)	ROI	916/2210	Resizing, ROI segmentation (thresholding), filtering, multiplicative scatter correction, wavelength selection	Classification	Statistical (PLS-DA), ML (SVM)
7	He (2018)	ROI	2932 total	ROI segmentation (watershed), resizing	Classification	PCA-ML (SVM, RF, *k*-NN)
8	Hoorali (2020)	Patch	1021/281	Patching, standardization, augmentation	Segmentation	CNN (UNet, UNet ++)
9	Ibrahim (2021)	Image	124/54, 371/157, 367/159	Resizing, augmentation	Classification	CNN (AlexNet)

Table 2.6 (cont'd)

No.	Reference	Data type	Data size (train/test)	Preprocessing	AI analysis method	Models
10	Kang (2020a)	ROI	Ranging from 500/100 to 50000/10000	ROI segmentation (thresholding), SNV, wavelength selection	Classification	PCA-statistical (LDA, SR), PCA-ML (SVM), ANN (SAE)-statistical (LDA, SR), ANN (SAE)-ML (SVM)
11	Kang (2020b)	ROI	200/100	Resizing, augmentation, ROI segmentation (U-Net), SNV	Segmentation, classification	Proposed: CNN (U-Net & 1D-CNN); Others: PCA-ML (SVM, *k*-NN)
12	Kang (2020c)	ROI	4500/500	ROI segmentation (manual single-cell selection), normalization, morphological descriptor extraction, SNV	Classification	Proposed: Multimodal network with RNN (LSTM) & CNN (ResNet, 1D-CNN); Others: PCA-ML (SVM, RF, *k*-NN)
13	Kang (2021)	ROI	900/100	ROI segmentation (thresholding), SNV, normalization, outlier detection	Classification	Proposed: RNN (LSTM); Others: PCA-ML (LDA, SVM, *k*-NN)
14	Kim (2023)	Image	NR/253, NR/114	NR	Classification	CNN (ResNet-18, RegNetY-16GF, EfficientNet-V2-S, SwinV2-S, SwinV2-T)
15	Ma (2023)	Image	1764/756	Resizing, bounding box annotation, augmentation	Object detection	CNN (YOLOv4)
16	Maeda (2018)	ROI	NR/125	Contrast enhancement, color inversion, ROI segmentation (Otsu thresholding), discriminative parameter extraction	Classification	Statistical (LDA), ML (SVM, RF, *k*-NN, naïve Bayes), ANN
17	Park (2023)	ROI	1083/191	ROI segmentation (U-Net), morphological descriptor extraction, SNV	Classification	Multimodal CNN (1D-CNN & ResNet)

Table 2.6 (cont'd)

No.	Reference	Data type	Data size (train/test)	Preprocessing	AI analysis method	Models
18	Rattray (2023)	Image	266/69	Resizing, normalization, morphological descriptor extraction, augmentation	Classification	Proposed: CNN (ResNet-50, VGG-19, MobileNetV2, Xception) Other: ML (SVM)
19	Seo (2013)	ROI	NR	Savitzky-Golay smoothing, ROI segmentation (manual colony selection)	Classification	Statistical (LDA, QDA, Mahalanobis distance), PCA-statistical, ML (SVM, *k*-NN), PCA-ML
20	Signoroni (2018)	ROI	11649/4993	Flat-field correction, Savitzky-Golay smoothing, ROI segmentation (watershed)	Classification	Proposed: 1D-CNN; Others: PCA-ML (SVM, RF)
21	Spahn (2022)	Patch or ROI	Small-to-moderate (e.g., 28/5, 94/5)	Resizing, patching, contrast enhancement, augmentation, ROI segmentation (manual selection, thresholding, U-Net)	Segmentation, object detection, denoising, digital labeling, super-resolution image prediction	CNN (U-Net, U-Net variants, YOLOv2), GAN (Pix2pix)
22	Tao (2023)	ROI	119000/51000, 630/1470	Manual single-cell cropping, flat-field correction, ROI segmentation (*k*-means), normalization	Classification	Proposed: Multimodal CNN; Others: CNN (1D-CNN, ResNet, DenseNet, multimodal network)
23	Treebupachatsakul (2019)	Image	320/80	NR	Classification	CNN (LeNet)
24	Treebupachatsakul (2020)	Image	160/40	NR	Classification	CNN (LeNet)

Table 2.6 (cont'd)

No.	Reference	Data type	Data size (train/test)	Preprocessing	AI analysis method	Models
25	Turra (2017)	ROI	11649/4993	Flat-field correction, Savitzky-Golay smoothing, ROI segmentation (watershed)	Classification	Proposed: 1D-CNN; Others: PCA-ML (SVM, RF)
26	Wu (2024)	ROI	1050/450	Contrast enhancement, ROI segmentation (edge detection, morphological filtering), Savitzky-Golay smoothing, normalization, augmentation	Classification	PCA-statistical (DA), PCA-ML (SVM, RF, *k*-NN), PCA-RNN (LSTM)
27	Yi (2023)	Image	342/114–164	Resizing, normalization, keypoint annotation, augmentation	Object detection	CNN (Faster R-CNN)
28	Zhu (2023)	ROI	NR	ROI segmentation (edge detection, morphological filtering), normalization	Classification	PCA-ML (SVM)

ANN: Artificial neural network. CLAHE: Contrast limited adaptive histogram equalization algorithm (contrast enhancement). CNN: Convolutional neural network. DA: Discriminant Analysis. GAN: Generative adversarial network. *k*-NN: *k*-nearest neighbors. LDA: Linear discriminant analysis. LSTM: Long short-term memory. MIL: Multiple instance learning. ML: Machine learning (traditional). NR: Not reported. OCSVM: Once-class SVM. PCA: Principal component analysis. PLS-DA: Partial least squares discriminant analysis. QDA: Quadratic discriminant analysis. RF: random forest. RNN: Recurrent neural network. ROI: Region of interest. SAE: Stacked autoencoder. SAM: Spectral angle mapping. SNV: Standard normal variate. SR: Softmax regression. SVM: Support vector machine.

2.4.2.3 Comparator characteristics

In this systematic review, the comparator was defined as conventional detection methods that did not involve AI algorithms for pathogen classification. **Table 2.7** provides details on the comparators used in each study, if applicable. Out of the 28 reviewed papers, only 7 reported the use of a comparator as a control for evaluating the AI-enabled detection methods. Of these, 6 studies used traditional plating techniques to initially identify bacteria before applying ML algorithms (Turra et al., 2017; Gu et al., 2020; Spahn et al., 2022; Borowa et al., 2023; Ma et al., 2023; Yi et al., 2023). Additionally, Yi et al. (2023) also utilized real-time quantitative polymerase chain reaction (RT-qPCR) methods. In one study, a team of microbiologists analyzed the same dataset used for model training and testing, serving as the comparator (Ibrahim et al., 2021).

2.4.2.4 Pathogen detection performance

Across the reviewed studies, there was a lot of variability in reporting pathogen detection performance. **Table 2.8** shows the most common evaluation metrics used in AI model evaluation, including classification accuracy, sensitivity, specificity, and area under the curve (AUC) values. In AI/ML benchmarking, a threshold of 70% is generally considered acceptable across these metrics. Values above 90% are typically regarded as excellent but optimal values vary by applications. However, extremely high accuracy or AUC close to 1 may indicate overfitting, particularly in studies using small or highly controlled datasets where the model may fail to generalize to real-world data.

Classification accuracy is the ratio of correctly predicted instances (i.e., true positive and true negative) to the total number of instances (i.e., all possible classifications). It is calculated as follows:

$$\text{Accuracy} = \frac{\text{TP} + \text{TN}}{\text{TP} + \text{TN} + \text{FP} + \text{FN}} \times 100 \quad (2.1)$$

where TP is true positive, TN is true negative, FP is false positive, and FN is false negative. Reporting an accuracy alone can be misleading, especially in imbalanced datasets where one class dominates. This metric ranged broadly from as low as 56.3% with a sample size of 620 in some cases (Borowa et al., 2021) to as high as 100% (Maeda et al., 2018; Park et al., 2023; Seo et al., 2013; Yi et al., 2023) Most studies consistently reported classification accuracy above 70%, demonstrating the potential of AI in imaging-based pathogen detection despite differences in approach. Studies achieving 100% accuracy were often conducted in controlled laboratory environments, where overfitting is a likely concern. However, none of the studies explicitly discussed the potential implications of overfitting in their analyses. Studies with lower accuracies tended to involve more complex, real-world datasets or broader classification challenges.

Fewer studies reported sensitivity (i.e., true positive rate or recall) and specificity (i.e., true negative rate) metrics. Sensitivity measures how well the model identifies actual positives as follows:

$$\text{Sensitivity} = \frac{\text{TP}}{\text{TP} + \text{FN}} \times 100 \quad (2.2)$$

In the studies reviewed, sensitivity values ranged from as low as 36% in Spahn et al. (2022) to 100% in Ma et al. (2023), Maeda et al. (2018) and Spahn et al. (2022). Specificity, on the other hand, measures how well the model identifies actual negatives as follows:

$$\text{Specificity} = \frac{\text{TN}}{\text{TN} + \text{FP}} \times 100 \quad (2.3)$$

Specificity values in the studies ranged from 80% (Hoorali et al., 2020) to 100% (Ibrahim et al., 2021; Maeda et al., 2018). These metrics highlight the variability in the performance of AI

models depending on dataset composition and the complexity of pathogen detection tasks. The pathogen detection task type, which often involves distinguishing between infected and non-infected samples, was commonly associated with these metrics.

AUC value reflects the balance between sensitivity and specificity, providing an overall picture of model performance. It is derived from the receiver operating characteristic (ROC) curve, which plots the true positive rate (i.e., sensitivity) against the false positive rate (e.g., 1–specificity) across different classification thresholds. AUC values range from 0 and 1, with values closer to 1 indicating better discrimination between positive and negative cases. AUC values in the included studies ranged from 68.3% (Borowa et al., 2021) to 100% (Kang et al., 2020c; Zhu et al., 2023). These metrics are crucial for evaluating the discriminatory power of AI models in distinguishing between classes. However, they remain unreported in 22 studies, indicating a gap in comprehensive performance assessment.

Table 2.7 Summary of comparators characteristics.

No.	Reference	Conventional methods	Sample preparation	Target detection level	Detection limit
1	Akbar (2021)	NR	NR	NR	NR
2	Ali (2020)	NR	NR	NR	NR
3	Borowa (2021)	NR	NR	NR	NR
4	Borowa (2023)	NR	NR	NR	NR
5	Fong (2020)	NR	NR	NR	NR
6	Gu (2020)	NR	NR	NR	NR
7	He (2018)	NR	NR	NR	NR
8	Hoorali (2020)	NR	NR	NR	NR
9	Ibrahim (2021)	Expert labeling	Same as index	N/A	N/A
10	Kang (2020a)	NR	NR	NR	NR
11	Kang (2020b)	NR	NR	NR	NR
12	Kang (2020c)	NR	NR	NR	NR
13	Kang (2021)	NR	NR	NR	NR
14	Kim (2023)	NR	NR	NR	NR
15	Ma (2023)	Plating	Same as index	Colony	NR
16	Maeda (2018)	NR	NR	NR	NR
17	Park (2023)	NR	NR	NR	NR
18	Rattray (2023)	NR	NR	NR	NR
19	Seo (2013)	NR	NR	NR	NR
20	Signoroni (2018)	NR	NR	NR	NR
21	Spahn (2022)	NR	NR	NR	NR
22	Tao (2023)	NR	NR	NR	NR
23	Treebupachatsakul (2019)	NR	NR	NR	NR
24	Treebupachatsakul (2020)	NR	NR	NR	NR
25	Turra (2017)	NR	NR	NR	NR
26	Wu (2024)	NR	NR	NR	NR
27	Yi (2023)	Plating, qPCR	Same as index	Colony	10^3 CFU/mL
28	Zhu (2023)	NR	NR	NR	NR

N/A: Not applicable. NR: Not reported. qPCR: Quantitative polymerase chain reaction.

Table 2.8 Summary of pathogen detection performance of AI-enabled detection methods.

No.	Reference	Accuracy (%)	Sensitivity (%)	Specificity (%)	AUC (%)	Other metrics
1	Akbar (2021)	99.24	99.20	99.87	NR	FPR
2	Ali (2020)	NR	41.07–91.6	NR	72–83	N/A
3	Borowa (2021)	56.3–64.8	56.3–64.8	NR	68.3–78.6	Precision, F1 score
4	Borowa (2023)	60.3–96.0	NR	NR	69.8–98.7	N/A
5	Fong (2020)	91.0–98.4	NR	NR	NR	N/A
6	Gu (2020)	NR	NR	NR	NR	Confusion matrix only
7	He (2018)	96.83–98.36	NR	NR	NR	F1 score
8	Hoorali (2020)	81–97	84–98	80–97	NR	Precision, DSC
9	Ibrahim (2021)	98.09–98.73	96.77–99.20	97.67–100	NR	N/A
10	Kang (2020a)	75.3–94.9	75–95	NR	NR	Precision, F1 score
11	Kang (2020b)	90	NR	NR	NR	N/A
12	Kang (2020c)	91.0–98.4	NR	NR	99–100	N/A
13	Kang (2021)	90.4–92.9	NR	NR	NR	N/A
14	Kim (2023)	79.8–97.9	NR	NR	NR	N/A
15	Ma (2023)	NR	87.4–100	NR	NR	IoU, Precision, AP, mAP
16	Maeda (2018)	74.4–100.0	64.0–100.0	86.0–100.0	NR	PPV
17	Park (2023)	64.13–100	NR	NR	NR	N/A
18	Rattray (2023)	62.75–90.73	NR	NR	NR	N/A
19	Seo (2013)	80.5–100	NR	NR	NR	Kappa coefficient
20	Signoroni (2018)	99.7	NR	NR	NR	N/A
21	Spahn (2022)	NR	36–100	NR	NR	IoU, Precision, mAP, SSIM, PSNR
22	Tao (2023)	92	NR	NR	99.09–99.97	Kappa coefficient
23	Treebupachatsakul (2019)	NR	NR	NR	NR	Train accuracy only
24	Treebupachatsakul (2020)	NR	NR	NR	NR	Train accuracy only
25	Turra (2017)	99.7	NR	NR	NR	N/A
26	Wu (2024)	65.56–98.22	NR	NR	NR	N/A
27	Yi (2023)	80–100	NR	NR	NR	N/A
28	Zhu (2023)	93.6	93.6	98.4	97–100	Precision

AP: Average precision. DSC: Dice similarity coefficient. FPR: False positive ratio. IoU: Intersection of union.

Table 2.8 (cont'd)

mAP: Mean average precision. N/A: Not applicable. NR: Not reported. PPV: Positive predictive value. PSNR: Peak-signal-to-noise ratio. SSIM: Structural similarity.

2.4.3 Risk of bias assessment

The results of the risk of bias assessment, based on the modified QUADAS-2 approached described in **Section 2.3.6**, are summarized in **Figure 2.2**. As detailed in **Section 2.3.6,** studies were assessed using 12 signaling questions across four domains: pathogen selection, index test (i.e., proposed AI-enabled detection methods), reference standard (i.e., conventional detection methods), and flow and timing (**Table 2.2**). Each study was categorized using a three-tier rating system according to the number of "yes" response to these questions, emphasizing methodological transparency, replicability, and comparative analysis. Among the studies, 11 were rated as "high risk of bias", 2 as "low risk of bias", and 15 as "unclear". Studies frequently demonstrated limited reporting on bacterial strain accessibility, dynamic data-driven preprocessing, or clear reference standards, highlighting areas critical for replicability and comparability in benchmarking. Overall, these findings underscore the promising yet evolving nature of AI-enabled pathogen detection research.

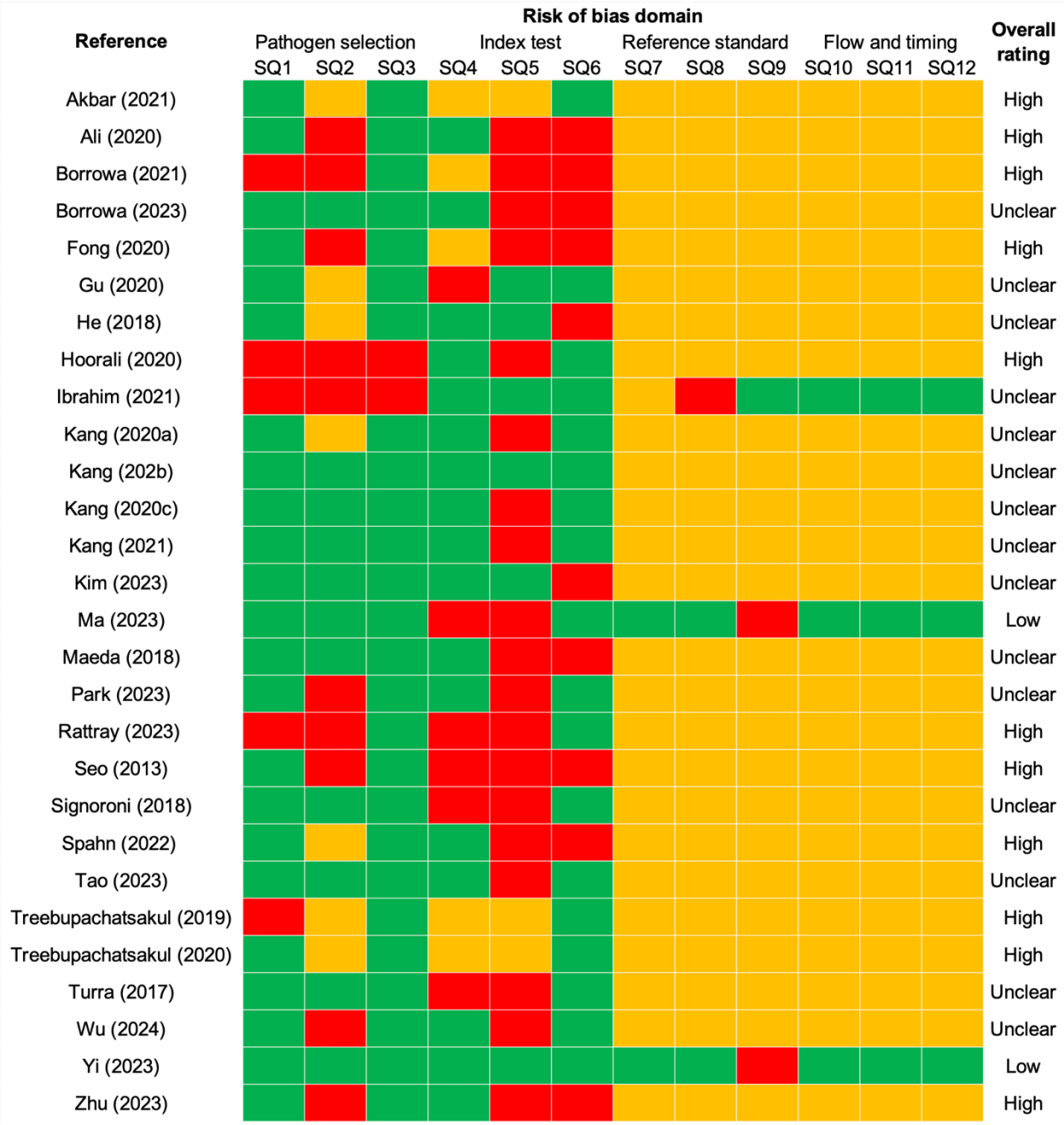

Figure 2.2 Summary of risk of bias assessments for the 28 included studies using the modified QUADAS-2 criteria with 12 signaling questions detailed in **Table 2.2**. Ratings: green (yes), yellow (unclear), and red (no). Studies were rated as "high" (<4 yes), "low" (>8 yes), or "unclear" (4–8 yes) risk of bias.

2.5 Discussion

In this systematic review, we revisited four key research questions: (1) identifying AI algorithms employed in imaging for pathogen classification, (2) evaluating how AI enhances the speed and accuracy of pathogen detection compared to traditional methods, (3) highlighting the recent advancements in the integration of AI with multimodal imaging for pathogen research, and (4) exploring how AI techniques facilitate early detection of pathogens under stress conditions.

2.5.1 There is no one-size-fits-all algorithm for AI-enabled pathogen classification

The reviewed studies demonstrated that diverse AI models, from traditional ML to advanced CNNs, have successfully achieved advanced pathogen classification performance by capturing spatial, spectral, and contextual features (**Table 2.8**. However, the effectiveness of these models is highly context-dependent, with no single model architecture consistently superior across all scenarios. Data preprocessing techniques were frequently used to improve data quality and extract relevant features and align with input requirements of the state-of-the-art model architectures (**Table 2.6**). Similar to the selection of AI model architectures, studies utilized diverse combinations of preprocessing techniques, further highlighting the context-dependent nature of AI-enabled pathogen detection. In particular, multimodal imaging produces high-dimensional and heterogeneous datasets characterized by distinct modalities, scales, and feature representations, making thorough and tailored preprocessing critical (Cozzolino et al., 2023; Fong et al., 2020; Kang et al., 2020c; Park et al., 2023; Tao et al., 2023). Consequently, effective pathogen classification relies heavily on context-specific optimization of preprocessing methods and AI model architectures.

Despite these advancements, this review identifies critical gaps arising from the multidisciplinary nature of research, where standardization and improvements could further enhance generalization and meta-analysis. Establishing consistent experimental protocols, including bacterial incubation conditions and concentrations, imaging settings, and data size, would significantly improve reproducibility and enable meaningful comparisons across studies. Moreover, while early studies predominantly emphasized achieving high accuracy, greater attention should be devoted to the entire data pipeline. Specifically, future research should carefully address overfitting and generalization by adopting validation methods, such as hold-out validation with train/validation/test splits (Hoorali et al, 2020; Kang et al., 2020a, 2020b, 2020c, 2021; Ma et al., 2023; Park et al., 2023; Rattray et al., 2023), cross-validation strategies (Ali et al., 2020; Gu et al., 2020; Ibrahim et al., 2021), or evaluation using fully independent test set from distinct sources (Yi et al., 2023). An unbiased assessment of model performance on unseen data can only be ensured by utilizing an independent test set that remains strictly separate from model training to prevent data leakage, thereby achieving genuine evaluation beyond the model-fitting stage. Class imbalance is another important factor in data science, often overlooked in the included studies. This is particularly critical in object detection tasks, even when starting with a balanced number of images per class (Ma et al., 2023; Yi et al., 2023) due to severe foreground-to-background imbalance and sparse or small object instances within images. This inherent imbalance requires specialized approaches (e.g., focal loss, tailored anchors) to ensure accurate detection of underrepresented or less prominent objects.

Furthermore, establishing standardized benchmarks is essential for rigorous and consistent evaluation of AI-enabled pathogen detection models. Computationally, this includes building open-source AI communities around publicly accessible food safety and agricultural

repositories hosting benchmark datasets (Joshi et al., 2023; Qian et al., 2025). Biologically, it involves adopting standardized reference protocols for pathogen detection, such as traditional plating methods and qPCR assays. Future research should also emphasize incorporating diverse real-world samples to enhance the generalizability and applicability of AI-enabled detection methods. As AI-enabled systems continue to evolve, fostering collaborative efforts across researchers to share datasets, imaging protocols, and algorithms could accelerate innovation and AI integrations in pathogen detection.

2.5.2 Pathogen detection accelerated and automated by AI modeling

A common motivation across the reviewed studies was the need for rapid pathogen detection methods, addressing limitations such as lengthy biological sample preparation and reliance on selective enrichment steps (Seo et al., 2013; Maeda et al., 2018; Treebupachatsakul et al., 2019; Ibrahim et al., 2020; Kang et al., 2021; Ma et al., 2023). Most reviewed studies involving non-AI comparator methods utilized culture-based plating method, considered the gold standard (**Table 2.6**). In contrast, AI-enabled imaging methods were investigated for their potential to substantially accelerate detection by reducing biological sample preparation time and automating complex data analysis workflows. Notably, several studies demonstrated that AI image classification achieved high accuracies using bacterial samples with less than 24 h of incubation, highlighting the strong potential of these methods for near real-time pathogen monitoring (Ali et al., 2020; Borowa et al., 2023; Gu et al., 2020; He et al., 2018; Kim et al., 2023; Ma et al., 2023; Maeda et al., 2018; Park et al., 2023; Seo et al., 2013; Signoroni et al., 2018; Spahn et al., 2022; Treebupachatsakul et al., 2019; Turra et al., 2017; Wu et al., 2024; Yi et al., 2023). This represents a significant improvement compared to traditional techniques, which typically require several days for accurate detection (Foddai & Grant 2020).

Due to the streamlined biological sample preparation and automated data analysis, AI models can rapidly detect and identify pathogens, potentially predicting cross-contamination risks in near real-time. AI algorithms enable simultaneous classification of multiple bacterial strains directly from a generic sample preparation, reducing the dependency on highly optimized reagents required for selective enrichment. Additionally, AI-enabled imaging allows pathogen detection across multiple scales, from single-cell to microcolony and colony levels, further reducing wait times compared to traditional methods. In particular, Ma et al. (2023) and Yi et al. (2023) demonstrated rapid pathogen detection capabilities, achieving classification within 4 h with accuracies above 90%. The speed and accuracy of AI models have broad application potentials in food safety, ranging from identifying contamination sources to predicting pathogen presence and cross-contamination risks.

2.5.3 Enhancing capabilities of multimodal imaging through AI integration

Hyperspectral imaging is one type of multimodal sensing, a non-invasive approach that generates comprehensive datasets capturing morphological, structural, and biochemical signatures of pathogens (Dale et al., 2013, Kang et al., 2020). Unlike single-modality imaging methods that primarily provide spatial information only, multimodal imaging offers richer, high-dimensional data by integrating both spectral and spatial features (Eady & Park 2016). This comprehensive approach allows for the detection of subtle pathogen characteristics, such as variations in intracellular structures and metabolic profiles, which may remain undetected with single-modality techniques (Barzan et al., 2021, Piqueras et al., 2011). When integrated with advanced deep learning algorithms, multimodal datasets can further reveal subtle biological variations among bacterial species and strains (**Tables 2.6 and 2.8**). For example, Park et al. (2023) demonstrated that AI-enabled hyperspectral microscopy could differentiate between live

and dead *Salmonella*, highlighting the potential for AI models to distinguish pathogens based on physiological states rather than morphology alone. Such advancements could enable the classification at more granular levels, including bacterial strain or serovar. Given the extensive diversity within pathogens like *Salmonella*, acknowledging unique phenotypic and genotypic variations among different strains and serovars is crucial (Khan et al., 2024; Sabbagh et al., 2010; Uzzau et al., 2001). Thus, hyperspectral imaging has been extensively utilized across pathogen detection studies at multiple scales (**Table 2.6**), ranging from microbial colonies (macroscopic) to single-cell characteristics (microscopic). Consequently, multimodal imaging studies typically report higher classification accuracies than those relying solely on single modality imaging (Fong et al., 2020; Kang et al., 2020c; Tao et al., 2023; Park et al., 2023).

Furthermore, effective data preprocessing techniques are essential for extracting meaningful biological insights and identifying hidden contextual patterns within high-dimensional, multimodal datasets. PCA, historically one of the most widely adopted preprocessing methods (**Table 2.8**, enables an efficient approach for dimensionality reduction and automated feature extraction of relevant features. By reducing dimensional complexity while retaining key informational content, PCA significantly enhances pathogen classification accuracy and computational efficiency (Ram et al., 2024; Seo et al., 2016). Despite these advantages, PCA has inherent limitations, including sensitivity to multicollinearity and reliance on linear transformations based on Euclidean distances, which may not fully capture complex, nonlinear relationships embedded within multimodal data. To overcome these constraints, advanced deep learning methods, particularly end-to-end learning frameworks and attention-based models, are gaining traction in many domains due to their capability to model complex, nonlinear interactions and dynamically prioritize relevant features (Hong et al., 2020; Li et al., 2024).

2.5.4 Emerging applications of AI-enabled imaging for detecting stressed pathogens

As shown in **Table 2.3,** despite the limited number of studies specifically addressing pathogen detection under stress conditions, emerging advancements in AI-enabled imaging methods demonstrate significant promise for improving early detection, particularly when pathogens undergo morphological and metabolic changes induced by stressors. Notably, two studies reviewed demonstrated that AI can accurately differentiate pathogens in stress-induced states, beyond the conventional viable and culturable conditions (Ali et al., 2020; Park et al., 2023; Wu et al., 2024). Additionally, Chapter 3 explores the capability of AI integrated with multimodal imaging accurately differentiate *E. coli* K-12 in its viable and culturable state from its viable but non-culturable (VBNC) state, included by low-level antimicrobial stressors. These findings highlight the importance and promise of using AI to detect pathogens at more nuanced classification levels, such as source-specific strains or serovars. Pathogen isolates originating from various geospatial regions may uniquely adapt to local environmental stressors, further influencing their biological expressions (Cheng et al., 2019; Marmion et al., 2022). Integrating these variations into AI model architectures and data pipeline is therefore an essential and promising future direction, capable of significantly improving detection accuracy and facilitating robust, near real-time pathogen monitoring across diverse conditions.

2.6 Conclusion

This systematic review explored the use of AI-enabled imaging techniques for pathogen detection, highlighting notable computational advancements alongside existing challenges related to biological methodology inconsistencies and reporting practices. AI-enabled methods have demonstrated significant potential in enhancing classification accuracy and reducing detection time across diverse conditions. However, critical gaps remain due to multidisciplinary

complexities, underscoring the need for improved standardization to enhance reproducibility, facilitate meta-analysis, and strengthen generalization. Establishing consistent laboratory protocols (e.g., bacterial incubation conditions, imaging settings) and refining data pipeline (e.g., contextual data preprocessing, overfitting mitigation, class imbalance correction) are crucial for meaningful cross-study comparisons. Additionally, the integration of AI with multimodal imaging has further advanced pathogen detection by leveraging high-dimensional data, yet challenges persist in optimizing feature extraction and fusion strategies. Incorporating diverse biological variations, including stress condition studies, will be essential for enhancing model robustness and real-world applicability. Standardizing computational benchmarks and biological reference protocols, while integrating multimodal imaging and diverse biological contexts, will significantly improve generalization and applicability, supporting broader adoption of AI-enabled pathogen detection in food safety, public health, and environmental monitoring.

BIBLIOGRAPHY

Acuff, J., & Ponder, M. (2020). Interactions of Foodborne Pathogens with the Food Matrix. In A. Demirci, H. Feng, & K. Krishnamurthy (Eds.), *Food Safety Engineering* (pp. 129–156). Springer International Publishing. https://doi.org/10.1007/978-3-030-42660-6_5

Akbar, S. A., Ghazali, K. H., Hasan, H., Mohamed, Z., & Aji, W. S. (2021). An Enhanced Classification of Bacteria Pathogen on Microscopy Images Using Deep Learning. *2021 4th International Seminar on Research of Information Technology and Intelligent Systems (ISRITI)*, 119–123. https://doi.org/10.1109/ISRITI54043.2021.9702809

Akbari, H., Halig, L. V., Schuster, D. M., Osunkoya, A., Master, V., Nieh, P. T., Chen, G. Z., & Fei, B. (2012). Hyperspectral imaging and quantitative analysis for prostate cancer detection. *Journal of Biomedical Optics*, *17*(7). https://doi.org/10.1117/1.JBO.17.7.076005

Akgönüllü, S., & Denizli, A. (2022). Recent advances in optical biosensing approaches for biomarkers detection. *Biosensors and Bioelectronics: X*, *12*, 100269. https://doi.org/10.1016/j.biosx.2022.100269

Ali, N., Kirchhoff, J., Onoja, P. I., Tannert, A., Neugebauer, U., Popp, J., & Bocklitz, T. (2020). Predictive Modeling of Antibiotic Susceptibility in *E. coli* Strains Using the U-Net Network and One-Class Classification. *IEEE Access*, *8*, 167711–167720. IEEE Access. https://doi.org/10.1109/ACCESS.2020.3022829

Barzan, G., Sacco, A., Mandrile, L., Giovannozzi, A. M., Portesi, C., & Rossi, A. M. (2021). Hyperspectral Chemical Imaging of Single Bacterial Cell Structure by Raman Spectroscopy and Machine Learning. *Applied Sciences*, *11*(8), Article 8. https://doi.org/10.3390/app11083409

Bliven, K. A., & Maurelli, A. T. (2016). Evolution of Bacterial Pathogens Within the Human Host. *Microbiology Spectrum*, *4*(1). https://doi.org/10.1128/microbiolspec.VMBF-0017-2015

Borowa, A., Rymarczyk, D., Ochońska, D., Brzychczy-Włoch, M., & Zieliński, B. (2021). Deep learning classification of bacteria clones explained by persistence homology. *2021 International Joint Conference on Neural Networks (IJCNN)*, 1–8. https://doi.org/10.1109/IJCNN52387.2021.9533954

Borowa, A., Rymarczyk, D., Ochońska, D., Sroka-Oleksiak, A., Brzychczy-Włoch, M., & Zieliński, B. (2023). Identifying Bacteria Species on Microscopic Polyculture Images Using Deep Learning. *IEEE Journal of Biomedical and Health Informatics*, *27*(1), 121–130. IEEE Journal of Biomedical and Health Informatics. https://doi.org/10.1109/JBHI.2022.3209551

Cheng, R. A., Eade, C. R., & Wiedmann, M. (2019). Embracing Diversity: Differences in Virulence Mechanisms, Disease Severity, and Host Adaptations Contribute to the Success of Nontyphoidal Salmonella as a Foodborne Pathogen. *Frontiers in Microbiology*, *10*. https://doi.org/10.3389/fmicb.2019.01368

Cozzolino, D., Williams, P. J., & Hoffman, L. C. (2023). An overview of pre-processing methods available for hyperspectral imaging applications. *Microchemical Journal*, *193*, 109129. https://doi.org/10.1016/j.microc.2023.109129

Dale, L. M., Thewis, A., Boudry, C., Rotar, I., Dardenne, P., Baeten, V., & Pierna, J. A. F. (2013). Hyperspectral Imaging Applications in Agriculture and Agro-Food Product Quality and Safety Control: A Review. *Applied Spectroscopy Reviews*, *48*(2), 142–159. https://doi.org/10.1080/05704928.2012.705800

Dupont, M. F., Elbourne, A., Cozzolino, D., Chapman, J., Truong, V. K., Crawford, R. J., & Latham, K. (2020). Chemometrics for environmental monitoring: A review. *Analytical Methods*, *12*(38), 4597–4620. https://doi.org/10.1039/D0AY01389G

Foddai, A. C. G., & Grant, I. R. (2020). Methods for detection of viable foodborne pathogens: Current state-of-art and future prospects. *Applied Microbiology and Biotechnology*, *104*(10), 4281–4288. https://doi.org/10.1007/s00253-020-10542-x

Fong, A., Shu, G., McDonogh, B., & Park, B. (2020). Detecting foodborne pathogens with darkfield hyperspectral microscopy. In *Hyperspectral Imaging and Applications* (pp. 9–16). SPIE. https://doi.org/10.1117/12.2584913

Gao, L., & Smith, R. T. (2015). Optical hyperspectral imaging in microscopy and spectroscopy – a review of data acquisition. *Journal of Biophotonics*, *8*(6), 441–456. https://doi.org/10.1002/jbio.201400051

Gowen, A. A., Feng, Y., Gaston, E., & Valdramidis, V. (2015). Recent applications of hyperspectral imaging in microbiology. *Talanta*, *137*, 43–54. https://doi.org/10.1016/j.talanta.2015.01.012

Gu, P., Feng, Y.-Z., Zhu, L., Kong, L.-Q., Zhang, X., Zhang, S., Li, S.-W., & Jia, G.-F. (2020). Unified Classification of Bacterial Colonies on Different Agar Media Based on Hyperspectral Imaging and Machine Learning. *Molecules*, *25*(8), Article 8. https://doi.org/10.3390/molecules25081797

Hameed, S., Xie, L., & Ying, Y. (2018). Conventional and emerging detection techniques for pathogenic bacteria in food science: A review. *Trends in Food Science & Technology*, *81*, 61–73. https://doi.org/10.1016/j.tifs.2018.05.020

He, Y., Xu, W., Zhi, Y., Tyagi, R., Hu, Z., & Cao, G. (2018). Rapid bacteria identification using structured illumination microscopy and machine learning. *Journal of Innovative Optical Health Sciences*, *11*(01), 1850007. https://doi.org/10.1142/S1793545818500074

Hong, D., Gao, L., Yao, J., Zhang, B., Plaza, A., & Chanussot, J. (2021). Graph Convolutional Networks for Hyperspectral Image Classification. *IEEE Transactions on Geoscience and Remote Sensing*, *59*(7), 5966–5978. IEEE Transactions on Geoscience and Remote Sensing. https://doi.org/10.1109/TGRS.2020.3015157

Hoorali, F., Khosravi, H., & Moradi, B. (2020). Automatic *Bacillus anthracis* bacteria detection and segmentation in microscopic images using UNet++. *Journal of Microbiological Methods*, *177*, 106056. https://doi.org/10.1016/j.mimet.2020.106056

Ibrahim, A. U., Guler, E., Guvenir, M., Suer, K., Serte, S., & Ozsoz, M. (2021). Automated detection of *Mycobacterium tuberculosis* using transfer learning. *The Journal of Infection in Developing Countries*, *15*(05), Article 05. https://doi.org/10.3855/jidc.13532

Joshi, A., Guevara, D., & Earles, M. (2023). Standardizing and centralizing datasets for efficient training of agricultural deep learning models. *Plant Phenomics*, *5*, 0084. https://doi.org/10.34133/plantphenomics.0084

Kang, R., Park, B., & Chen, K. (2020a). Identifying non-O157 Shiga toxin-producing *Escherichia coli* (STEC) using deep learning methods with hyperspectral microscope images. *Spectrochimica Acta Part A: Molecular and Biomolecular Spectroscopy*, *224*, 117386. https://doi.org/10.1016/j.saa.2019.117386

Kang, R., Park, B., Eady, M., Ouyang, Q., & Chen, K. (2020b). Classification of foodborne bacteria using hyperspectral microscope imaging technology coupled with convolutional neural networks‡. *Applied Microbiology and Biotechnology*, *104*(7), Article 7. https://doi.org/10.1007/s00253-020-10387-4

Kang, R., Park, B., Eady, M., Ouyang, Q., & Chen, K. (2020c). Single-cell classification of foodborne pathogens using hyperspectral microscope imaging coupled with deep learning frameworks. *Sensors and Actuators B: Chemical*, *309*, 127789. https://doi.org/10.1016/j.snb.2020.127789

Kang, R., Park, B., Ouyang, Q., & Ren, N. (2021). Rapid identification of foodborne bacteria with hyperspectral microscopic imaging and artificial intelligence classification algorithms. *Food Control*, *130*, 108379. https://doi.org/10.1016/j.foodcont.2021.108379

Kim, M. J., Park, J., Kang, M., Jeong, U., Jeong, D., Kang, N.-G., Hwang, S. J., Youn, S. H., Hwang, B. K., Hyun, Y., & Kim, D. (2023). Bacteria detection and species identification at the single-cell level using super-resolution fluorescence imaging and AI analysis. *Biosensors and Bioelectronics*, *240*, 115603. https://doi.org/10.1016/j.bios.2023.115603

Law, J. W.-F., Ab Mutalib, N.-S., Chan, K.-G., & Lee, L.-H. (2015). Rapid methods for the detection of foodborne bacterial pathogens: Principles, applications, advantages and limitations. *Frontiers in Microbiology*, *5*. https://doi.org/10.3389/fmicb.2014.00770

Li, N., Wang, Z., & Cheikh, F. A. (2024). Discriminating Spectral-Spatial Feature Extraction for Hyperspectral Image Classification: A Review. *Sensors (Basel, Switzerland)*, *24*(10), 2987. https://doi.org/10.3390/s24102987

Ma, L., Yi, J., Wisuthiphaet, N., Earles, M., & Nitin, N. (2022). Accelerating the Detection of Bacteria in Food Using Artificial Intelligence and Optical Imaging. *Applied and Environmental Microbiology*, *89*(1), e01828-22. https://doi.org/10.1128/aem.01828-22

Maeda, Y., Sugiyama, Y., Kogiso, A., Lim, T.-K., Harada, M., Yoshino, T., Matsunaga, T., & Tanaka, T. (2018). Colony Fingerprint-Based Discrimination of *Staphylococcus* species with Machine Learning Approaches. *Sensors*, *18*(9), Article 9. https://doi.org/10.3390/s18092789

Marmion, M., Macori, G., Ferone, M., Whyte, P., & Scannell, A. G. M. (2022). Survive and thrive: Control mechanisms that facilitate bacterial adaptation to survive manufacturing-related stress. *International Journal of Food Microbiology*, *368*, 109612. https://doi.org/10.1016/j.ijfoodmicro.2022.109612

Paniel, N., & Noguer, T. (2019). Detection of *Salmonella* in Food Matrices, from Conventional Methods to Recent Aptamer-Sensing Technologies. *Foods*, *8*(9), 371. https://doi.org/10.3390/foods8090371

Park, B., Shin, T., Wang, B., McDonogh, B., & Fong, A. (2023). Classification between live and dead foodborne bacteria with hyperspectral microscope imagery and machine learning. *Journal of Microbiological Methods*, *209*, 106739. https://doi.org/10.1016/j.mimet.2023.106739

Pinto-Coelho, L. (2023). How Artificial Intelligence Is Shaping Medical Imaging Technology: A Survey of Innovations and Applications. *Bioengineering*, *10*(12), Article 12. https://doi.org/10.3390/bioengineering10121435

Piqueras, S., Duponchel, L., Tauler, R., & de Juan, A. (2011). Resolution and segmentation of hyperspectral biomedical images by Multivariate Curve Resolution-Alternating Least Squares. *Analytica Chimica Acta*, *705*(1), 182–192. https://doi.org/10.1016/j.aca.2011.05.020

Qian, C., Yang, H., Acharya, J., Liao, J., Ivanek, R., & Wiedmann, M. (2025). Initializing a public repository for hosting benchmark datasets to facilitate machine learning model development in food safety. *Journal of Food Protection*, 100463. https://doi.org/10.1016/j.jfp.2025.100463

Ram, B. G., Oduor, P., Igathinathane, C., Howatt, K., & Sun, X. (2024). A systematic review of hyperspectral imaging in precision agriculture: Analysis of its current state and future prospects. *Computers and Electronics in Agriculture*, *222*, 109037. https://doi.org/10.1016/j.compag.2024.109037

Rattray, J. B., Lowhorn, R. J., Walden, R., Márquez-Zacarías, P., Molotkova, E., Perron, G., ... & Brown, S. P. (2023). Machine learning identification of *Pseudomonas aeruginosa* strains from colony image data. PLoS Computational Biology, 19(12), e1011699. https://doi.org/10.1371/journal.pcbi.1011699

Rudi, K., Moen, B., Drømtorp, S. M., & Holck, A. L. (2005). Use of Ethidium Monoazide and PCR in Combination for Quantification of Viable and Dead Cells in Complex Samples. *Applied and Environmental Microbiology*, *71*(2), 1018–1024. https://doi.org/10.1128/AEM.71.2.1018-1024.2005

Sabbagh, S. C., Forest, C. G., Lepage, C., Leclerc, J.-M., & Daigle, F. (2010). So similar, yet so different: Uncovering distinctive features in the genomes of *Salmonella enterica* serovars Typhimurium and Typhi. *FEMS Microbiology Letters*, *305*(1), 1–13. https://doi.org/10.1111/j.1574-6968.2010.01904.x

Schardt, C., Adams, M. B., Owens, T., Keitz, S., & Fontelo, P. (2007). Utilization of the PICO framework to improve searching PubMed for clinical questions. *BMC Medical Informatics and Decision Making*, *7*, 16. https://doi.org/10.1186/1472-6947-7-16

Seo, Y., Park, B., Hinton, A., Yoon, S.-C., & Lawrence, K. C. (2016). Identification of *Staphylococcus* species with hyperspectral microscope imaging and classification algorithms. *Journal of Food Measurement and Characterization*, *10*(2), 253–263. https://doi.org/10.1007/s11694-015-9301-0

Seo, Y. W., Yoon, S. C., Park, B., Hinton Jr, A., Windham, W. R., & Lawrence, K. C. (2013). Development of classification models to detect *Salmonella* Enteritidis and *Salmonella* Typhimurium found in poultry carcass rinses by visible-near infrared hyperspectral imaging. In *Sensing for Agriculture and Food Quality and Safety V* (pp. 70–78). SPIE. https://doi.org/10.1117/12.2016336

Shamseer, L., Moher, D., Clarke, M., Ghersi, D., Liberati, A., Petticrew, M., Shekelle, P., Stewart, L. A., & PRISMA-P Group. (2015). Preferred reporting items for systematic review and meta-analysis protocols (PRISMA-P) 2015: Elaboration and explanation. *BMJ (Clinical Research Ed.)*, *350*, g7647. https://doi.org/10.1136/bmj.g7647

Shao, Z., Zhao, R., Yuan, S., Ding, M., & Wang, Y. (2022). Tracing the evolution of AI in the past decade and forecasting the emerging trends. *Expert Systems with Applications*, *209*, 118221. https://doi.org/10.1016/j.eswa.2022.118221

Signoroni, A., Savardi, M., Pezzoni, M., Guerrini, F., Arrigoni, S., & Turra, G. (2018). Combining the use of CNN classification and strength-driven compression for the robust identification of bacterial species on hyperspectral culture plate images. *IET Computer Vision*, *12*(7), 941–949. https://doi.org/10.1049/iet-cvi.2018.5237

Spahn, C., Gómez-de-Mariscal, E., Laine, R. F., Pereira, P. M., von Chamier, L., Conduit, M., Pinho, M. G., Jacquemet, G., Holden, S., Heilemann, M., & Henriques, R. (2022). DeepBacs for multi-task bacterial image analysis using open-source deep learning approaches. *Communications Biology*, *5*(1), 1–18. https://doi.org/10.1038/s42003-022-03634-z

Tao, C., Du, J., Wang, J., Hu, B., & Zhang, Z. (2023). Rapid Identification of Infectious Pathogens at the Single-Cell Level via Combining Hyperspectral Microscopic Images and Deep Learning. *Cells*, *12*(3), Article 3. https://doi.org/10.3390/cells12030379

Treebupachatsakul, T., & Poomrittigul, S. (2019). Bacteria Classification using Image Processing and Deep learning. *2019 34th International Technical Conference on Circuits/Systems, Computers and Communications (ITC-CSCC)*, 1–3. https://doi.org/10.1109/ITC-CSCC.2019.8793320

Treebupachatsakul, T., & Poomrittigul, S. (2020). Microorganism Image Recognition based on Deep Learning Application. *2020 International Conference on Electronics, Information, and Communication (ICEIC)*, 1–5. https://doi.org/10.1109/ICEIC49074.2020.9051009

Turra, G., Arrigoni, S., & Signoroni, A. (2017, September). CNN-Based Identification of Hyperspectral Bacterial Signatures for Digital Microbiology. In *Image Analysis and Processing-ICIAP 2017*, Catania, Italy (pp. 500–510). Springer International Publishing. https://doi.org/10.1007/978-3-319-68548-9_46

Uzzau, S., Brown, D. J., Wallis, T., Rubino, S., Leori, G., Bernard, S., Casadesús, J., Platt, D. J., & Olsen, J. E. (2000). Host adapted serotypes of *Salmonella enterica*. *Epidemiology & Infection*, *125*(2), 229–255. https://doi.org/10.1017/S0950268899004379

Vicente-Santos, A., Willink, B., Nowak, K., Civitello, D. J., & Gillespie, T. R. (2023). Host-pathogen interactions under pressure: A review and meta-analysis of stress-mediated effects on disease dynamics. *Ecology Letters*, *26*(11), 2003–2020. https://doi.org/10.1111/ele.14319

Wang, Y., & Salazar, J. K. (2016). Culture-Independent Rapid Detection Methods for Bacterial Pathogens and Toxins in Food Matrices. *Comprehensive Reviews in Food Science and Food Safety*, *15*(1), 183–205. https://doi.org/10.1111/1541-4337.12175

Whiting, P. F., Rutjes, A. W., Westwood, M. E., Mallett, S., Deeks, J. J., Reitsma, J. B., ... & QUADAS-2 Group. (2011). QUADAS-2: a revised tool for the quality assessment of diagnostic accuracy studies. *Annals of internal medicine*, *155*(8), 529-536. https://doi.org/10.7326/0003-4819-155-8-201110180-00009

Wu, C., Xie, Y., Xi, Q., Han, X., Li, Z., Li, G., Zhao, J., & Liu, M. (2024). Rapid and high accurate identification of *Escherichia coli* active and inactivated state by hyperspectral microscope imaging combing with machine learning algorithm. *Vibrational Spectroscopy*, *130*, 103645. https://doi.org/10.1016/j.vibspec.2023.103645

Yi, J., Wisuthiphaet, N., Raja, P., Nitin, N., & Earles, J. M. (2023). AI-enabled biosensing for rapid pathogen detection: from liquid food to agricultural water. *Water Research*, *242*, 120258. https://doi.org/10.1016/j.watres.2023.120258

Zeng, D., Chen, Z., Jiang, Y., Xue, F., & Li, B. (2016). Advances and Challenges in Viability Detection of Foodborne Pathogens. *Frontiers in Microbiology*, *7*, 1833. https://doi.org/10.3389/fmicb.2016.01833

Zhu, F., Zhang, H., Shao, Y., He, Y., & Ngadi, M. (2014). Mapping of Fat and Moisture Distribution in Atlantic Salmon Using Near-Infrared Hyperspectral Imaging. *Food and Bioprocess Technology*, *7*(4), 1208–1214. https://doi.org/10.1007/s11947-013-1228-z

Zhu, H., Luo, J., Liao, J., & He, S. (2023). High-accuracy Rapid Identification and Classification of Mixed Bacteria Using Hyperspectral Transmission Microscopic Imaging and Machine Learning. *Progress In Electromagnetics Research*, *178*, 49–62. https://doi.org/10.2528/PIER23082303

CHAPTER 3: DETECTION OF VIABLE BUT NONCULTURABLE E. COLI INDUCED BY LOW-LEVEL ANTIMICROBIALS USING AI-ENABLED HYPERSPECTRAL MICROSCOPY[1]

3.1 Abstract

Rapid detection of bacterial pathogens is essential for food safety and public health, yet bacteria can evade detection by entering a viable but non-culturable (VBNC) state under sublethal stress, such as antimicrobial residues. These bacteria remain active but undetectable by standard culture-based methods without extensive enrichment, necessitating advanced detection methods. This study developed an AI-enabled hyperspectral microscope imaging (HMI) framework for rapid VBNC detection under low-level antimicrobials. The objectives were to: i) induce the VBNC state in *Escherichia coli* K-12 by exposure to selected antimicrobial stressors, ii) obtain hyperspectral data capturing physiological changes in VBNC cells, and iii) automate the classification of normal and VBNC cells using deep learning image classification. The VBNC state was induced by low-level oxidative (0.01% hydrogen peroxide) and acidic (0.001% peracetic acid) stressors for 3 days, confirmed by live-dead staining and plate counting. Hyperspectral microscopy provided spatial and spectral data, extracted into pseudo-RGB images using three characteristic spectral wavelengths. An EfficientNetV2-based convolutional neural network architecture was trained on these pseudo-RGB images, achieving 97.1% accuracy of VBNC classification (n = 200), outperforming the model trained on standard color images at 83.3%. The results highlight the potential for rapid, automated VBNC detection using AI-enabled hyperspectral microscopy, contributing to timely intervention to prevent foodborne illnesses and outbreaks.

[1] Note: This chapter has been published in *Journal of Food Protection (2025).*

3.2 Introduction

Detection of enteric pathogens is crucial for safeguarding public health from infectious diseases, however pathogens that bypass detection cause significant challenges. Under adverse environmental conditions, bacteria such as *Escherichia coli* (including EHEC strains) can enter a viable but non-culturable (VBNC) state as a survival strategy (Oliver 2010; Pinto et al., 2015). Various environmental stressors, such as low temperatures, pH fluctuations, salt concentrations, and nutrient limitations, have been shown to induce the VBNC state (Oliver et al., 2010; Liu et al., 2017; Chen et al., 2018; Li et al., 2020a). Bacteria in the VBNC state fail to grow on culture media on which they would normally grow but remain alive and capable of renewed metabolic activity and pathogenicity (Oliver 2000; Ramamurthy et al., 2014). In addition, previous studies have found that processes which are normally assumed to be bactericidal may instead result in cells entering the VBNC state (Oliver 2010). These include antimicrobial treatments and residues such as peracetic acid in wastewater treatment or hydrogen peroxide in food packaging. (Li et al., 2020b; Scaramuzza et al., 2020; Ao et al., 2021). Therefore, understanding and detecting VBNC states is critical for accurate bacterial detection to improve food safety and public health.

Standard culture-based methods may vastly underestimate the occurrence of VBNC bacteria that pose a threat to food and health safety (Oliver 2010). Despite efforts to develop advanced molecular methods for improving VBNC detection, these methods often require extensive sample preparation and high-quality labor, and they may face challenges with non-viable cell DNAs (Guo et al., 2021; Pinto et al., 2015). Optical detection of VBNCs using microscopy have shown promise, yet relying on fluorescence staining, which extends the overall detection time (Wideman et al., 2021). The extended time to detection is a critical limitation of bacterial detection methods, especially for products with shorter shelf lives. Thus, there is a need

for advanced imaging techniques that can minimize sample preparation requirements while enhancing data analysis for detecting VBNC bacteria.

Recent studies have incorporated AI into diagnostic applications for early detection, utilizing deep convolutional neural networks (CNNs) for microscopy data analysis (Litjens et al., 2017; Mousavizadegan et al., 2024; Chen et al., 2024). Specifically, microscopy coupled with deep learning has demonstrated significant potential in the rapid identification of bacteria (Ma et al., 2023; Chen et al., 2024). Moreover, when paired with advanced sensing techniques to capture detailed imagery data, CNNs trained on lab-cultured bacteria can adapt to detect pathogens in unseen real-world samples, highlighting the applicability of AI-enabled microscopy when provided with sufficient information (Yi et al., 2023). Recently, hyperspectral microscope imaging (HMI) has been implemented for pathogen detection, as it offers richer information with spectral and spatial data of biological samples. Beyond the spatial morphological features captured by optical microscopy, hyperspectral microscopy provides spectrochemical information on sample constituents, intracellular components, and metabolic activity (Barzan et al., 2021; Piqueras et al., 2011). Additionally, hyperspectral microscopy benefits from its non-invasive and high-throughput analysis capabilities, complemented by advanced deep learning approaches that enable accelerated and automated interpretation of abstract features extracted from its high-dimensional data (Kang et al., 2020; Park et al., 2023a; Tao et al., 2022; Tao et al., 2023). These advanced techniques have the potential to improve rapid detection by capturing physiological changes in bacteria through imagery data.

The primary goal of this study was to develop a data-efficient AI-enabled hyperspectral microscopy framework for the rapid detection of VBNC bacteria under low-level antimicrobials. Specifically, we selected *E. coli* K-12 as a model bacterium and surrogate for the foodborne

pathogen *E. coli* O157:H7. The objectives were to: i) induce the VBNC state in *E. coli* K-12 by exposure to low-concentration antimicrobial stressors, ii) obtain hyperspectral data capturing physiological changes between normal and VBNC cells, and iii) automate the classification of normal and VBNC cells deep learning image classification. As illustrated in **Figure 3.1**, the overall workflow of this study includes key steps. First, the VBNC state in *E. coli* was induced using low concentrations of peracetic acid (PAA) and hydrogen peroxide (H_2O_2). Viability and culturability of the cells were confirmed using live-dead staining and standard plate counting methods. Hyperspectral microscopy was then employed to acquire detailed imagery data of both normal and VBNC cells. These images were subsequently preprocessed and used for model training and evaluation in the classification of normal and VBNC cells. This study was designed to demonstrate the feasibility of a rapid, resource-efficient framework for detecting specific models of stressed bacteria, i.e., VBNC *E. coli* under low-level antimicrobial stress. It serves as foundational work that could lead to expanded biological validation and refined algorithms for capturing more subtle and diverse physiological states. Overall, this study highlights the potential of AI-enabled hyperspectral microscopy for the rapid detection of VBNC bacteria.

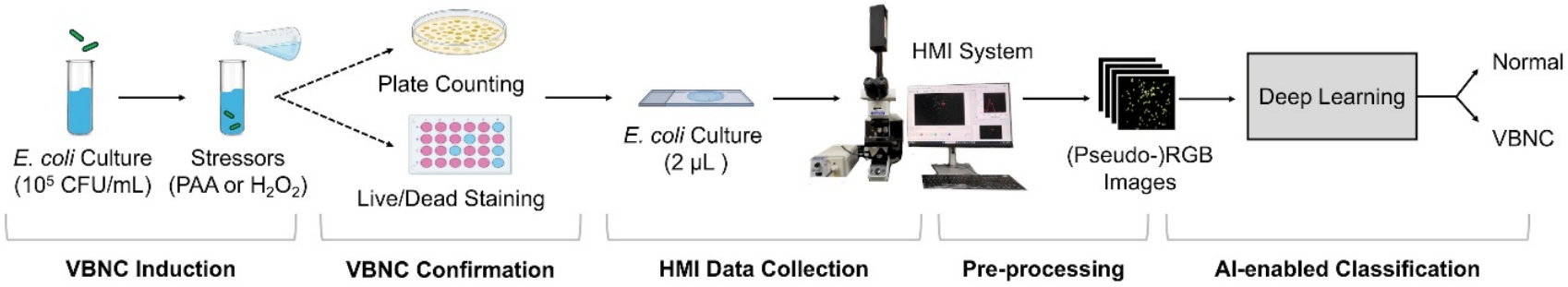

Figure 3.1 Schematic diagram of viable but non-culturable (VBNC) detection using artificial intelligence (AI)-enabled hyperspectral microscopy.

3.3 Materials and methods

3.3.1 Bacterial strains and preparation of bacterial suspension

In this study, *E. coli* K-12 (strain MG1655, from ATCC) was selected as a surrogate for *E. coli* O157:H7 due to its genetic and physiological similarities (Hu and Gurtler, 2017). The *E. coli* stock cultures were maintained at 4°C on LB Lennox agar plate (Thermo Fisher, Waltham, MA, USA). A single bacterial colony was inoculated into 9 mL of tryptic soy broth (Difco, BD, Sparks, MD, USA) supplemented with 0.6% (w/v) yeast extract (Difco, BD) and incubated at 37°C for 16 h. Cells in the logarithmic phase were harvested by centrifugation at 4,450 ×*g* for 15 min at 4°C (SYTO 9, SLA-1500, Hampton, NH, USA). The cells were then washed once in sterile 0.85% NaCl solution to remove excess culture medium residue to limit nutrients for VBNC induction. The final pellet was suspended in sterile 0.85% NaCl for a final concentration of 10^9 CFU/mL before exposure to antimicrobial stressors.

3.3.2 VBNC induction using antimicrobial stressors

E. coli suspension was subjected to low concentrations of oxidative and acid stressors to induce the VBNC state. Using a modified version of a previously published method (Salive et al., 2020), two stressors at low concentrations were applied: 0.01–0.1% (v/v) H_2O_2 (Fisher Scientific, Ann Arbor, MI, USA) and 0.001–0.1% (v/v) PAA (Sigma Aldrich, St. Louis, MO, USA). These stressors were chosen due to their proven ability to induce a VBNC state and their use in food processing sanitation (Li et al., 2020b; Scaramuzza et al., 2020; Ao et al., 2021; Kim et al., 2023). To assess the effectiveness of these stressors, positive and negative controls were included: a positive control consisting of 0.85% NaCl for live cells in a normal state (i.e., “normal cells” hereafter) and a negative control consisting of 100% ethanol for completely dead cells. Based on preliminary work following the viability and culturability assays described below

(data not shown), the final concentrations of H_2O_2 and PAA were determined to be 0.01% and 0.001%, respectively, with an exposure period of 3 days. These stress solutions were prepared by adding 1 mL of the bacterial suspension at 10^9 CFU/mL to 9 mL of either stress solution, resulting in final concentrations of 10^8 CFU/mL with 0.01% H_2O_2 or 0.001% PAA. All stress solutions were then incubated at 4°C.

3.3.3 Viability and culturability assays

The final concentrations of H_2O_2 and PAA used for imaging of VBNC cells were determined based on the results of viability and culturability assays. The stressor concentrations resulting in 100% of the population in the VBNC state were selected for further imaging. This was defined as when fluorescence intensity indicated 50% or more viable cells (i.e., "viable"), while no culturable bacterial colonies were detected by plating (i.e., "non-culturable").

To monitor the viability of stressed *E. coli* samples over time, an aliquot was stained with the Live/Dead BacLight Bacterial Viability Kit (L7012, Fisher Scientific), following the manufacturer's instructions. Briefly, the staining solution was prepared by mixing 6 µL of 3.34 mM SYTO 9 dye (green fluorescence) with 6 µL of 20 mM propidium iodide dye (red fluorescence). This mixture was then added to 2 mL of filter-sterilized de-ionized water. To stain the stressed *E. coli* samples, 100 µL of each bacterial suspension was pipetted into separate wells of a black opaque 96-well flat bottom microplate. Then 100 µL of the staining solution was added to each well and mixed thoroughly by pipetting up and down 5 times. The integrated fluorescence intensity in relative fluorescent units (RFU) was collected at two different emission ranges using a SpectraMax iD3 Multi-Mode Microplate Reader (Molecular Devices, San Jose, CA, USA): green fluorescence (510–540 nm) and red fluorescence (620–650 nm). These measurements were used to calculate the percent viable cells using Equation 3.1.

$$\text{Viable Cell (\%)} = \frac{F_S^{\text{green}}/F_N^{\text{green}}}{F_S^{\text{green}}/F_N^{\text{green}} + F_S^{\text{red}}/F_D^{\text{red}}} \times 100 \quad (3.1)$$

where F_S is the green or red fluorescence intensity of stressed cells (RFU), F_N is the fluorescence intensity of normal cells (RFU), and F_D is the fluorescence intensity of completely dead cells (RFU). All fluorescence intensity measurements were adjusted for background fluorescence.

The culturability of each stressed *E. coli* sample was assessed until no culturable bacterial colonies were detected by the standard plate counting method. At selected intervals, 100 µL of the bacterial suspension was neutralized in de-ionized water and was plated onto sterile tryptic soy agar plates. A total of three serial dilutions were plated, and the plates were incubated at 37°C for 24 h. After incubation, the number of culturable colonies were counted as colony forming units (CFU). The results were then converted to log CFU/mL, taking into account the dilution factors. The detection limit was determined by calculating the bacterial counts corresponding to the presence of one colony after plating (i.e., 2 log CFU/mL).

3.3.4 Statistical Analysis

One-way analysis of variance in Python Statsmodels library (Seabold and Perktold, 2010) was used to test for significant differences ($p < 0.05$) in viability and culturability measurements. These assays were conducted in triplicate. Tuckey's Honest Significant Difference test was used to indicate significantly different values across different incubation time points within the same treatment group.

3.3.5 Hyperspectral data collection for normal and VBNC cells

Hyperspectral data were conducted for two conditions: i) freshly grown overnight subcultures of normal cells and ii) VBNC cells induced by exposure to the selected stress condition of 0.001% PAA for 3 days. This specific condition was chosen after confirming VBNC induction by low antimicrobial exposures, as described above, as the representative VBNC

condition for hyperspectral data collection. Microscope slides of bacterial cells were prepared following a modified version of a previously published method (Park et al., 2023b). Briefly, *E. coli* cells were washed three times by centrifugation at 4,450 ×*g* for 15 min at 4°C with sterile phosphate-buffered saline (Thermo Fisher). The final pellet was suspended in sterile de-ionized water for a final concentration of 10^5 CFU/mL. Subsequently, 2 µL of the bacterial suspension was deposited onto a sterile glass slide and allowed to air dry for 12 min at 23°C with an average relative humidity of 42% in a biosafety cabinet. An additional 2 µL of sterile de-ionized water was added to affix a plastic coverslip, securing the cells in place.

Our hyperspectral microscopy system comprises of an Olympus BX43 upright optical microscope (Evident Scientific, Waltham, MA, USA) equipped with CytoViva patented enhanced darkfield illumination optics and tungsten halogen lamp (CytoViva, Auburn, AL, USA) and a HinaLea 4250 hyperspectral camera (HinaLea, Emeryville, CA, USA) (**Figure 3.2**). The spatial resolution of the imaging system was 1936 × 1216 pixels, covering a spectral range was 399–1,000 nm with 303 spectral bands. Imaging was performed using a 100× oil immersion objective lens, with an exposure time of 200 ms and a gain setting of 16 dB. These parameters were carefully chosen to maximize the signal-to-noise ratio, minimizing background noise while ensuring optimal brightness. Hyperspectral microscopy was conducted on ten biological replicates for normal and VBNC cells. For each biological replicate, 10 distinct regions of interests were imaged per microscope slide, ensuring that there were no overlapping cells. A total of 200 hyperspectral datasets (100 normal and 100 VBNC) were obtained for further analysis.

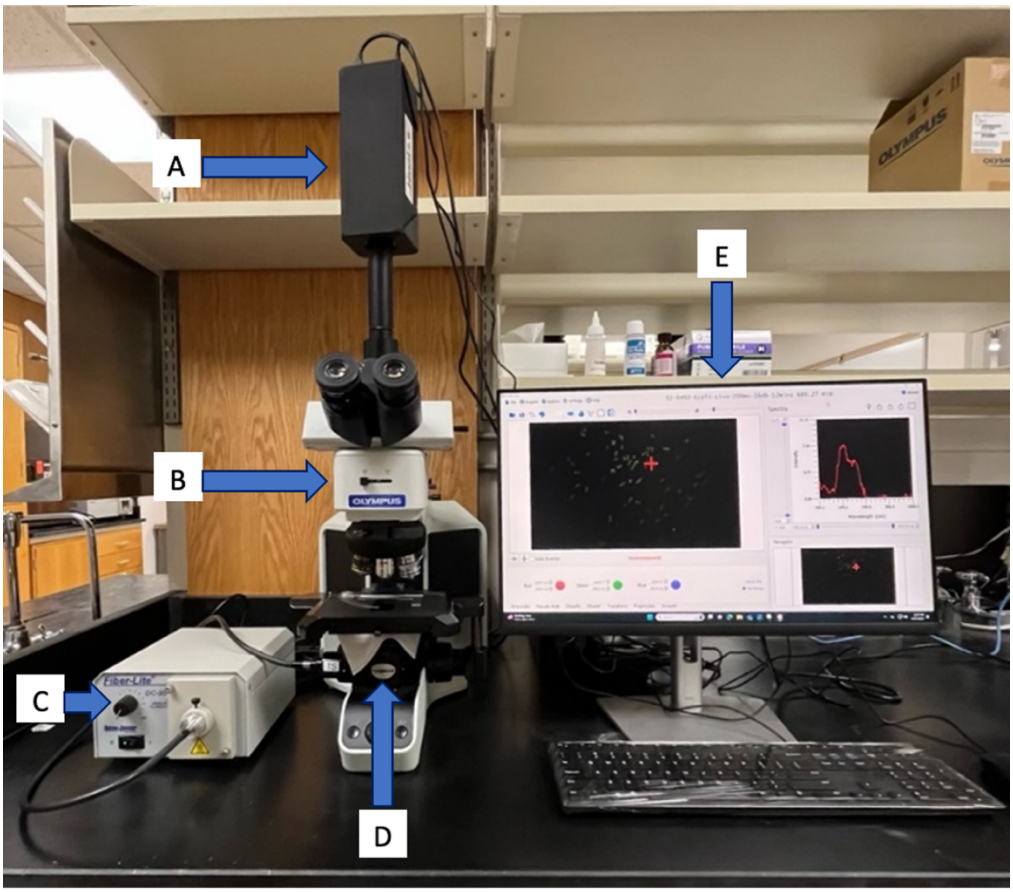

Figure 3.2 Hyperspectral microscope imaging (HMI) system: (**A**) Hyperspectral camera, (**B**) upright optical microscope, (**C**) tungsten halogen lamp, (**D**) enhanced darkfield illumination optics, and (**E**) desktop.

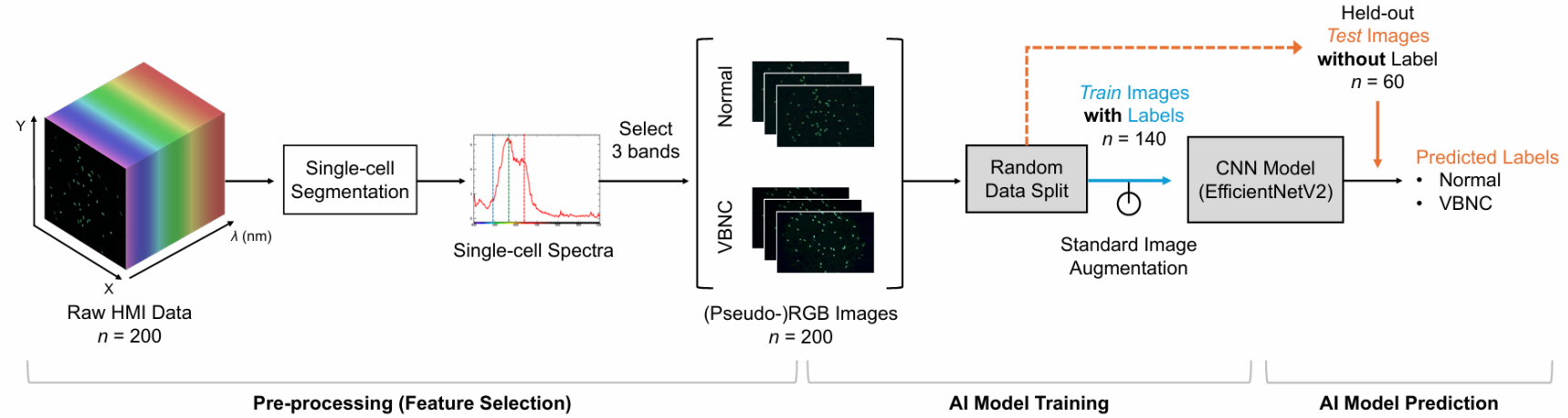

Figure 3.3 Overview of the data pipeline for classifying normal and VBNC *E. coli* cells using CNN. The diagram illustrates how raw hyperspectral data cubes were processed into pseudo-RGB or standard color images, followed by CNN image classification.

3.3.6 Data preprocessing and CNN image classification

The data pipeline for classifying normal and VBNC cells is shown in **Figure 3.3**. This diagram provides an overview of how the raw hyperspectral data cubes were processed into pseudo-RGB or standard color images, which were then classified using a CNN model. The collected hyperspectral data were preprocessed to extract pseudo-RGB and standard color images, which were then used for deep learning image classification to compare the effectiveness of hyperspectral microscopy and conventional optical microscopy in VBNC detection. Pseudo-RGB images were extracted using a modified version of a previously published automated bacterial segmentation (Park et al., 2023b), followed by the Spectral Python (Spy) library, while standard color images were extracted directly using Spy. The automated bacterial segmentation code identified data points corresponding to single bacterial cells, reducing the hypercube dimensions and providing the respective spectral profiles. Three characteristic spectral wavelengths were then selected and mapped to the red, green, and blue channels to create pseudo-RGB images. The extracted images were split, reserving 20% for testing and using the remaining 80% for model training.

The pseudo-RGB images were used to discriminate between normal and VBNC cells by training a CNN architecture based on an EfficientNetV2 variant (Tan and Le, 2021) with the PyTorch Lightning deep learning library. The modified version of the EfficientNetV2 architecture was employed with different combinations of standard augmentation strategies from the Albumentations library (Buslaev et al., 2020). The pre-trained EfficientNetV2 variant was loaded and trained on our training dataset with a total batch size of 4, using a cross-entropy loss function. An AdamW optimizer was implemented with an initial learning rate of 0.001 and a weight decay of 0.01. A step-based learning rate scheduler was incorporated, reducing the

learning rate by a factor of 0.3 every 10 epochs. Early stopping applied when the validation loss stopped improving. Model performance was evaluated on the held-out testing dataset, using a confusion matrix to assess the accuracy of the classification. The same steps were repeated with standard color images to compare VBNC classification based solely on cell morphology without spectral information.

3.4 Results

3.4.1 VBNC induction by low-concentration antimicrobial stressors

E. coli K-12 cells were exposed to various concentrations of H_2O_2 and PAA stress solutions to induce the VBNC state. By day three, live-dead staining results indicated that both H_2O_2 and PAA stress solutions at specific low concentrations maintained notable viability levels above 50% while being non-culturable by plating (**Figure 3.4**). Specifically, *E. coli* samples exposed to 0.01% H_2O_2 exhibited no culturable bacterial colonies after 72 h, indicating a loss of culturability. These samples showed fluorescence intensity values of $16.3 \pm 1.25 \times 10^5$ RFU for green and $4.76 \pm 7.13 \times 10^5$ RFU for red, resulting in $52.11 \pm 4.34\%$ viable cells, confirming the induction of a VBNC state. Similarly, *E. coli* samples exposed to 0.001% PAA exhibited minimal survival with concentrations of 1.43 ± 1.25 log CFU/mL after 72 h. These samples showed fluorescence intensity values of $12.5 \pm 2.62 \times 10^5$ RFU for green and $7.01 \pm 2.12 \times 10^5$ RFU for red, with $46.92 \pm 4.35\%$ viable cells, also indicating the induction of the VBNC state. These stress conditions, which effectively induced the VBNC state in *E. coli* K-12 cells, were subsequently selected for hyperspectral data collection.

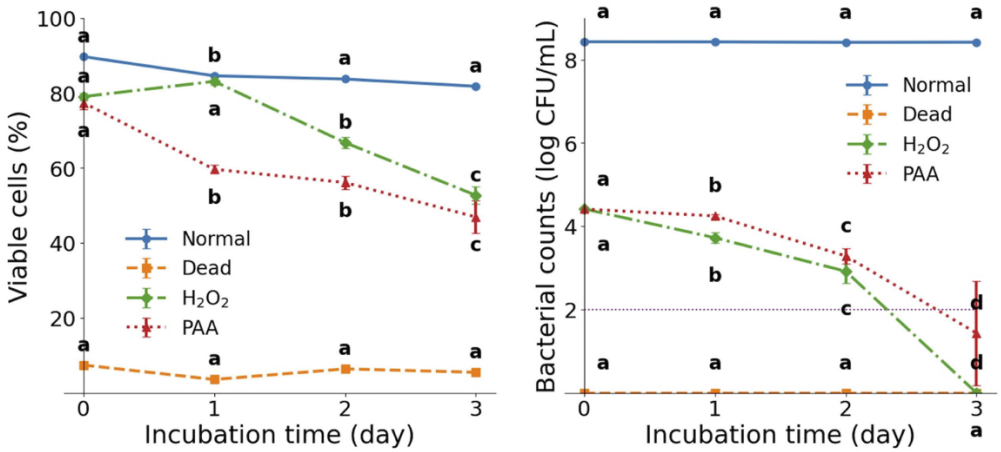

Figure 3.4 Viability and culturability of *E. coli* K-12 exposed to low-level antimicrobials: (A) Viable cells (%) measured by live-dead staining. The data are mean values with their standard deviations (n = 3). Different letters denote significant ($p < 0.05$) differences in values between days within a treatment. (B) Culturable bacterial counts (log CFU/mL) measured by the standard plate counting. Normal: Live cells in a normal state. H_2O_2: Cells exposed to hydrogen peroxide at a concentration of 0.01% (v/v) for 3 days. PAA: Cells exposed to peracetic acid at a concentration of 0.001% (v/v) for 3 days. Dead: Completely dead cells exposed to 100% ethanol. The purple dotted line indicates the detection limit.

3.4.2 Comparison of hyperspectral data of normal and VBNC cells

Following the confirmation of VBNC induction, both normal and VBNC *E. coli* cells were visualized using hyperspectral microscopy to extract pseudo-RGB and standard color images. These images were then used for VBNC classification, as illustrated in **Figure 3.3**, which shows how the feature extraction in **Figure 3.5** leads to the classification results presented in **Figure 3.6**. As shown in **Figures 3.5A** and 3.**5D**, the hyperspectral datasets provided hypercubes capturing distinct spectral profiles for normal and VBNC cells. These spectra were extracted from single cells, and the average raw spectra for normal and VBNC cells showed substantial differences across most wavelengths. Notably, normal cells exhibited higher spectral intensities on average compared to VBNC cells. Based on these average values, three characteristic spectral wavelengths were identified: 410, 559, and 634 nm for normal cells, and 416, 556, and 642 nm for VBNC cells, respectively. Representative pseudo-RGB images of normal and VBNC cells are shown in **Figures 3.5B** and **3.5E**, respectively, demonstrating higher signal intensity compared to the corresponding standard color images shown in **Figures 3.5C** and **3.5F**. While the morphologies of these cells appeared qualitatively similar, their selected spectral wavelengths exhibited different intensities per channel.

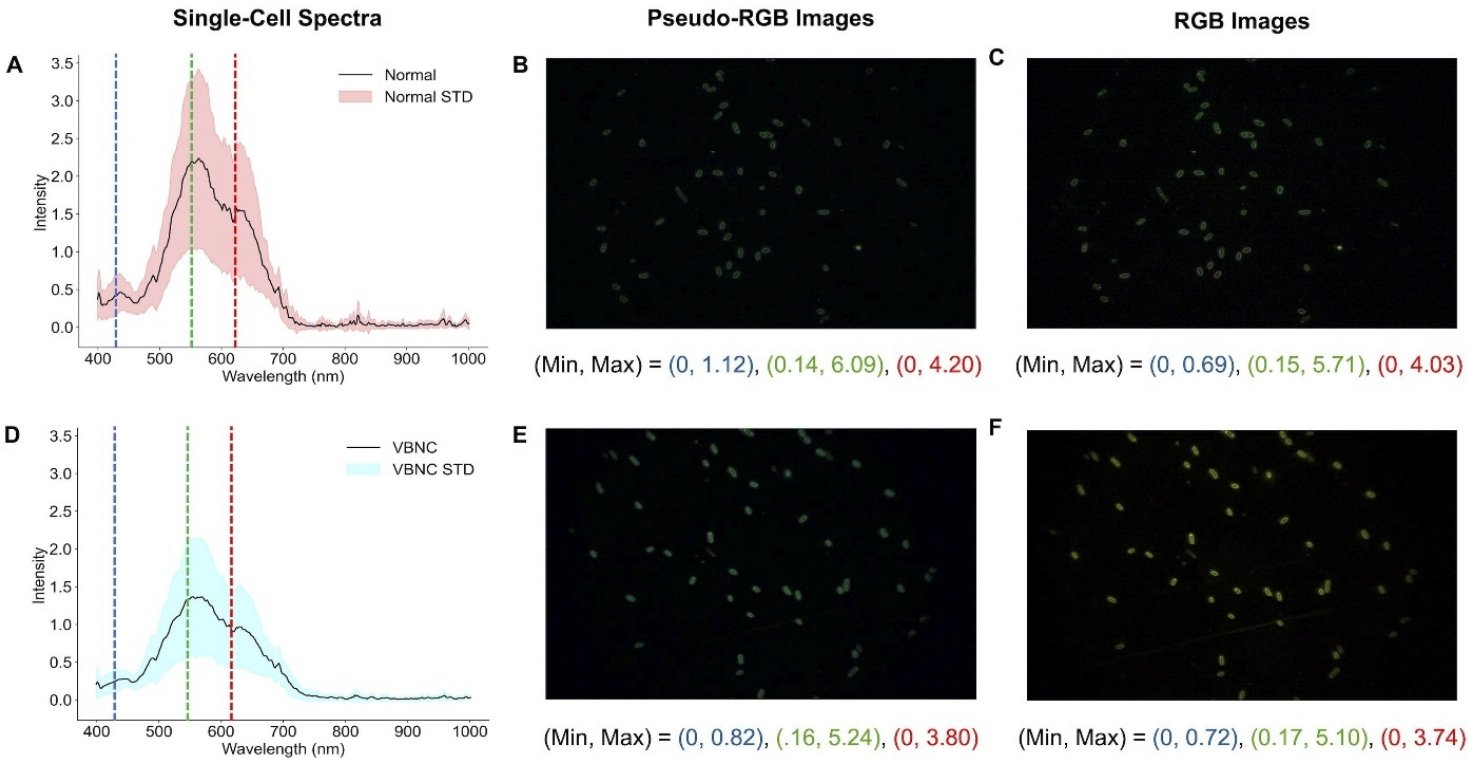

Figure 3.5 Single-cell spectra and example images extracted from hyperspectral data for (A–C) normal and (D–F) VBNC *E. coli* cells. The single-cell spectra (A, D) show mean values with their standard deviations (n = 15). The dotted lines within these spectra indicate the characteristic spectral wavelengths used in each pseudo-RGB channel. Pseudo-RGB images (B, E) and RGB images (C, F) are displayed with their respective minimum and maximum spectral intensities for each channel. The brightness (+25%) and contrast (−25%) of the example images were adjusted for publication clarity.

3.4.3 CNN classification of imagery from hyperspectral data

To capture physiological changes in *E. coli* cells represented by their spectral profiles, pseudo-RGB images were used to train the EfficientNetV2-based CNN architecture to distinguish between normal and VBNC cells. As shown in **Figure 3.6A**, the model trained on pseudo-RGB images achieved an accuracy of 97.1% on the held-out set of 20 testing hyperspectral datasets. In comparison, **Figure 3.6B** shows that the model trained on standard color images achieved an accuracy of 83.3% on the same testing dataset. These results highlight the improved classification performance, particularly with VBNCs, when using pseudo-RGB images derived from characteristic spectral wavelengths.

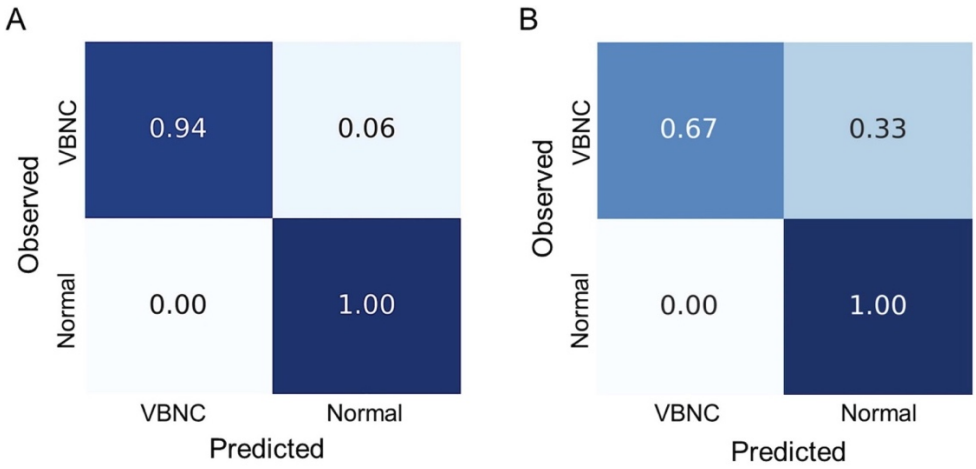

Figure 3.6 Confusion matrices for the classification of normal and VBNC cells using the EfficientNetV2 variant for (A) pseudo-RGB images and (B) standard color images extracted from the held-out testing hyperspectral datasets.

3.5 Discussion

3.5.1 Low-concentration antimicrobial stressors can induce VBNC state in E. coli

The oxidative and acidic stressors induced by 0.01% H_2O_2 and 0.001% PAA led to the entry of *E. coli* K-12 into the VBNC state within 72 h (**Figure 3.4**). This can be attributed to the mechanisms by which each stressor affects bacterial cells. Acidic stress results in protein and DNA damage, while oxidative stress impairs protein production (Guan and Liu, 2019; Fasnacht and Polacek, 2021). The demonstrated induction of the VBNC state by these low-concentration oxidative and acidic stress solutions highlights the impact of the potential mechanisms behind VBNC induction, raising concerns about the effectiveness of commonly used disinfectants (Oliver 2010; Robben 2018). It is noteworthy that the concentrations in this study are much lower than those recommended for disinfection, suggesting that exposure is more likely to occur through residues rather than direct application. Similar findings have been reported for *L. monocytogenes* and *Listeria* spp. Exposed to low levels of benzalkonium chloride, where most isolates acquired tolerance to low levels of this antimicrobial (Bolten et al., 2022). Additionally, chlorination and UV radiation have been shown to induce the VBNC state in *E. coli*, highlighting the potential risk associated with antimicrobial residues (Zhu et al., 2022). However, there remains ongoing debate regarding the confirmation of VBNC viability, with some researchers suggesting that membrane integrity-based dyes, such as those used in this study, may misidentify non-viable cells as viable (Liu et al., 2023). While the SYTO 9 dye in the Live/Dead viability kit is widely used to indicate membrane integrity, some viable bacteria may exclude it. Recent perspectives emphasize the need for species-specific nucleic acid amplification and resuscitation to more accurately confirm VBNC states (Liu et al., 2023). Future studies could integrate additional validation techniques to improve VBNC confirmation while using hyperspectral data

to further characterize physiological states, providing a more comprehensive analysis of VBNC detection.

3.5.2 Hyperspectral microscopy captures physiological changes in VBNC cells as imagery

Hyperspectral microscopy allowed for detailed spatial and spectral characterization of both normal and VBNC cells. Unlike traditional optical microscopy techniques, hyperspectral microscopy is non-invasive and captures a spectrum for each pixel, providing a rich dataset that includes both spatial and spectral information (Park et al., 2023a). The differences in spectral intensities between normal and VBNC cells reflect the effects of stressors on cellular biochemical activities. The overall lower spectral intensity observed in VBNC cells compared to normal cells (**Figure 3.5**) can be attributed to the reduced metabolic activity inherent to the survival state of VBNC cells (Oliver 2010). In contrast, it has been reported that dead cells may exhibit much higher spectral intensities than live cells (Park et al., 2023b). This discrepancy can be attributed to the different mechanisms underlying cell death and the induction of the VBNC state. In the study by Park et al. (2023b), cell death was induced by autoclaving, whereas VBNC cells in this study were subjected to sublethal stressors. While this study focused on VBNC induction due to low-level antimicrobials, the spectrochemical signatures identified, such as shifts in characteristic spectral wavelengths and reduced spectral intensity linked to metabolic activity, may also reflect similar changes in VBNC cells induced by other stressors. For instance, İzgördü et al. (2024) identified spectral bands associated with biomolecular signatures of RNA as consistent biomarkers for detecting VBNC cells under stress conditions, including temperature, metal, and antibiotics. These findings suggest that hyperspectral microscopy could be further investigated to detect VBNC cells induced by a broader range of stressors through the identification of additional spectrochemical biomarkers. Future studies could build on this

framework by exploring how diverse stress-induced VBNC states produce unique spectrochemical features and by integrating hyperspectral microscopy with advanced chemometric analyses to enhance its applicability. Overall, the success of hyperspectral microscopy in capturing physiological signals sufficient for classifying VBNC cells induced by low-level antimicrobials suggests that this framework could be further explored and adapted for detecting VBNCs induced by other stressors, including low temperatures, pH, high salt concentrations, and oligotrophic conditions.

3.5.3 CNN automates the rapid detection of VBNCs from hyperspectral data

By leveraging the physiological differences between normal and VBNC cells captured in hyperspectral datasets, this study demonstrates improved VBNC classification with pseudo-RGB images compared to standard color images (**Figure 3.6**). The dual capability of hyperspectral datasets enables accurate identification of such physiological differences, which may not be visible with standard imaging methods that provide only morphological information. Our CNN architecture could quickly and effectively learn patterns and features in the spatial distributions of spectral intensities that differentiate the physiological states of bacterial cells. A key advantage of this AI-enabled hyperspectral microscopy framework is its speed, as it allows for imaging bacterial suspensions without the need for time-consuming enrichment steps, which typically take additional days in conventional culture-based techniques (Foddai and Grant 2020).

Another important advantage is its ability to classify VBNC cells without requiring specialized reagents, making it particularly suitable for resource-limited environments. Unlike species-specific nucleic acid amplification methods, our approach leverages spectrochemical signatures to detect VBNC cells using simple resources, such as de-ionized water, offering a rapid and resource-efficient screening tool. This capability complements advanced molecular

methods by offering early insights into bacterial species and their physiological states, which can guide the selection of species-specific amplification techniques for further precise testing. Future work could integrate this framework with molecular methods to validate consistency and enhance the reliability of testing results. This detection framework holds strong potential for food safety inspections, where fast and reliable detection of VBNC cells is essential to reducing the risk of foodborne outbreaks. By enabling real-time monitoring as a primary screening tool in food processing facilities, it allows for early pathogen detection and guides further lab testing. This approach could prevent large-scale recalls, reduce the spread of foodborne illness, and improve public health by addressing risks before products reach consumers.

Furthermore, the model's robustness and data efficiency were enhanced by a combination of standard augmentation strategies that simulate variations in illumination, focusing, sensor noise, and missing information during microscope imaging. These augmentations maximized data diversity for effective feature extraction and led to an increase in classification accuracy from 91.4% to 97.1% for pseudo-RGB images (data not shown). Follow-on studies may further strengthen this framework by developing advanced augmentation techniques tailored for hyperspectral datasets, employing domain adaptation techniques commonly used in biomedical imaging to improve data diversity and enhance generalization of AI-enabled imaging across different setups (Gu et al., 2019; Azizi et al., 2023).

Additionally, utilized the state-of-the-art CNN architecture, EfficientNetV2, an image classification model selected for its high accuracy and computational efficiency. This follows the standard progression in deep learning, where image classification models often serve as the foundation for more advanced computer vision tasks, such as localization, quantification, and segmentation. While our study demonstrated strong classification performance, precise

quantification of viable cells remains a challenge compared to molecular methods, such as propidium monoazide-quantitative polymerase chain reaction (PMA-qPCR) (Truchado et al., 2020; Shi et al., 2022). PMA-qPCR is well-established in research for its ability to distinguish viable bacterial cells from dead ones by targeting DNA in cells with intact membranes. Its demonstrated utility in complex food matrices highlights its importance for food safety assessments, where detecting viable cells is critical. In our previous work, the Faster R-CNN object detection model was applied to quantify viable *E. coli* cells (Yi et al., 2023), demonstrating the feasibility of using object detection for such tasks. Faster R-CNN, however, predates EfficientNetV2, and we anticipate that leveraging the superior accuracy and computational efficiency of EfficientNetV2 as the backbone for object detection could further improve quantification performance. Extending the hyperspectral microscopy framework in this manner could address a key limitation of the current study by enabling quantification of individual cells while preserving the advantage of not requiring species-specific amplification. Thus, combining quantification with VBNC detection could offer a more comprehensive pathogen detection framework, validated through quantitative molecular techniques like PMA-qPCR to ensure accuracy and reliability.

3.6 Conclusions

The findings of this study underscore the potential of AI-enabled hyperspectral microscopy as a valuable tool for accurate and efficient detection of VBNCs induced by low-concentration antimicrobial stressors. This study demonstrated that exposing *E. coli* to low-level antimicrobials (0.001% PAA and 0.01% H_2O_2) for 3 days can induce the VBNC state, confirming that antimicrobial residues can lead to VBNCs. By training a CNN architecture using pseudo-RGB images from HMI, the study achieved up to 97% accuracy in classifying normal

and VBNC cells without extended incubation time. These results highlight the potential of automating and accelerating VBNC detection, demonstrating the applicability of integrating hyperspectral microscopy and CNN image classification for rapid bacterial detection. Future applications may include testing on various foodborne pathogens at different levels of discrimination, exploring other stressors, and detecting VBNCs in real-world food samples without the need for enrichment, offering enhanced capabilities for ensuring food safety and public health.

Data availability

The code and extracted image datasets will be available at https://github.com/food-ai-engineering-lab/VBNC-Detection-JFP. Future updates will be integrated into this repository.

BIBLIOGRAPHY

Ao, X., Eloranta, J., Huang, C.-H., Santoro, D., Sun, W., Lu, Z., & Li, C. (2021). Peracetic acid-based advanced oxidation processes for decontamination and disinfection of water: A review. *Water Research*, *188*, 116479. https://doi.org/10.1016/j.watres.2020.116479

Azizi, S., Culp, L., Freyberg, J., Mustafa, B., Baur, S., Kornblith, S., Chen, T., Tomasev, N., Mitrović, J., Strachan, P., Mahdavi, S. S., Wulczyn, E., Babenko, B., Walker, M., Loh, A., Chen, P.-H. C., Liu, Y., Bavishi, P., McKinney, S. M., … Natarajan, V. (2023). Robust and data-efficient generalization of self-supervised machine learning for diagnostic imaging. *Nature Biomedical Engineering*, *7*(6), 756–779. https://doi.org/10.1038/s41551-023-01049-7

Barzan, G., Sacco, A., Mandrile, L., Giovannozzi, A. M., Chiara Portesi, & Rossi, A. M. (2021). Hyperspectral chemical imaging of single bacterial cell structure by Raman spectroscopy and machine learning. *Applied Sciences*, *11*(8), 3409–3409. https://doi.org/10.3390/app11083409

Bolten, S., Harrand, A. S., Skeens, J., & Wiedmann, M. (2022). Nonsynonymous mutations in fepR are associated with adaptation of *Listeria monocytogenes* and other *Listeria* spp. to low concentrations of benzalkonium chloride but do not increase survival of *L. monocytogenes* and other *Listeria* spp. after exposure to benzalkonium chloride concentrations recommended for use in food processing environments. *Applied and Environmental Microbiology*, *88*(11), e00486-22. https://doi.org/10.1128/aem.00486-22

Buslaev, A., Iglovikov, V. I., Khvedchenya, E., Parinov, A., Druzhinin, M., & Kalinin, A. A. (2020). Albumentations: fast and flexible image augmentations. *Information*, *11*(2), 125. https://doi.org/10.3390/info11020125

Chen, Q., Bao, H., Li, H., Wu, T., Qi, X., Zhu, C., ... & Qi, Y. (2024). Microscopic identification of foodborne bacterial pathogens based on deep learning method. *Food Control*, 110413. https://doi.org/10.1016/j.foodcont.2024.110413

Chen, S., Li, X., Wang, Y., Zeng, J., Ye, C., Li, X., ... & Yu, X. (2018). Induction of *Escherichia coli* into a VBNC state through chlorination/chloramination and differences in characteristics of the bacterium between states. *Water research*, *142*, 279-288.

Cho, I.-H., & Ku, S. (2017). Current technical approaches for the early detection of foodborne pathogens: challenges and opportunities. *International Journal of Molecular Sciences*, *18*(10), 2078. https://doi.org/10.3390/ijms18102078

Fasnacht, M., & Polacek, N. (2021). Oxidative stress in bacteria and the central dogma of molecular biology. *Frontiers in Molecular Biosciences*, *8*, 671037. https://doi.org/10.3389/fmolb.2021.671037

Foddai, A. C. G., & Grant, I. R. (2020). Methods for detection of viable foodborne pathogens: current state-of-art and future prospects. *Applied Microbiology and Biotechnology*, *104*(10), 4281–4288.

Guan, N., & Liu, L. (2020). Microbial response to acid stress: mechanisms and applications. *Applied Microbiology and Biotechnology*, *104*(1), 51–65. https://doi.org/10.1007/s00253-019-10226-1

Gu, Y., Ge, Z., Bonnington, C. P., & Zhou, J. (2019). Progressive transfer learning and adversarial domain adaptation for cross-domain skin disease classification. *IEEE Journal of Biomedical and Health Informatics*, *24*(5), 1379–1393. https://doi.org/10.1109/JBHI.2019.2942429

Guo, L., Wan, K., Zhu, J., Ye, C., Chabi, K., & Yu, X. (2021). Detection and distribution of vbnc/viable pathogenic bacteria in full-scale drinking water treatment plants. *Journal of Hazardous Materials*, *406*, 124335. https://doi.org/10.1016/j.jhazmat.2020.124335

Hu, M., & Gurtler, J. B. (2017). Selection of surrogate bacteria for use in food safety challenge studies: A review. *Journal of Food Protection*, *80*(9), 1506–1536. https://doi.org/10.4315/0362-028x.jfp-16-536

İzgördü, Ö. K., Gurbanov, R., & Darcan, C. (2024). Understanding the transition to viable but non-culturable state in *Escherichia coli* W3110: a comprehensive analysis of potential spectrochemical biomarkers. *World Journal of Microbiology and Biotechnology*, *40*(7), 1–15. https://doi.org/10.1007/s11274-024-04019-6

Kang, R., Park, B., Eady, M., Ouyang, Q., & Chen, K. (2020). Single-cell classification of foodborne pathogens using hyperspectral microscope imaging coupled with deep learning frameworks. *Sensors and Actuators B: Chemical*, *309*, 127789. https://doi.org/10.1016/j.snb.2020.127789

Kim, J.-M., Zhang, B.-Z., & Park, J.-M. (2023). Comparison of sanitization efficacy of sodium hypochlorite and peroxyacetic acid used as disinfectants in poultry food processing plants. *Food Control*, *152*, 109865. https://doi.org/10.1016/j.foodcont.2023.109865

Li, Y., Huang, T. Y., Ye, C., Chen, L., Liang, Y., Wang, K., & Liu, J. (2020a). Formation and control of the viable but non-culturable state of foodborne pathogen *Escherichia coli* O157: H7. *Frontiers in Microbiology*, *11*, 1202.

Li, Y., Huang, T.-Y., Mao, Y., Chen, Y., Shi, F., Peng, R., Chen, J., Yuan, L., Bai, C., Chen, L., Wang, K., & Liu, J. (2020b). Study on the viable but non-culturable (VBNC) state formation of *Staphylococcus aureus* and its control in food system. *Frontiers in Microbiology*, *11*, 599739. https://doi.org/10.3389/fmicb.2020.599739

Litjens, G., Kooi, T., Bejnordi, B. E., Setio, A. A. A., Ciompi, F., Ghafoorian, M., van der Laak, J. A. W. M., van Ginneken, B., & Sánchez, C. I. (2017). A survey on deep learning in medical image analysis. *Medical Image Analysis*, *42*, 60–88. https://doi.org/10.1016/j.media.2017.07.005

Liu, J., Zhou, R., Li, L., Peters, B. M., Li, B., Lin, C. W., ... & Shirtliff, M. E. (2017). Viable but non-culturable state and toxin gene expression of enterohemorrhagic *Escherichia coli* O157 under cryopreservation. *Research in Microbiology*, *168*(3), 188-193.

Liu, J., Yang, L., Kjellerup, B. V., & Xu, Z. (2023). Viable but nonculturable (VBNC) state, an underestimated and controversial microbial survival strategy. *Trends in Microbiology*, *31*(10), 1013–1023.

Ma, L., Yi, J., Wisuthiphaet, N., Earles, M., & Nitin, N. (2023). Accelerating the detection of bacteria in food using artificial intelligence and optical imaging. *Applied and Environmental Microbiology*, *89*(1), e01828-22. https://doi.org/10.1128/aem.01828-22

Mousavizadegan, M., Shalileh, F., Mostajabodavati, S., Mohammadi, J., & Hosseini, M. (2024). Machine learning-assisted image-based optical devices for health monitoring and food safety. *TrAC Trends in Analytical Chemistry*, 117794. https://doi.org/10.1016/j.trac.2024.117794

Oliver, J. D. (2000). The public health significance of viable but nonculturable bacteria. *Nonculturable Microorganisms in the Environment*, 277–300. https://doi.org/10.1007/978-1-4757-0271-2_16

Oliver, J. D. (2010). Recent findings on the viable but nonculturable state in pathogenic bacteria. *FEMS Microbiology Reviews*, *34*(4), 415–425. https://doi.org/10.1111/j.1574-6976.2009.00200.x

Park, B., Shin, T., Kang, R., Fong, A., McDonogh, B., & Yoon, S.-C. (2023a). Automated segmentation of foodborne bacteria from chicken rinse with hyperspectral microscope imaging and deep learning methods. *Computers and Electronics in Agriculture*, *208*, 107802. https://doi.org/10.1016/j.compag.2023.107802

Park, B., Shin, T., Wang, B., McDonogh, B., & Fong, A. (2023b). Classification between live and dead foodborne bacteria with hyperspectral microscope imagery and machine learning. *Journal of Microbiological Methods*, *209*, 106739. https://doi.org/10.1016/j.mimet.2023.106739

Paszke, A., Gross, S., Massa, F., Lerer, A., Bradbury, J., Chanan, G., Killeen, T., Lin, Z., Gimelshein, N., Antiga, L., Desmaison, A., Kopf, A., Yang, E., DeVito, Z., Raison, M., Tejani, A., Chilamkurthy, S., Steiner, B., Fang, L., … Chintala, S. (2019). PyTorch: An Imperative Style, High-Performance Deep Learning Library. *Advances in Neural Information Processing Systems*, *32*.

Pinto, D., Santos, M. A., & Chambel, L. (2015). Thirty years of viable but nonculturable state research: Unsolved molecular mechanisms. *Critical Reviews in Microbiology*, *41*(1), 61–76. https://doi.org/10.3109/1040841X.2013.794127

Piqueras, S., Duponchel, L., Tauler, R., & de Juan, A. (2011). Resolution and segmentation of hyperspectral biomedical images by multivariate curve resolution-alternating least squares. *Analytica Chimica Acta*, *705*(1), 182–192. https://doi.org/10.1016/j.aca.2011.05.020

Ramamurthy, T., Ghosh, A., Pazhani, G. P., & Shinoda, S. (2014). Current Perspectives on Viable but Non-Culturable (VBNC) Pathogenic Bacteria. *Frontiers in Public Health*, *2*, 91118. https://doi.org/10.3389/fpubh.2014.00103

Robben, C., Fister, S., Witte, A. K., Schoder, D., Rossmanith, P., & Mester, P. (2018). Induction of the viable but non-culturable state in bacterial pathogens by household cleaners and inorganic salts. *Scientific Reports*, *8*(1), 15132. https://doi.org/10.1038/s41598-018-33595-5

Salive, A. F. V., Prudêncio, C. V., Baglinière, F., Oliveira, L. L., Ferreira, S. O., & Vanetti, M. C. D. (2020). Comparison of stress conditions to induce viable but non-cultivable state in *Salmonella*. *Brazilian Journal of Microbiology*, *51*(3), 1269–1277. https://doi.org/10.1007/s42770-020-00261-w

Scaramuzza, N., Cigarini, M., Mutti, P., & Berni, E. (2020). Sanitization of packaging and machineries in the food industry: Effect of hydrogen peroxide on ascospores and conidia of filamentous fungi. *International Journal of Food Microbiology*, *316*, 108421. https://doi.org/10.1016/j.ijfoodmicro.2019.108421

Seabold, S., & Perktold, J. (2010). Statsmodels: econometric and statistical modeling with python. *Proceedings of the 9th Python in Science Conference*.

Shi, Z., Li, X., Fan, X., Xu, J., Liu, Q., Wu, Z., & Pan, D. (2022). PMA-qPCR method for the selective quantitation of viable lactic acid bacteria in fermented milk. *Frontiers in Microbiology*, *13*, 984506.

Tan, M., & Le, Q. V. (2021). EfficientNetV2: smaller models and faster training. *International Conference on Machine Learning.* 10096–10106.

Tao, C., Du, J., Tang, Y., Wang, J., Dong, K., Yang, M., Hu, B., & Zhang, Z. (2022). A deep-learning based system for rapid genus identification of pathogens under hyperspectral microscopic images. *Cells*, *11*(14), 2237. https://doi.org/10.3390/cells11142237

Tao, C., Du, J., Wang, J., Hu, B., & Zhang, Z. (2023). Rapid identification of infectious pathogens at the single-cell level via combining hyperspectral microscopic images and deep learning. *Cells*, *12*(3), 379. https://doi.org/10.3390/cells12030379

Truchado, P., Gil, M. I., Larrosa, M., & Allende, A. (2020). Detection and quantification methods for viable but non-culturable (VBNC) cells in process wash water of fresh-cut produce: industrial validation. *Frontiers in Microbiology*, *11*. https://doi.org/10.3389/fmicb.2020.00673

Wideman, N. E., Oliver, J. D., Crandall, P. G., & Jarvis, N. A. (2021). Detection and potential virulence of viable but non-culturable (VBNC) *Listeria monocytogenes*: a review. *Microorganisms*, *9*(1), 194. https://doi.org/10.3390/microorganisms9010194

Yi, J., Wisuthiphaet, N., Raja, P., Nitin, N., & Earles, J. M. (2023). AI-enabled biosensing for rapid pathogen detection: From liquid food to agricultural water. *Water Research*, *242*, 120258. https://doi.org/10.1016/j.watres.2023.120258

Zhu, L., Shuai, X., Xu, L., Sun, Y., Lin, Z., Zhou, Z., ... & Chen, H. (2022). Mechanisms underlying the effect of chlorination and UV disinfection on VBNC state *Escherichia coli* isolated from hospital wastewater. *Journal of Hazardous Materials*, *423*, 127228.

CHAPTER 4: RAPID SALMONELLA SEROVAR CLASSIFICATION USING AI-ENABLED HYPERSPECTRAL MICROSCOPY WITH ENHANCED DATA PREPROCESSING AND MULTIMODAL FUSION

4.1 Abstract

Traditional *Salmonella* serovar identification involves lengthy enrichment steps using selective media, delaying timely food safety interventions. This study presents a rapid one-step method combining hyperspectral microscopy with artificial intelligence (AI) for detection and identification of *Salmonella* serovars. Five serovars (Enteritidis, Infantis, Kentucky, Johannesburg, 4,[5],12:i:-) were analyzed using fresh cultures placed onto glass slides and rehydrated only with sterilized deionized water. Hyperspectral microscopy acquired 100 hyperspectral data cubes per serovar (n=500) from 6 biological replicates, from which multiple single-cell spectra and corresponding standard color images were obtained. Two preprocessing approaches were compared for spectral feature engineering: i) manual feature selection based on domain knowledge, and ii) data-driven feature extraction using principal component analysis. Classification performance of k-nearest neighbors, support vector machine, random forest, and multilayer perceptron (MLP) was evaluated by accuracy, precision, and recall. Additionally, multimodal fusion integrated spectral features with spatial information from standard color images analyzed by a convolutional neural network. PCA-derived features consistently outperformed manual feature selection, achieving highest accuracy with MLP (81.08%). A multimodal model further improved accuracy (82.40%) while reducing overfitting. Our findings demonstrate that AI-enabled hyperspectral microscopy accelerates *Salmonella* serovar classification through enhanced data preprocessing and multimodal fusion, effectively leveraging critical insights from high-dimensional data.

4.2 Introduction

Salmonella is one of the most significant foodborne pathogens, with serovars that exhibit distinct host reservoirs, pathogenicity, and epidemiological profiles, making accurate serovar-level discrimination essential (Bell et al., 2016; CDC, 2024). The current standard for detection and identification of *Salmonella* serovars in food relies on a multi-step culture-based method outlined in regulatory guidelines such as the Food and Drug Administration (FDA) Bacteriological Analytical Manual (BAM). This method involves an initial 24-h non-selective pre-enrichment, followed by a 24-h selective enrichment, and subsequent isolation on selective agar media for an additional 24–48 h. Confirmatory serotyping via slide agglutination using O and H antigen-specific antisera (the Kauffmann-White scheme) further extends the identification process by 2–3 days (Daquigan et al., 2016; FDA, 2024; Patel et al., 2024). Efforts to reduce the overall processing times have led to the development of rapid molecular detection methods, which partially minimize the need for selective enrichment (Ranieri et al., 2013; Herrera-León et al., 2007; Grinevich et al., 2024). However, these methods still require initial enrichment steps, may detect non-viable cells, and continue to necessitate pure isolates for definitive serovar identification (Patel et al., 2024). Additionally, robust data analysis often involves specialized domain expertise and skilled personnel. Therefore, there remains an unmet need for a rapid one-step method capable of simultaneously detecting and identifying viable *Salmonella* serovars without extensive enrichment, thereby complementing and enhancing rapid screening approaches.

To address these unmet needs, recent advancements in optical imaging and artificial intelligence (AI) present promising solutions. Optical imaging techniques that leverage intrinsic bacterial characteristics, such as scattering patterns, autofluorescence, and refractive index, allow

for label-free analysis, minimizing extensive sample preparation and reducing dependence on selective enrichment process (Bhunia et al., 2022; Wang et al., 2022; McGoverin et al., 2021). Similarly, classical microscopy-based approaches have been enhanced by image processing algorithms that differentiate bacterial species based on observable parameters such as shape, size, and refractive index (Franco-Duarte et al., 2019). More recently, incorporating deep convolutional neural networks (CNNs) further accelerated the analysis of high-resolution image data by leveraging convolutional filters to extract fine-grained spatial features and hierarchical relationships, thus enabling simultaneous detection and identification of viable bacteria (Ma et al., 2023; Yi et al., 2023). The integration of AI models underscores the value of spatial relationships within image data, highlighting hidden yet informative patterns that can enhance rapid classification of pathogens.

Hyperspectral microscopy provides an advanced optical imaging by capturing high-dimensional data across a broader electromagnetic spectrum, significantly enhancing pathogen classification capabilities. This non-invasive technique utilizes intrinsic bacterial light-scattering fingerprints, offering detailed insights into biochemical, metabolic, and structural properties beyond basic cellular morphology (Kang et al., 2020a). Historically, hyperspectral microscopy applications primarily focused on spectral data for pathogen classification, using spatial data mainly for identifying cellular regions of interest (ROIs) (Kang et al., 2020a, Wu et al., 2024; Zhu et al., 2023). These studies employed various data preprocessing methods, followed by comparative evaluations of traditional machine learning classifiers, such as random forest (RF), support vector machine (SVM), and k-nearest neighbors (k-NN), to determine optimal algorithm. Early studies demonstrated successful differentiation of closely related *Salmonella* serovars (Eady et al., 2015; Eady & Park 2016), yet their emphasis on model optimization, rather than

end-to-end automation, necessitated manual preprocessing steps for data quality and interpretation. More recent advancements in AI-enabled hyperspectral microscopy have effectively integrated spatial data through CNNs, enabling automated extraction of spatial features and hierarchical modeling. These improvements have enhanced classification accuracy at the species level (Kang et al., 2020; Tao et al., 2023) and facilitated discrimination of physiological states such as viability (Park et al., 2023a) or stress responses (Papa et al., 2024). Furthermore, some of these studies have shown that multimodal fusion of spectral and spatial data improves classification performance. Given these promising advancements in other pathogens, applying multimodal fusion specifically to *Salmonella* serovar classification represents a critical next step toward achieving rapid, accurate, and generalizable serovar-level classification.

Thus, this study introduces a rapid AI-enabled hyperspectral microscopy method for the rapid classification of *Salmonella* serovars with enhanced generalizability. The objectives of this study are to i) develop a rapid serovar classification approach requiring minimal sample preparation without enrichment, ii) compare manual feature selection and data-driven feature extraction approaches to optimize spectral data preprocessing, and iii) evaluate multimodal fusion of spectral and spatial data to enhance classification accuracy and reduce overfitting. As illustrated in **Figure 4.1**, our AI-enabled hyperspectral microscopy method addresses these objectives by directly analyzing fresh overnight cultures of five *Salmonella* serovars (Kentucky, Infantis, Enteritidis, 4,[5],12:i:-, and Johannesburg), without prolonged enrichment and extensive reagents. To leverage the rich information present in hyperspectral data, the analysis employed two parallel branches: a spectral branch and a spatial branch. Within the spectral branch, single-cell spectral derived from hyperspectral data cubes were preprocessed using manual feature

selection and data-driven feature extraction approaches, followed by traditional machine learning algorithms to determine the optimal combination. In the spatial branch, standard color images derived from hyperspectral data cubes were analyzed using a CNN. Outputs from both branches were then integrated using prediction-level multimodal fusion. Overall, this study not only accelerates serovar-level classification but also establishes the groundwork for automated end-to-end pathogen classification, significantly enhancing food safety monitoring and enabling timely interventions.

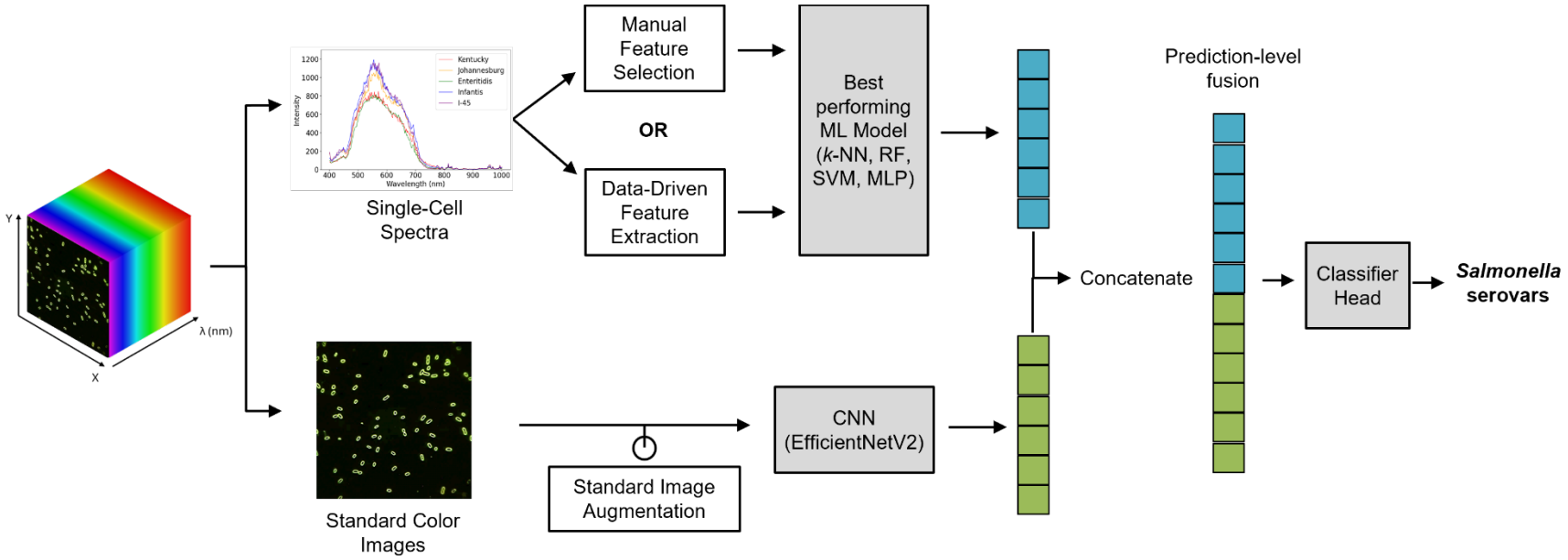

Figure 4.1 Overall workflow of hyperspectral data collection, preprocessing, and classification. ML: Machine learning. CNN: Convolutional neural network.

4.3 Materials and methods

4.3.1 Data acquisition

4.3.1.1 Bacterial strains and sample preparation

In this study, a total of five *Salmonella* serovars (Enteritidis, Infantis, Kentucky, Johannesburg, and 4,[5],12:i:-) were selected due to their critical roles in food safety and public health and obtained from the Food Safety Laboratory at Cornell University. The *Salmonella* stock cultures were maintained at 4°C on LB Lennox agar plates (Thermo Fisher, Waltham, MA, USA). Fresh cultures for data collection were inoculated into 9 mL of tryptic soy broth (Difco, BD, Sparks, MD, USA) supplemented with 0.6% (w/v) yeast extract (Difco, BD) and incubated at 37°C for 16 h. Cells in the logarithmic phase were harvested by centrifugation at 4,450 rpm for 15 min at 4°C (SYTO 9, SLA-1500, Hampton, NH, USA). The final pellet was suspended in sterile de-ionized (DI) water for a final concentration of 10^5 CFU/mL for hyperspectral microscopy image acquisition. Microscope slides of bacterial cells were prepared following a modified version of a previously published method (Papa et al., 2024; Park et al., 2023a). For each serovar, 2 µL of bacterial suspension was deposited onto a sterile glass microscope slide and air dried for 15 min at 23°C with an average relative humidity of 43% in a fume hood. After 15 min, 1 µL of sterile DI water was added to affix a plastic coverslip, securing the cells in place.

4.3.1.2 Hyperspectral microscopy and data consistency check

Hyperspectral microscopy data collection was conducted for all five serovars following our previously published method (Papa et al., 2024). A total of 500 hyperspectral data cubes (100 for each serovar) were acquired using an Olympus BX43 upright optical microscope (Evident Scientific, Waltham, MA, USA) equipped with CytoViva patented enhanced darkfield illumination optics, a tungsten halogen lamp (CytoViva, Auburn, AL, USA), and a HinaLea

4250 hyperspectral camera (HinaLea, Emeryville, CA, USA). The spatial resolution of the imaging system was 1936 × 1216 pixels, covering a spectral range of 399–1,000 nm with 303 spectral bands. Imaging was performed using a 100× oil immersion objective lens, with an exposure time of 200 ms and a gain setting of 16 dB.

For each data collection session, three subcultures per serovar were incubated across two independent sessions to yield a total of six biological replicates. Each subculture was allocated 3 microscope slides for data collection, serving as technical replicates. For each technical replicate, 6 distinct fields of view were imaged per microscope slide, with careful selection to prevent overlapping cells. This approach yielded a total of 500 hyperspectral data cubes (100 per serovar) for further analysis. Raw hyperspectral data were analyzed with the Environment for Visualizing Images (ENVI) software (version 6.0) to ensure consistency between the dataset within each serovar.

4.3.2 Data preprocessing and spectral feature engineering

After confirming data consistency, raw hyperspectral data were processed following the workflow illustrated in **Figure 4.1**. The dataset was initially partitioned into training and testing sets (70:30 split ratio, fixed random state = 42) to prevent data leakage during preprocessing and ensure reproducibility. Spectral information from bacterial cells were obtained following previously published methods. Briefly, automated segmentation of single-cell regions of interest (ROIs) was performed using attention-gated residual U-Net (ARG2U-Net) (Park et al., 2023) to derive average single-cell spectra. The resulting spectra were then transformed using standard normal variate (SNV) to remove baseline effects caused by imaging conditions (Kang et al., 2020a).

These averaged spectral data served as inputs in the spectral branch for subsequent comparisons between two feature engineering approaches: i) manual feature selection and ii) data-driven feature extraction. For manual feature selection, three characteristic wavebands corresponding to the most intense regions near the red, green, and blue ranges across all serovars were manually selected, following the methods in our previous study (Papa et al., 2024). For data-driven feature extraction, principal component analysis (PCA) was applied to the training set to reduce dimensionality by capturing the most informative linear combinations across all wavebands, as opposed to manually selecting only three bands. PCA was implemented using the singular value decomposition function from the Python library NumPy. Before PCA, the training data were mean-centered, and the same mean value was used for test data transformation. The number of principal components (PCs) was chosen to retain 99% of the original variance, ensuring minimal information loss. The PCA transformation was fitted exclusively on the training set and subsequently applied to the test set.

4.3.3 Machine learning classification for spectral branch

4.3.3.1 Model architectures

Four supervised machine learning algorithms were implemented in the spectral branch using Python scikit-learn library to determine the best performing model for *Salmonella* serovar classification. These included three traditional machine learning models widely used in food safety research, *k*-NN, RF, and SVM (Fong et al., 2020; He et al., 2018; Turra et al., 2017; Wu et al., 2024; Seo et al., 2013; Maeda et al., 2018; Signoroni et al., 2018; Kang et al., 2021), as well as a shallow multilayer perceptron (MLP) model. *k*-NN uses a distance-based metric to classify data points based on their nearest neighbors. RF employs an ensemble approach, combining multiple decision trees to improve classification accuracy and reduce overfitting. SVM classifies

samples by identifying an optimal hyperplane to maximize the margin between different classes in feature space. The shallow MLP model was designed to include one hidden layer containing 100 neurons with a ReLU activation function to introduce non-linearity, followed by a linear output layer.

4.3.3.2 Model training

All machine learning models were trained using the PyTorch library for Python (Paszke et al., 2019). Hyperparameter tuning for each model was performed via grid search and 10-fold cross-validation. For k-NN, hyperparameter tuning optimized the number of neighbors (k), leaf size, and distance metric (p), with a search space including k values from 1 to 4, leaf sizes from 1 to 50, and distance metrics of 1 and 2. For RF, hyperparameters optimized included tree depth, minimum samples per split, minimum samples per leaf, and the number of features considered for splitting. The search space included maximum depths of 10, 25, or unlimited, minimum samples per split (5, 7), and leaf sizes (3, 5), with the number of estimators fixed at 100. SVM was optimized with a search space that included a fixed regularization parameter (C = 1), a radial basis function kernel, and polynomial kernel degrees of 3 and 4. Model selection was based on classification accuracy. MLP was trained was trained for 50 epochs using the Adam optimizer (initial learning rate = 0.001) and cross-entropy loss.

4.3.4 Multimodal spectral-spatial fusion

4.3.4.1 CNN for spatial branch

In the spatial branch, standard color images (i.e., RGB images) derived from raw hyperspectral data were analyzed using a CNN to leverage morphological context. The standard color images were created by combining data points at wavelengths of 620 nm (red), 550 nm (green), and 450 nm (blue). Building on methods described by Papa et al. (2024), a modified

EfficientNetV2 architecture was trained using the PyTorch Lightning deep learning framework (Tan & Le, 2021). Various combinations of standard augmentation strategies from the Albumentations library (Buslaev et al., 2020) were applied to enhance model robustness. The pretrained EfficientNetV2 variant (`efficientnetv2_rw_s`) was fine-tuned on the training dataset with a total batch size of 16, using a cross-entropy loss function. Optimization was performed using the AdamW optimizer with an initial learning rate of 0.0001 and a weight decay of 0.001, while a step-based learning rate scheduler reduced the learning rate by a factor of 0.3 every 10 epochs. To mitigate overfitting, early stopping was implemented based on validation loss monitored throughout each epoch.

4.3.4.2 Fusion of spectral and spatial prediction outputs

The multimodal fusion model concatenated prediction-level outputs from the best-performing spectral machine learning model and the CNN spatial model, as shown in **Figure 4.1**. Note that the output dimensions from the spatial and spectral branches differ, as EfficientNetV2 typically outputs a prediction vector matching the number of classes (5 serovars in this case), whereas the spectral branch outputs a vector of length 32. Thus, we modified the EfficientNetV2 model to output a length-32 feature vector that can be concatenated with the output of the spectral branch. The resulting spectral-spatial fused vector had a length of 64. This vector was then fed into the final classifier head, a feed-forward neural network consisting of one hidden layer with 64 neurons, followed by an output layer with 5 neurons corresponding to the number of *Salmonella* serovar classes. The fusion model was trained for 50 epochs using an AdamW optimizer, with different learning rates for the spatial (0.0001) and spectral (0.0001) branches and the fusion classifier head (0.001) to balance learning. The batch size, weight decay, and the remaining training procedures and hyperparameters were the same as in **Section 4.3.4.1**.

4.3.5 Model evaluation and performance metrics

Each model's performance was assessed using classification accuracy, precision, and recall, ensuring a comprehensive evaluation. The formulas used for evaluation were as follows:

$$\text{Accuracy} = \frac{\text{TP} + \text{TN}}{\text{TP} + \text{TN} + \text{FP} + \text{FN}} \times 100 \tag{4.1}$$

$$\text{Precision} = \frac{\text{TP}}{\text{TP} + \text{FP}} \times 100 \tag{4.2}$$

$$\text{Recall} = \frac{\text{TP}}{\text{TP} + \text{FN}} \times 100 \tag{4.3}$$

where TP, TN, FP, FN are true positive, true negative, false positive, and false negative, respectively.

4.4 Results

4.4.1 Comparison of hyperspectral data of *Salmonella* serovars

The results in **Figure 4.2** illustrate spatial and spectral data derived from the raw hyperspectral data cubes. **Figure 4.2** shows example standard color images of a bacterial cell from each *Salmonella* serovar, created by combining data points from red, green, and blue channels. Spatially and morphologically, bacterial cells from all serovars appear visually similar to the human eye. However, **Figure 4.2** reveals clear spectral distinction by the average single-cell spectra obtained from individual bacterial cells. Each serovar shows characteristic variations in spectral intensity and peak wavelengths. *Salmonella* Kentucky exhibited a maximum intensity of 848 at 570 nm, *Salmonella* Johannesburg had a maximum intensity of 1,095 at 564 nm, *Salmonella* Enteritidis had a maximum intensity of 812 at 562 nm, *Salmonella* Infantis had a maximum intensity of 1191 at 555 nm, and *Salmonella* 4,[5],12:i:- had a maximum intensity of 1159 at 553 nm.

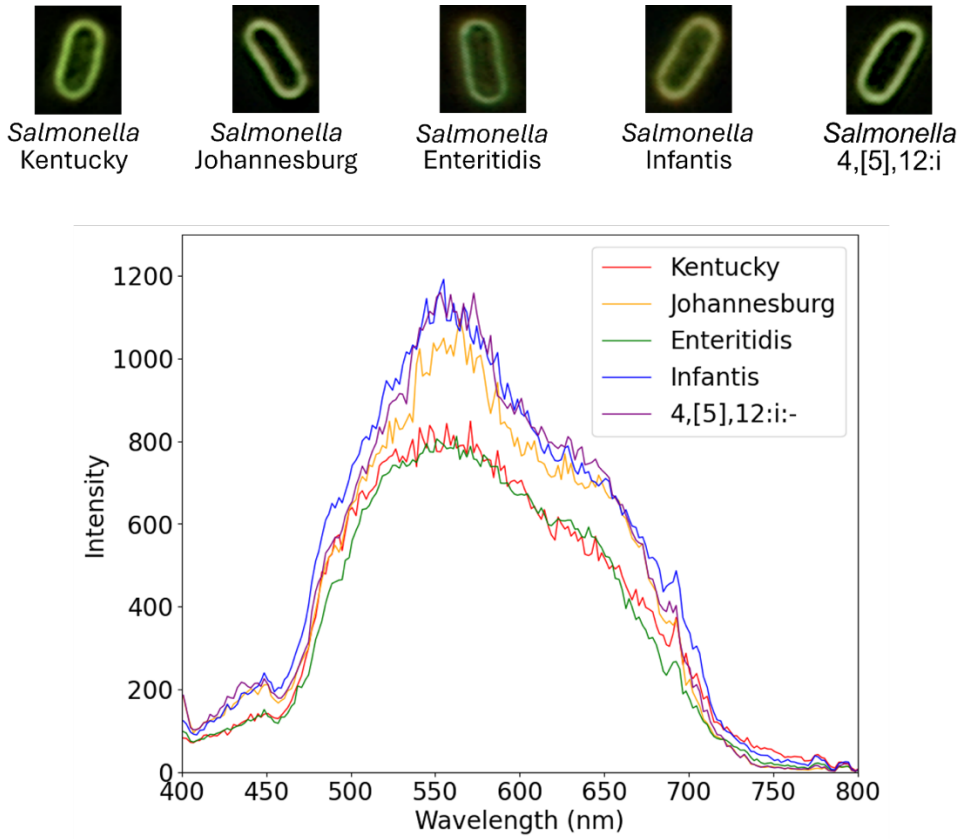

Figure 4.2 Hyperspectral data collected for *Salmonella* serovars: (A) Example standard color images and (B) average single-cell spectra derived from raw hyperspectral data cube.

4.4.2 Selection of the optimal classification model within the spectral branch

4.4.2.1 Influences of manual feature selection and data-driven feature extraction

Global manual feature selection was performed on the average single-cell spectra to identify characteristic wavebands useful for *Salmonella* serovar classification. By analyzing these spectra, three characteristic spectral wavebands at 499, 555, and 628 nm were identified. These wavebands exhibited significantly higher intensity levels compared to those typically captured by wavebands represented by standard red, green, blue channels. This observation highlights the potential importance of these specific wavebands for differentiating among *Salmonella* serovars. Additionally, data-driven feature extraction using PCA was performed on the single-cell spectral dataset. It was found that retaining 18 principal components (PCs) was sufficient to explain 99% of the total data variance. By selecting these 18 PCs, dimensionality was effectively reduced without loss of critical information needed for accurate classification.

4.4.2.2 Performance comparison of machine learning models using spectral features

To identify the best-preforming model within the spectral branch, the classification performance of machine learning algorithms were compared using both manually selected spectral wavebands and PCA-derived spectral features. **Table 4.1** summarizes the classification accuracies obtained from each approach. When employing the three manually selected wavebands, classification accuracies on the test sets (n = 350) for k-NN, SVM, RF, and MLP were 60.13%, 54.05%, 59.45%, and 62.16%, respectively, with corresponding precision values of 60.10%, 55.99%, 58.83%, and 62.09%, and recall values of 60.13%, 54.05%, 59.46%, and 62.16%. In contrast, the use of 18 PCA-derived spectral features, which captured 99% of the total data variance, substantially improved the performance of all models. Specifically, test-set classification accuracies increased to 73.65%, 75.00%, 77.70%, and 81.08%, for k-NN, SVM,

RF, and MLP, respectively, along with improved precision values of 74.19%, 76.26%, 78.63%, and 81.08%, and recall values of 73.65%, 75.00%, 77.70%, and 81.08%.

Table 4.1 Impact of feature engineering on spectral data with machine learning models using manual feature selection and data-driven feature extraction.

Spectral features	Model	Accuracy (%)		Precision (%)		Recall (%)	
		Train	Test	Train	Test	Train	Test
Manual selection[1]	k-NN	67.24	60.13	67.65	60.10	67.24	60.13
	SVM	55.94	54.05	58.06	55.99	55.94	54.05
	RF	100.00	59.45	100.00	58.83	100.00	59.46
	MLP	**64.64**	**62.16**	**65.00**	**62.09**	**64.64**	**62.16**
Data-driven extraction[2]	k-NN	81.74	73.65	81.86	74.19	81.74	73.65
	SVM	81.74	75.00	82.10	76.26	81.74	75.00
	RF	100.00	77.70	100.00	78.63	100.00	77.70
	MLP	**99.42**	**81.08**	**99.43**	**81.08**	**99.42**	**81.08**

[1]The three characteristic spectral wavebands were manually selected based on domain knowledge, retaining physical interpretability. [2]The top 18 principal components (PCs) were extracted through principal component analysis, representing 99% of data variance. These PCs are linear combinations of all original spectral bands, creating abstract feature representations optimized for variance and reducing correlation or collinearity, but lack direct physical interpretability.

4.4.3 Multimodal classification by fusion of spectral and spatial features

The multimodal fusion model demonstrated superior classification performance compared to the standalone spatial and spectral models (**Table 4.2**). Specifically, the multimodal approach achieved a test-set classification accuracy of 82.40%, precision of 82.40%, and recall of 82.40%, surpassing the standalone spatial model (i.e., EfficientNetV2) accuracy, precision, and recall of 66.44% obtained from standard color images, as well as the best-performing standalone spectral model (i.e., PCA-MLP) accuracy of 81.08%. By integrating spectral and spatial features, the multimodal fusion reduced classification ambiguity, especially among serovars with overlapping spatial characteristics or subtle biochemical differences. Additionally, multimodal fusion substantially reduced overfitting observed in standalone models, narrowing the performance gap between training and test datasets (e.g., accuracy gap reduced from spectral-only model: 99.42% train vs. 81.08% test, to multimodal model: 93.62% train vs. 82.40% test). This demonstrates improved generalization and highlights the advantage of combining complementary spectral and spatial information.

Serovar-specific classification performance is further illustrated in **Figure 4.3**. The multimodal model performed particularly well for the serovar 4,[5],12:i:-, achieving the highest classification accuracy of 97%. The lowest accuracy was observed for Infantis (73%), which was commonly misclassified as Johannesburg. Enteritidis (81%) and Johannesburg (82%) showed strong classification results with minimal confusion. Kentucky achieved moderate accuracy (79%) but showed occasional misclassification with Enteritidis. These serovar-specific patterns emphasize the model's strength as well as highlight areas requiring further refinement.

Table 4.2 Enhanced classification through multimodal fusion of spatial data with the best-performing model on spectral data.

	Accuracy (%)		Precision (%)		Recall (%)	
Model	**Train**	**Test**	**Train**	**Test**	**Train**	**Test**
Spectral only[1]	99.42	81.08	99.43	81.08	99.42	81.08
Spatial only[2]	68.22	57.33	77.78	57.33	77.78	57.33
Spectral-spatial fusion	**93.62**	**82.40**	**86.43**	**82.40**	**86.43**	**82.40**

[1]PCA-MLP was selected as the best model in Table 1. [2]EfficientNetV2 variant was used as the CNN model architecture.

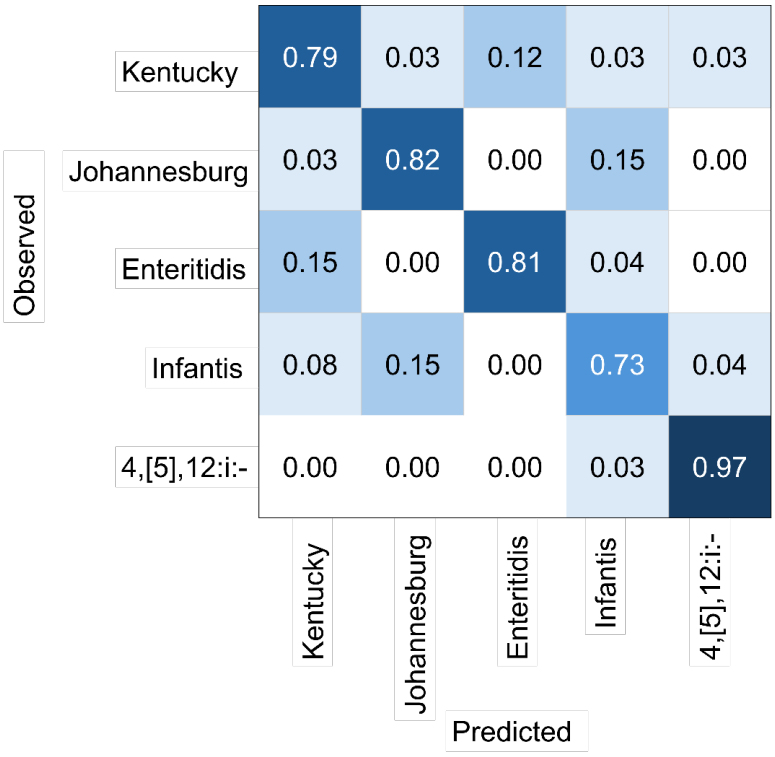

Figure 4.3 Confusion matrix results for the classification of *Salmonella* serovars using the multimodal fusion model.

4.5 Discussion

4.5.1 Hyperspectral microscopy captures inherent differences in *Salmonella* serovars

Hyperspectral microscopy data in this study provided a comprehensive spatial and spectral characterization of each *Salmonella* serovar, enabling the simultaneous capture of morphological details and spectral signatures at the single-cell level. As shown in **Figure 4.2**, the spectral profiles revealed distinct intensity patterns for each serovar, although the overall variability among the serovars was relatively small compared to the differences observed between distinct bacterial species or between bacteria of the same species in different viability states (Park et al., 2023a; Papa et al., 2025). This limited variability highlights the phenotypic similarities shared among *Salmonella* serovars, while still reflecting subtle biochemical and structural differences that can be leveraged for classification. This aligns with previous findings using hyperspectral microscopy with different light sources, further supporting that the captured features reflect inherent characteristics of *Salmonella* (Eady & Park, 2016a,b). In Eady & Park 2016b, they found spectral profiles of *Salmonella* serovars to have three distinct peaks between 400nm and 800nm while using a tungsten halogen lamp. This characteristic is consistent with our data as seen in **Figure 4.2**, with 3 more subtle peaks at 446nm, 555nm, and 628nm**.** These subtle differences in spectral profiles can be attributed primarily to variations in the surface structures of each serovar, such as differences in lipopolysaccharide composition, outer membrane proteins, and other cell envelope components (Andino & Hanning, 2015; CDC, 2020). Such molecular differences influence the way each serovar interacts with incident light, leading to distinct spectral signatures (Park et al., 2016; Zheng et al., 2021). Additionally, a serovars' places of origin, whether environmental, clinical, or food-related, may contribute to

variations in surface chemistry and morphology, further affecting their spectral characteristics (Buncic et al., 2002; Ferrari et al., 2019; Khan et al., 2024).

4.5.2 Data-driven feature extraction outperformed manual feature selection in spectral data representation for classification

The results of this study demonstrate that data preprocessing plays a crucial role in preparing the hyperspectral microscopy data for accurate *Salmonella* serovar classification (**Table 4.1**). The high dimensionality and complexity of hyperspectral datasets often introduce challenges such as noise, redundancy, and irrelevant information, all of which can negatively impact the performance and accuracy of AI models (Jia et al., 2024; Signoroni et al., 2019; Wang et al., 2020). To overcome these challenges, effective preprocessing techniques such as normalization and dimensionality reduction are essential (Ramirez Rochac et al., 2019; Alimi et al., 2023). Normalization ensures that variations in data scales do not bias the classification process, while noise reduction techniques help remove unwanted spectral variations that could obscure meaningful patterns (Yao & Lewis, 2010; Cao et al., 2017; Vaddi & Manoharan, 2020). Dimensionality reduction methods, such as PCA, are particularly important for hyperspectral data, as they enable the extraction of the most important features while discarding redundant or irrelevant spectral bands (Rodarmel & Shan, 2002; Datta et al., 2017). These preprocessing steps ensure that only the most relevant spectral features are retained, thereby improving classification accuracy and model generalization.

In our study, while manual feature selection based on domain expertise successfully achieved accurate classification among hyperspectral microscopy data of *E. coli* in different physiological states in our previous study (Papa et al., 2025), a similar approach resulted in lower classification accuracies for *Salmonella* serovar classification when applied to spectral data, as

shown in **Table 4.1**. The reduced performance can be attributed to the limited spectral information retained by selecting only three bands, which may not capture the subtle yet critical differences among the serovars. Manual feature selection can also introduce bias, potentially overlooking spectral regions that contribute significantly to classification when analyzed collectively. Although this approach reduces computational and data storage demands, it risks discarding spectral information that could differentiate serovars. This reliance on a small subset of the spectral data can lead to suboptimal performance, as subtle differences may span multiple wavelengths outside the chosen bands. This concept is similar with hyperspectral imaging at the macroscale. In Tonskin et al., 2017, they found that feature selection based on their High Dimensional Model Representation outperformed other feature selection algorithms such as Chi2 and Fisher.

In contrast, data-driven feature extraction using PCA substantially improved classification performance, as shown in **Table 4.1**. These improvements demonstrate that PCA effectively captures the most informative spectral patterns and relationships that may not be apparent through manual feature selection. The superior performance of PCA-based preprocessing highlights the importance of data-driven feature extraction methods in hyperspectral data analysis (Rodamel & Shan, 2002; Eady et al., 2015). Using hyperspectral images at the macroscale, Rodamel & Shan 2002 concluded that using the most important bands from PCA resulted in high classification rates and lower computation time. Eady et al., 2015 showed that hyperspectral microscope images processed with PCA resulted in classification accuracies above 90%. By leveraging statistical techniques to identify and retain the most informative components, PCA offers a systematic and unbiased approach to capturing the underlying spectral complexity of bacteria while allowing machine learning models to focus on

relevant features, leading to enhanced classification performance. Overall, these findings align with broader research showing that analytical decisions, including the choice of preprocessing methods, can significantly influence model outcomes. Variations in preprocessing such as normalization, noise reduction, and baseline correction directly affect feature selection and, consequently, classification performance (Gould et al., 2025). Therefore, selecting appropriate preprocessing techniques is essential to ensure that classification results reflect true biological variation rather than artifacts of data handling.

4.5.3 Multimodal fusion of spectral and spatial features reduces overfitting and improves serovar classification

The improved performance of the multimodal fusion model highlights the value of leveraging multiple feature types in high-dimensional hyperspectral microscopy data. In our model, spatial and spectral feature vectors were combined to capture a more comprehensive representation of each *Salmonella* serovar, resulting in more accurate predictions with reduced overfitting on the training dataset (**Table 4.2**). Spatial data captures morphological characteristics, while spectral data provide rich biochemical information (Imani & Ghassemian, 2020). Spatial data, derived from the structural aspects of hyperspectral images provide critical insights into cell morphology and patterns related to cellular structure. These morphological characteristics are highly effective for distinguishing microorganisms that exhibit clear physical differences. On the other hand, spectral data independently provide powerful biochemical fingerprints of biological samples (Li et al., 2024). By analyzing how samples scatter light across 303 spectral bands, spectral data reveal variations in chemical compositions (Eady et al., 2015; Eady & Park 2016a). These biochemical signatures are especially useful for differentiating between *Salmonella* serovars that are morphologically similar but biochemically distinct.

However, while both spatial and spectral features individually contribute significantly to classification performance, their combination yields even better results. In Liu et al., 2021, the use of spectral and spatial features to classify *Bacillus megaterium* and *Bacillus* cereus resulted in classification accuracies above 95% with different machine learning models. Additionally, other studies in spectral-spatial fusion have explored CNNs and transformer-based architectures to improve generalization, demonstrating that leveraging both spatial and spectral information leads to higher classification accuracy and better adaptation to unseen variations (Kang et al., 2020b; Praveen & Menon, 2021). Kang et al., 2020b combined LSTM, ResNet, and a 1D-CNN to create Fusion-Net that process hyperspectral data and resulted in a 98.4% classification accuracy. Praveen & Menon 2021 utilized Gabor filtering with a 3D-CNN to classify

4.6 Conclusion

This study demonstrates that hyperspectral microscopy, combined with AI-driven analysis, provides a rapid, one-step method for accurate *Salmonella* serovar classification. By capturing both spatial and spectral features, hyperspectral microscopy enables a comprehensive characterization of microbial differences, utilizing both morphological and biochemical signatures. The findings also confirm that data-driven feature extraction compared to expert feature selection, greatly improves classification accuracy by preserving critical spectral information while also reducing the dimensionality of the data. The integration of spatial and spectral modalities through multimodal fusion improved generalization and reduces overfitting, ensuring robust classification of serovars with subtle biochemical or morphological differences. This fusion-based approach outperformed traditional machine learning models, reinforcing the value of multimodal hyperspectral analysis in pathogen detection. The ability to perform non-invasive, high-throughput classification in a single analytical step highlights the potential of this

method for real-time food safety monitoring, offering a scalable and efficient solution for microbial identification in complex environments.

Data availability

The code and data will be made available in a public repository at https://github.com/food-ai-engineering-lab upon publication. Future updates will be integrated into this repository.

BIBLIOGRAPHY

AL-Alimi, D., Al-qaness, M. A. A., Cai, Z., & Alawamy, E. A. (2023). IDA: Improving distribution analysis for reducing data complexity and dimensionality in hyperspectral images. *Pattern Recognition*, *134*, 109096. https://doi.org/10.1016/j.patcog.2022.109096

Andino, A., & Hanning, I. (2015). *Salmonella* enterica: Survival, Colonization, and Virulence Differences among Serovars. *The Scientific World Journal*, *2015*, 520179. https://doi.org/10.1155/2015/520179

Park, B., Sundaram, J., Hinton, A., Yoon, S.-C., Windham, W., & Lawrence, K. (2016). *Detection and Characterization of Salmonella with Hyperspectral Microscope Imaging*.

Bell, R. L., Jarvis, K. G., Ottesen, A. R., McFarland, M. A., & Brown, E. W. (2016). Recent and emerging innovations in *Salmonella* detection: a food and environmental perspective. Microbial biotechnology, 9(3), 279-292.

Bhunia, A. K., Singh, A. K., Parker, K., & Applegate, B. M. (2022). Petri-plate, bacteria, and laser optical scattering sensor. *Frontiers in Cellular and Infection Microbiology*, *12*. https://doi.org/10.3389/fcimb.2022.1087074

Buncic, S., Avery, S. M., Rocourt, J., & Dimitrijevic, M. (2001). Can food-related environmental factors induce different behaviour in two key serovars, 4b and 1/2a, of Listeria monocytogenes? *International Journal of Food Microbiology*, *65*(3), 201–212. https://doi.org/10.1016/s0168-1605(00)00524-9

Ferrari, R. G., Rosario, D. K. A., Cunha-Neto, A., Mano, S. B., Figueiredo, E. E. S., & Conte-Junior, C. A. (2019). Worldwide Epidemiology of *Salmonella* Serovars in Animal-Based Foods: A Meta-analysis. *Applied and Environmental Microbiology*, *85*(14), e00591-19. https://doi.org/10.1128/AEM.00591-19

Khan, H. A., Neyaz, L. A., Malak, H. A., Alshehri, W. A., Elbanna, K., Organji, S. R., Asiri, F. H., Aldosari, M. S., & Abulreesh, H. H. (2024). Diversity and antimicrobial susceptibility patterns of clinical and environmental *Salmonella* enterica serovars in Western Saudi Arabia. *Folia Microbiologica*, *69*(6), 1305–1317. https://doi.org/10.1007/s12223-024-01172-1

Wang, Z., Liang, S., Xu, L., Song, W., Wang, D., & Huang, D. (2020). Dimensionality reduction method for hyperspectral image analysis based on rough set theory. *European Journal of Remote Sensing*, *53*(1), 192–200. https://doi.org/10.1080/22797254.2020.1785949

Jia, J., Zheng, X., Wang, Y., Chen, Y., Karjalainen, M., Dong, S., Lu, R., Wang, J., & Hyyppä, J. (2024). The effect of artificial intelligence evolving on hyperspectral imagery with different signal-to-noise ratio, spectral and spatial resolutions. *Remote Sensing of Environment*, *311*, 114291. https://doi.org/10.1016/j.rse.2024.114291

Cao, F., Yang, Z., Ren, J., Jiang, M., & Ling, W.-K. (2017). *Does Normalization Methods Play a Role for Hyperspectral Image Classification?* (arXiv:1710.02939). arXiv. https://doi.org/10.48550/arXiv.1710.02939

CDC. (2024, October 4). *About Salmonella Infection*. *Salmonella* Infection (Salmonellosis). https://www.cdc.gov/salmonella/about/index.html

Daquigan, N., Grim, C. J., White, J. R., Hanes, D. E., & Jarvis, K. G. (2016). Early Recovery of *Salmonella* from Food Using a 6-Hour Non-selective Pre-enrichment and Reformulation of Tetrathionate Broth. *Frontiers in microbiology*, *7*, 2103. https://doi.org/10.3389/fmicb.2016.02103

Datta, A., Ghosh, S., & Ghosh, A. (2018). PCA, Kernel PCA and Dimensionality Reduction in Hyperspectral Images. In G. R. Naik (Ed.), *Advances in Principal Component Analysis: Research and Development* (pp. 19–46). Springer. https://doi.org/10.1007/978-981-10-6704-4_2

Eady, M., & Park, B. (2016a). Classification of *Salmonella* enterica serotypes with selective bands using visible/NIR hyperspectral microscope images. *Journal of Microscopy*, *263*(1), 10–19. https://doi.org/10.1111/jmi.12368

Eady, M. & Park, B. (2016b). Rapid identification of *Salmonella* serotypes through hyperspectral microscopy with different lighting sources. *Journal of Spectral Imaging*. 5. 10.1255/jsi.2016.a4.

Eady, M., Park, B., & Choi, S. (2015). Rapid and Early Detection of *Salmonella* Serotypes with Hyperspectral Microscopy and Multivariate Data Analysis. *Journal of Food Protection*, *78*(4), 668–674. https://doi.org/10.4315/0362-028X.JFP-14-366

Fong, A., Shu, G., McDonogh, B., & Park, B. (2020). Detecting foodborne pathogens with darkfield hyperspectral microscopy. In *Hyperspectral Imaging and Applications* (pp. 9–16). SPIE. https://doi.org/10.1117/12.2584913

Franco-Duarte, R., Černáková, L., Kadam, S., S. Kaushik, K., Salehi, B., Bevilacqua, A., Corbo, M. R., Antolak, H., Dybka-Stępień, K., Leszczewicz, M., Relison Tintino, S., Alexandrino de Souza, V. C., Sharifi-Rad, J., Melo Coutinho, H. D., Martins, N., & Rodrigues, C. F. (2019). Advances in Chemical and Biological Methods to Identify Microorganisms—From Past to Present. *Microorganisms*, *7*(5), 130. https://doi.org/10.3390/microorganisms7050130

Gould, E., Fraser, H. S., Parker, T. H., Nakagawa, S., Griffith, S. C., Vesk, P. A., Fidler, F., Hamilton, D. G., Abbey-Lee, R. N., Abbott, J. K., Aguirre, L. A., Alcaraz, C., Aloni, I., Altschul, D., Arekar, K., Atkins, J. W., Atkinson, J., Baker, C. M., Barrett, M., … Whelan, S. (2025). Same data, different analysts: Variation in effect sizes due to analytical decisions in ecology and evolutionary biology. *BMC Biology*, *23*(1), 35. https://doi.org/10.1186/s12915-024-02101-x

Grinevich, D., Harden, L., Thakur, S., & Callahan, B. (2024). Serovar-level identification of bacterial foodborne pathogens from full-length 16S rRNA gene sequencing. *mSystems*, *9*(3), e0075723. https://doi.org/10.1128/msystems.00757-23

He, Y., Xu, W., Zhi, Y., Tyagi, R., Hu, Z., & Cao, G. (2018). Rapid bacteria identification using structured illumination microscopy and machine learning. *Journal of Innovative Optical Health Sciences*, *11*(01), 1850007. https://doi.org/10.1142/S1793545818500074

Herrera-León, S., Ramiro, R., Arroyo, M., Díez, R., Usera, M. A., & Echeita, M. A. (2007). Blind comparison of traditional serotyping with three multiplex PCRs for the identification of *Salmonella* serotypes. *Research in Microbiology*, *158*(2), 122–127. https://doi.org/10.1016/j.resmic.2006.09.009

Imani, M., & Ghassemian, H. (2020). An overview on spectral and spatial information fusion for hyperspectral image classification: Current trends and challenges. *Information Fusion*, *59*, 59–83. https://doi.org/10.1016/j.inffus.2020.01.007

Kang, R., Park, B., & Chen, K. (2020a). Identifying non-O157 Shiga toxin-producing *Escherichia coli* (STEC) using deep learning methods with hyperspectral microscope images. *Spectrochimica Acta Part A: Molecular and Biomolecular Spectroscopy*, *224*, 117386. https://doi.org/10.1016/j.saa.2019.117386

Kang, R., Park, B., Eady, M., Ouyang, Q., & Chen, K. (2020b). Single-cell classification of foodborne pathogens using hyperspectral microscope imaging coupled with deep learning frameworks. *Sensors and Actuators B: Chemical*, *309*, 127789. https://doi.org/10.1016/j.snb.2020.127789

Kang, R., Park, B., Ouyang, Q., & Ren, N. (2021). Rapid identification of foodborne bacteria with hyperspectral microscopic imaging and artificial intelligence classification algorithms. *Food Control*, *130*, 108379. https://doi.org/10.1016/j.foodcont.2021.108379

Li, N., Wang, Z., & Cheikh, F. A. (2024). Discriminating Spectral–Spatial Feature Extraction for Hyperspectral Image Classification: A Review. *Sensors (Basel, Switzerland)*, *24*(10), 2987. https://doi.org/10.3390/s24102987

Liu, K., Ke, Z., Chen, P., Zhu, S., Yin, H., Li, Z., & Chen, Z. (2021). Classification of two species of Gram-positive bacteria through hyperspectral microscopy coupled with machine learning. *Biomedical Optics Express*, *12*(12), 7906–7916. https://doi.org/10.1364/BOE.445041

Ma, L., Yi, J., Wisuthiphaet, N., Earles, M., & Nitin, N. (2022). Accelerating the Detection of Bacteria in Food Using Artificial Intelligence and Optical Imaging. *Applied and Environmental Microbiology*, *89*(1), e01828-22. https://doi.org/10.1128/aem.01828-22

Maeda, Y., Sugiyama, Y., Kogiso, A., Lim, T.-K., Harada, M., Yoshino, T., Matsunaga, T., & Tanaka, T. (2018). Colony Fingerprint-Based Discrimination of *Staphylococcus* species with Machine Learning Approaches. *Sensors*, *18*(9), Article 9. https://doi.org/10.3390/s18092789

McGoverin, C., Steed, C., Esan, A., Robertson, J., Swift, S., & Vanholsbeeck, F. (2021). Optical methods for bacterial detection and characterization. *APL Photonics*, *6*(8), 080903. https://doi.org/10.1063/5.0057787

Nutrition, C. for F. S. and A. (2020). BAM Chapter 5: Salmonella. *FDA*. https://www.fda.gov/food/laboratory-methods-food/bam-chapter-5-salmonella

Papa, M., Wasit, A., Pecora, J., Bergholz, T. M., & Yi, J. (2025). Detection of Viable but Nonculturable *E. coli* Induced by Low-Level Antimicrobials Using AI-Enabled Hyperspectral Microscopy. *Journal of Food Protection*, *88*(1), 100430. https://doi.org/10.1016/j.jfp.2024.100430

Park, B., Shin, T., Wang, B., McDonogh, B., & Fong, A. (2023a). Classification between live and dead foodborne bacteria with hyperspectral microscope imagery and machine learning. *Journal of Microbiological Methods*, *209*, 106739. https://doi.org/10.1016/j.mimet.2023.106739

Park, B., Shin, T., Kang, R., Fong, A., McDonogh, B., & Yoon, S.-C. (2023b). Automated segmentation of foodborne bacteria from chicken rinse with hyperspectral microscope imaging and deep learning methods. *Computers and Electronics in Agriculture*, *208*, 107802. https://doi.org/10.1016/j.compag.2023.107802

Park, B., Sundaram, J., Hinton, A., Yoon, S.-C., Windham, W., & Lawrence, K. (2016). *Detection and Characterization of Salmonella with Hyperspectral Microscope Imaging ‡*.

Paszke, A., Gross, S., Massa, F., Lerer, A., Bradbury, J., Chanan, G., Killeen, T., Lin, Z., Gimelshein, N., Antiga, L., Desmaison, A., Kopf, A., Yang, E., DeVito, Z., Raison, M., Tejani, A., Chilamkurthy, S., Steiner, B., Fang, L., … Chintala, S. (2019). PyTorch: An Imperative Style, High-Performance Deep Learning Library. *Advances in Neural Information Processing Systems*, *32*.

Patel, A., Wolfram, A., & Desin, T. S. (2024). Advancements in Detection Methods for *Salmonella* in Food: A Comprehensive Review. *Pathogens (Basel, Switzerland)*, *13*(12), 1075. https://doi.org/10.3390/pathogens13121075

Praveen, B., & Menon, V. (2021). Study of Spatial–Spectral Feature Extraction Frameworks With 3-D Convolutional Neural Network for Robust Hyperspectral Imagery Classification. *IEEE Journal of Selected Topics in Applied Earth Observations and Remote Sensing*, *14*, 1717–1727. IEEE Journal of Selected Topics in Applied Earth Observations and Remote Sensing. https://doi.org/10.1109/JSTARS.2020.3046414

Ramirez Rochac, J. F., Zhang, N., Thompson, L., & Oladunni, T. (2019). A Data Augmentation-Assisted Deep Learning Model for High Dimensional and Highly Imbalanced Hyperspectral Imaging Data. *2019 9th International Conference on Information Science and Technology (ICIST)*, 362–367. https://doi.org/10.1109/ICIST.2019.8836913

Ranieri, M. L., Shi, C., Moreno Switt, A. I., den Bakker, H. C., & Wiedmann, M. (2013). Comparison of Typing Methods with a New Procedure Based on Sequence

Characterization for *Salmonella* Serovar Prediction. *Journal of Clinical Microbiology*, *51*(6), 1786–1797. https://doi.org/10.1128/JCM.03201-12

Rodarmel, C., & Shan, J. (2002a). *Principal Component Analysis for Hyperspectral Image Classification*. https://www.semanticscholar.org/paper/Principal-Component-Analysis-for-Hyperspectral-Rodarmel-Shan/c9eb2d77f24673dde1d5105feb6c2d75915d682c

Seo, Y. W., Yoon, S. C., Park, B., Hinton Jr, A., Windham, W. R., & Lawrence, K. C. (2013). Development of classification models to detect *Salmonella* Enteritidis and *Salmonella* Typhimurium found in poultry carcass rinses by visible-near infrared hyperspectral imaging. In *Sensing for Agriculture and Food Quality and Safety V* (pp. 70–78). SPIE. https://doi.org/10.1117/12.2016336

Signoroni, A., Savardi, M., Baronio, A., & Benini, S. (2019). Deep Learning Meets Hyperspectral Image Analysis: A Multidisciplinary Review. *Journal of Imaging*, *5*(5), 52. https://doi.org/10.3390/jimaging5050052

Tan, M., & Le, Q. V. (2021). EfficientNetV2: smaller models and faster training. *International Conference on Machine Learning.* 10096–10106.

Tao, C., Du, J., Wang, J., Hu, B., & Zhang, Z. (2023). Rapid Identification of Infectious Pathogens at the Single-Cell Level via Combining Hyperspectral Microscopic Images and Deep Learning. *Cells*, *12*(3), Article 3.

Taşkın, G., Kaya, H., & Bruzzone, L. (2017). Feature Selection Based on High Dimensional Model Representation for Hyperspectral Images. *IEEE Transactions on Image Processing*, *26*(6), 2918–2928. IEEE Transactions on Image Processing. https://doi.org/10.1109/TIP.2017.2687128

Turra, G., Arrigoni, S., & Signoroni, A. (2017, September). CNN-Based Identification of Hyperspectral Bacterial Signatures for Digital Microbiology. In *Image Analysis and Processing-ICIAP 2017*, Catania, Italy (pp. 500–510). Springer International Publishing. https://doi.org/10.1007/978-3-319-68548-9_46

Vaddi, R., & Manoharan, P. (2020). Hyperspectral image classification using CNN with spectral and spatial features integration. *Infrared Physics & Technology*, *107*, 103296. https://doi.org/10.1016/j.infrared.2020.103296

Wang, P., Sun, H., Yang, W., & Fang, Y. (2022). Optical Methods for Label-Free Detection of Bacteria. *Biosensors*, *12*(12), 1171. https://doi.org/10.3390/bios12121171

Wang, Z., Liang, S., Xu, L., Song, W., Wang, D., & Huang, D. (2020). Dimensionality reduction method for hyperspectral image analysis based on rough set theory. *European Journal of Remote Sensing*, *53*(1), 192–200. https://doi.org/10.1080/22797254.2020.1785949

Wu, C., Xie, Y., Xi, Q., Han, X., Li, Z., Li, G., Zhao, J., & Liu, M. (2023). Rapid and high accurate identification of Escherichia coli active and inactivated state by hyperspectral

microscope imaging combing with machine learning algorithm. *Vibrational Spectroscopy*, *130*, 103645. https://doi.org/10.1016/j.vibspec.2023.103645

Wu, C., Xie, Y., Xi, Q., Han, X., Li, Z., Li, G., Zhao, J., & Liu, M. (2024). Rapid and high accurate identification of *Escherichia coli* active and inactivated state by hyperspectral microscope imaging combing with machine learning algorithm. *Vibrational Spectroscopy*, *130*, 103645. https://doi.org/10.1016/j.vibspec.2023.103645

Yao, H., & Lewis, D. (2010). CHAPTER 2—Spectral Preprocessing and Calibration Techniques. In D.-W. Sun (Ed.), *Hyperspectral Imaging for Food Quality Analysis and Control* (pp. 45–78). Academic Press. https://doi.org/10.1016/B978-0-12-374753-2.10002-4

Yi, J., Wisuthiphaet, N., Raja, P., Nitin, N., & Earles, J. M. (2023). AI-enabled biosensing for rapid pathogen detection: From liquid food to agricultural water. *Water Research*, *242*, 120258. https://doi.org/10.1016/j.watres.2023.120258

Zheng, S., Bawazir, M., Dhall, A., Kim, H.-E., He, L., Heo, J., & Hwang, G. (2021). Implication of Surface Properties, Bacterial Motility, and Hydrodynamic Conditions on Bacterial Surface Sensing and Their Initial Adhesion. *Frontiers in Bioengineering and Biotechnology*, *9*, 643722. https://doi.org/10.3389/fbioe.2021.643722

Zhu, H., Luo, J., Liao, J., & He, S. (2023). High-accuracy Rapid Identification and Classification of Mixed Bacteria Using Hyperspectral Transmission Microscopic Imaging and Machine Learning. *Progress in Electromagnetics Research*, *178*, 49–62. https://doi.org/10.2528/pier23082303

CHAPTER 5: CONCLUSIONS AND FUTURE WORK

This study successfully developed an AI-enabled hyperspectral microscopy framework capable of classifying pathogens, accounting for subtle biological variations in microbial physiology and the nuanced differences among closely related serovars. Chapter 2 initially identified critical research gaps in AI-enabled imaging for pathogen detection under diverse conditions. These gaps included a lack of integrated reporting of standardized laboratory protocols and data pipelines and limited research addressing stressed pathogen detection. Additionally, recent advancements in multimodal imaging were highlighted as promising areas for future exploration. To address these identified gaps, research chapters in this work advanced beyond conventional image classification techniques by establishing an optimized and reproducible laboratory protocol specifically tailored for microbiological sample preparation. This ensured consistent, high-quality hyperspectral data acquisition from viable bacteria. Moreover, multiple data processing strategies were evaluated, ranging from manual feature selection to advanced data-driven feature extraction, as well as multimodal fusion approaches.

In Chapter 3, the laboratory protocol was meticulously optimized to consistently capture high-quality hyperspectral data reflecting stressed physiological state of *E. coli*. Results demonstrated successful induction of the VBNC state using low-level antimicrobial stressors, with distinct spectral profiles observable between normal and VBNC cells. The optimized protocol involved minimal sample preparation, using sterilized DI water without selective media or additional reagents. Utilizing hyperspectral pseudo-RGB composites and a state-of-the-art deep CNN model (i.e., EfficientNetV2), VBNC and normal cells were classified with 97.1% accuracy, outperforming the 83.3% achieved with standard color images alone. This improvement highlights the enhanced pathogen detection capability achieved through selection

of characteristic wavebands enabled by hyperspectral microscopy. Overall, these results confirm the successful establishment of an AI-enhanced hyperspectral microscopy framework for rapidly detecting microbial stress-induced physiological states.

Chapter 4 further expanded on the laboratory protocol from Chapter 3, exploring advanced data processing pipelines for another type of subtle biological variation, i.e., serovar classification of *Salmonella* spp. To fully leverage the rich information present in hyperspectral data, the data pipeline employed two parallel branches: i) a spectral branch, obtaining single-cell spectra from raw hyperspectral data, which were preprocessed and analyzed using machine learning algorithms; and ii) a spatial branch, applying the CNN (i.e., EfficientNetV2) to standard color images. Within the spectral branch, manual feature selection was directly compared with data-driven feature extraction method (i.e., PCA). Subsequently, the outputs of both branches were combined through prediction-level multimodal fusion for comprehensive data analysis. This multimodal approach enabled accurate classification of *Salmonella* serovars (i.e., Kentucky, Johannesburg, Infantis, Enteritidis, and 4,[5],12:i:-) with up to 82.40% accuracy, even using minimal sample preparation as in Chapter 3. Data-driven feature extraction outperformed manual feature selection in terms of accuracy, precision, recall, and multimodal fusion further enhanced classification performance while mitigating overfitting. Overall, this demonstrates that data-driven preprocessing coupled with multimodal fusion allowed for improved *Salmonella* serovar classification.

For future work, several critical areas should be explored to enhance the accuracy, reliability, and practical applicability of AI-enabled hyperspectral microscopy in pathogen classification. One essential step is to perform direct comparative studies of hyperspectral microscopy with conventional detection method (i.e., culture-based) and advanced molecular

method (e.g. PCR and qPCR). Such comparisons will help establish clear performance benchmarks and validate efficacy of AI-enabled microscopy methods. Additionally, exploring more sophisticated AI and machine learning algorithms, such as physics-informed neural network, multi-task learning, and generative models, can further improve classification performance, particularly in distinguishing closely related serovars and identifying pathogens under various stress conditions. Extending this technology into complex food matrices also represent a critical area for future development. Detecting pathogens in food and food processing environments presents significant challenges due to inherent background noise and sample heterogeneity. Future efforts should aim to develop frameworks for near real-time pathogen detection and refine data pipelines specifically to manage the complexities of food samples effectively. Additionally, integrating hyperspectral microscopy with affordable and accessible imaging modalities, such as standard color imaging or conventional light microscopy, offers substantial potential through domain adaptation and transfer learning. Leveraging insights gained from high-resolution hyperspectral data to develop simplified image-based models could significantly improve pathogen detection performance while expanding the practicality and cost-effectiveness of AI-enabled imaging solutions.